IN SITU MONITORING OF PHARMACEUTICAL CRYSTALLISATION

ADEYINKA TEMITOPE AINA, BSc, MSc, MRSC

Thesis submitted to the University of Nottingham for the degree of Doctor of Philosophy

July 2012

Abstract

Using confocal Raman spectroscopy/microscopy, we have monitored pharmaceutical crystallisation 'in situ' in three model (well characterised polymorphic systems) Active Pharmaceutical Ingredients (APIs) and one previously unstudied system where polymorphism had not being reported prior to this study: flufenamic acid, a Non Steroidal Non-Inflammatory Drug (NSAID); nifedipine, an anti-hypertensive; tolbutamide, used in the treatment of type II diabetes; and imipramine hydrochloride, an antidepressant respectively. Constrained crystallisation from the solid amorphous state was utilised to kinetically trap polymorphs via the Ostwald's rule of stages. Particular emphasis was placed on the phonon-mode/low wavenumber region (4-400cm^{-1}) of the Raman spectral window (this region provides useful information about lattice environment).

In all cases our results from the Raman experiments were complemented with similar experiments using Differential Scanning Calorimetry (DSC) and Variable Temperature X-ray Powder Diffraction (VTXRPD). To reduce data complexity, principal component analysis was deployed and found to be extremely effective.

In chapter two, a multi-technique study of flufenamic acid (FFA) was carried out which served as a groundwork for later chapters. A solid-solid transformation between two forms of FFA (forms I and III) was observed, due to the abrupt nature of this transition, the 'Lindemann vibrational catastrophe' was envisaged as a possible mechanism for the transformation.

Using FFA as a test case in chapter three, polymorphic transformations was monitored in both FFA forms I and III using in situ Raman spectroscopy (as well as VTXRPD) by adopting the constrained crystallisation approach. The approach showed excellent promise (with the XRPD patterns of FFA form II and one unknown form uncovered) and was further explored in later chapters using a variety of pharmaceutical materials.

While in chapter four, the interconversion between the different polymorphs of nifedipine was studied using the constrained crystallisation approach monitored using in situ Raman spectroscopy (together with VTXRPD and DSC), our results compared favourably well with those previously published in literature. We also reported for the first time the phonon-mode Raman spectral for this system as earlier publications focussed only on the 'traditional' fingerprint region.

Similarly in chapter five, in situ Raman spectroscopy was also used to monitor the polymorphic transformations in tolbutamide (using the constrained crystallisation approach), results from the Raman analysis was compared with those obtained from VTXRPD and found to be in agreement. Thus further showing that Raman spectroscopy combined with the constrained crystallisation approach is a veritable tool for monitoring polymorphic transitions.

In chapter six, preliminary results (Raman/XRPD/DSC) showed for the first time that imipramine hydrochloride exhibits polymorphism, with the possibility of at least two new polymorphs. Combination of state of the art spectroscopic techniques with appropriate statistical methods, X-ray powder diffraction and DSC was shown to be an extremely effective approach to investigating and characterising polymorphism in drugs, often using only milligram or sub-milligram sample quantities.

Lastly in chapter seven, the novel technique of Transmission Raman Spectroscopy (TRS) was employed in carrying out a quantitative study of polymorphic content in a model pharmaceutical formulation and the results obtained compared with those from traditional backscattering geometry. The transmission method is shown to provide a true bulk measurement of the composition, being unaffected by systematic or stochastic sub-sampling issues that can plague traditional backscattering geometries.

ACKNOWLEDGEMENT

I will like to express my heart felt appreciation to my supervisor, Dr. Jonathan Burley, for his excellent supervision and for creating an enabling environment for learning, I will remain eternally grateful to him. I will also like to thank my co-supervisor Dr. Jonas Emsley and my internal assessor, Prof. Clive Roberts for their invaluable contributions without which my training would not have been successful.

I will also like to thank every member of the Laboratory of Biophysics and Surface Analysis (LBSA) for their help and assistance during my stay here at Nottingham. My appreciation goes to the members of the Jonathan Burley group, Jagadeesh, Andrew and Aalae for their support.

Finally, I will like to thank the Biotechnology and Biological Sciences Research Council (BBSRC), the East Midlands Development Agency (EMDA) and the Research Councils UK (RCUK), for providing funding for my doctoral training.

Lists of Tables and Figures

Lists of Tables

Table 1: Physical properties that differ among various solid forms. Modified from[8]

Table 2: The seven crystal systems and their corresponding Bravais lattices symmetries

Table 3: Solubility table for flufenamic acid as received

Table 4: Result of solvent drop milling experiments of FFA forms I and III

Table 5: Summary of previous publications on the polymorphic modification of nifedipine

Lists of Figures

Figure 1: Picture of the Raman system at the Nottingham Nanotechnology and Nanoscience Centre

Figures 2a and 2b: Enantiotropism versus Monotropism

Figure 3: A typical DSC scan for an amorphous material

Figure 4: Schematic diagram of the two types of DSC

Figure 5: A nucleus precessing in a magnetic field

Figure 6: Schematic representation of the theory of Raman Spectroscopy

Figure 8: Schematic diagram of transmission Raman spectroscopy

Figure 9: Microscope heating stage (Linkam) mounted on the rotating stage of a polarizing light microscope in the Laboratory of Biophysics and Surface Analysis, School of pharmacy, University of Nottingham

Figure 2.1: Molecular structure of Flufenamic acid

Figure 2.2: XRPD patterns of FFA

Figure 2.3: Patterns obtained from the dry milling experiment with FFA III

Figure 2.4a: Raman spectra of the phonon-mode of both forms I and III

Figure 2.4b: Raman spectra of the molecular-mode of both forms I and III

Figure 2.5: Raman spectra showing FFA III→I transformation upon dry milling

Figure 2.6: XRPD patterns of the solid-solid transformation between FFA forms I and III

Figure 2.7a: XRPD patterns of FFA I after solvent drop milling

Figure 2.7b: XRPD patterns of FFA III after solvent drop milling

Figure 2.8a: Molecular structure of FFA

Figure 2.8b: Energy of gas-phase FFA molecule as a function of the two nitrogen-centred torsion angles

Figure 2.9: Solid-state NMR spectral of FFA I and III

Figure 2.10: DSC plots for both FFA forms I and III

Figure 2.11a: Phonon-mode Raman spectra of FFA forms I and III

Figure 2.11b: Molecular-mode Raman spectra of FFA forms I and III

Figure 2.12a: Variable temperature Raman Spectroscopy experiment of FFA form I

Figure 2.12b: Variable temperature Raman Spectroscopy experiment of FFA form III

Figure 2.13: Representative Raman spectra from the heating FFA form III taken between 113-116°C

Figure 2.14: Plot of peak width and peak position as a function of temperature

Figure 3.1: Figure 3.1: In situ XRPD pattern from the heating of the amorphous form prepared from FFA I

Figure 3.2a: Variations in the Raman spectra (top right), PC1, PC2 (top left) with temperature and loadings (bottom), for the slow heating of of the amorphous form obtained from FFA I

Figure 3.2b: Variations in the Raman spectra (top right), PC1, PC2 (top left) with temperature and loadings (bottom), for the slow heating of the amorphous form obtained from FFA III

Figure 3.3a: Phonon-mode projection of the heating of amorphous form (prepared by melting FFA I)

Figure 3.3b: Molecular-mode projection of the heating of amorphous form (prepared by melting FFA I

Figure 3.4a: Phonon-mode projection of the heating of amorphous form (obtained by melting FFA III)

Figure 3.4b: Molecular-mode projection of the heating of amorphous form (obtained by melting FFA III)

Figure 3.5a: DSC trace of the slow heating of amorphous sample prepared by melting and quenching FFA I: inset are the two weak exotherms

Figure 3.5b: DSC trace of the slow heating of amorphous sample prepared by melting and quenching FFA III

Figure 4.1: Molecular structure of nifedipine

Figure 4.2a: DSC trace of the slow heating of amorphous sample prepared from nifedipine form I

Figure 4.2b: DSC plot of the slow heating of nifedipine form II

Figure 4.3a: In situ Raman spectra from heating amorphous form of nifedipine

Figure 4.3b: In situ Raman spectra of reheating nifedipine form II (phonon-mode only)

Figure 4.3c: In situ Raman spectra of nifedipine (molecular-mode region only)

Figure 4.4a: Raman spectra showing changes in the symmetric NO_2 stretching mode

Figure 4.4b: Raman spectra showing changes in the υ(C=O) vibration stretching mode

Figure 4.5a: Phonon mode Raman spectra of nifedipine

Figure 4.5b: Molecular mode Raman spectra of nifedipine

Figure 4.6a: Principal component projection of the heating of amorphous form of nifedipine

Figure 4.6b: Principal component projection of the reheating of nifedipine form II

Figure 4.7a: Phonon-mode projection of the heating of amorphous form of nifedipine

Figure 4.7b: Molecular-mode projection of the heating of amorphous form of nifedipine

Figure 4.8a: Phonon-mode projection of the reheat of nifedipine form II

Figure 4.8b: Molecular-mode projection of the reheat of nifedipine form II

Figure 4.9a: In situ XRPD pattern showing the crystallisation of amorphous nifedipine

Figure 4.9b: In situ XRPD pattern from the reheating of nifedipine form II

Figure 4.9c: Principal component projection of the heating of amorphous nifedipine (VTXRPD)

Figure 4.9d: Principal component projection from the reheating of nifedipine form II (VTXRPD)

Figure 5.1: Molecular structure of tolbutamide

Figure 5.2: Variations in the Raman spectra (top right), PC1, PC2 (top left) with temperature and loadings (bottom), for the slow heating of amorphous tolbutamide

Figure 5.3: Variations in the Raman spectra (top right), PC1, PC2 (top left) with temperature and loadings (bottom), for the low wave number bands (20-340cm^{-1})

Figure 5.4: Variations in the Raman spectra (top right), PC1, PC2 (top left) with temperature and loadings (bottom), due to the O=N-C stretching vibrations (780-825cm^{-1})

Figure 5.5: Variations in the Raman spectra (top right), PC1, PC2 (top left) with temperature and loadings (bottom),for the symmetric phenyl breathing mode (1120-1190cm^{-1})

Figure 5.6: Variations in the Raman spectra (top right), PC1, PC2 (top left) with temperature and loadings (bottom), for the symmetric C=C stretching vibrations (1580-1620cm^{-1})

Figure 5.7: Variations in patterns (top right), PC1, PC2 (top left) with temperature and loadings (bottom), for the VTXRPD experiment

Figure 6.1: Molecular structure of imipramine hydrochloride

Figure 6.2: DSC plot obtained from the heating of the supercooled melt of imipramine HCl at different temperature

Figure 6.3: In situ Raman spectra of imipramine hydrochloride (phonon-mode region only)

Figure 6.4: Variations in the Raman spectra (top right), PC1, PC2 (top left) with temperature and loadings (bottom), for the slow heating of amorphous imipramine hydrochloride

Figure 6.5a: Raman spectra showing changes in the C-N stretching vibration

Figure 6.5b: Raman spectra showing changes in the phenyl breathing mode

Figure 6.5c: Phonon-mode Raman spectra of imipramine hydrochloride

Figure 6.5d: Molecular-mode Raman spectra of imipramine hydrochloride

Figure 6.6a: Plot of peak position as a function of temperature

Figure 6.6b: Plot of peak width as a function of temperature

Figure 6.7: Variations in the X-ray patterns (top right), PC1, PC2 (top left) with temperature and loadings (bottom), for the slow heating of amorphous imipramine hydrochloride

Figure 7.1: Raman spectra of polymorphic mixtures of FFA, collected in backscattering geometry, for entire spectral range (LHS). Composition (mole fraction of form I) is given at the right, spectra for 0.1, 0.5, and 0.9 are in bold. Signature peaks for forms I and III are l labelled

Figure 7.2: Raman spectra of polymorphic mixtures of FFA, collected in transmission geometry, for entire spectral range (LHS) and phononmode bands (RHS). Composition (mole fraction of form I) is given at the right, spectra for 0.1, 0.5, and 0.9 samples are in bold. Signature peaks for forms I and III are labelled and the symmetric phenyl breathing mode is indicated with *.

Figure 7.3: Results of PLS analysis (validation plot, all data) for transmission and backscattering data

Figure 7.4: Results of fitting the two symmetric breathing bands of the phenyl rings in forms I and III with a single Gaussian

Figure 7.5a: Results of PLS analysis (validation plot, all data) for backscattering data (mean-centring off and esd normalisation on)

Figure 7.5b: Results of PLS analysis (validation plot, all data) for transmission data (mean-centring off and esd normalisation on)

Figure 7.6a: Results of PLS analysis (validation plot, all data) for backscattering data (mean-centring on and esd normalisation off)

Figure 7.6b: Results of PLS analysis (validation plot, all data) for transmission data (mean-centring on and esd normalisation off)

Figure 7.7a: Results of PLS analysis (validation plot, all data) for backscattering data (mean-centring off and esd normalisation off)

Figure 7.7b: Results of PLS analysis (validation plot, all data) for transmission data (mean-centring off and esd normalisation off)

Figure 7.8: Scanning electron micrographs of: (a) FFA I; (b) FFA III; and (c) 50 : 50 mixture milled for 60 seconds. Scale bars are 500, 500 and 200 microns respectively

Lists of Abbreviations

FFA - Flufenamic Acid

DSC - Differential Scanning Calorimetry

MTDSC - Modulated Temperature Differential Scanning Calorimetry

XRPD - X-Ray Powder Diffraction

PXRD - Powder X-ray Diffraction

VTXRPD - Variable Temperature X-Ray Powder Diffraction

NMR - Nuclear Magnetic Resonance

IUPAC - International Union of Pure and Applied Chemistry

TG - Thermogravimetry

HSM - Hot Stage Microscopy

SEM - Scanning Electron Microscopy

TRS - Transmission Raman Spectroscopy

NIR - Near Infra Red

IR - Infra Red

FT - Fourier Transform

API - Active Pharmaceutical Ingredient

PCA - Principal Component Analysis

CCD - Charged-Coupled Device

EMCCD - Electron Multiplying Charged-Coupled Device

ESD - Estimated Standard Deviation

Table of Contents

Cover page ..... **I**
Abstract ..... **II**
Acknowledgement ..... **III**
List of tables and figures ..... **IV**
List of abbreviations ..... **X**
Table of contents ..... **XI**

1.0 Introduction 1

1.1 Polymorphism 1
1.2 Relevance of solid state properties 2
1.3 Polymorphs/Solid state screening 5
1.4 Enantiotropism versus Monotropism 5
1.5 Ostwald Rule 8
1.6 Characterisation of polymorphic systems 9
1.7 Data handling using principal component analysis 18
1.8 General introduction 19

2.0 Polymorphism in Flufenamic Acid 21

2.1 Analysis and mechanistic study of a solid-solid transformation 21
2.2 Review of relevant literature 21
2.3 Experimental 23
2.4 Results and discussion 25
2.4.1 X-ray powder diffraction 25
2.4.2 Solubility assays 33
2.4.3 Solvent milling experiment 34
2.4.4 Molecular modelling 35
2.4.5 Solid state NMR 36
2.4.6 Differential scanning calorimetry 37
2.4.7. In situ Raman spectroscopy/microscopy 39

3.0 Polymorphic Transformations in Flufenamic Acid ….....46

3.1 Monitoring polymorphic changes in flufenamic acid using variable temperature X-ray powder diffraction and in situ Raman spectroscopy ….....46

3.2 Experimental ….....47

3.3 Results and discussion ….....49

3.3.1 X-ray powder diffraction ….....49

3.3.2 Confocal Raman spectroscopy ….....50

3.3.3 DSC analysis ….....53

4.0 Polymorphism in Nifedipine ….....56

4.1 In situ investigation of the polymorphic transformations from amorphous nifedipine using Raman spectroscopy ….....….....56

4.2 Introduction ….....57

4.3 Experimental ….....61

4.4 Results and discussion ….....63

4.4.1 DSC 63

4.4.2 Confocal Raman spectroscopy ….....65

4.4.3 Variable temperature XRPD 76

5.0 Polymorphism in Tolbutamide ….....80

5.1 Monitoring polymorphic transformations in tolbutamide using constrained crystallisation ...80

5.2 Introduction ….....80

5.3 Experimental ….....82

5.4 Results and discussion ….....83

5.4.1 Confocal Raman spectroscopy 83

5.4.2 X-ray powder diffraction …..….....88

6.0 Polymorphism in Imipramine Hydrochloride ….....97

6.1 Polymorphic fingerprinting using phonon-mode Raman spectroscopy ….....…90
6.2 Introduction ….....90
6.3 Experimental ….....92
6.4 Results and discussion ….....93
6.4.1 DSC analysis ….....….....93
6.4.2 Confocal Raman spectroscopy ….....….....95
6.4.3 X-ray powder diffraction ….....102

7.0 Raman spectroscopy: Backscattering versus transmission geometries ….....104

7.1 Transmission Raman spectroscopy as a tool for quantifying polymorphic content of pharmaceutical formulations ….....104
7.2 Introduction ….....104
7.3 Experimental ….....107
7.4 Results and discussion ….....109
7.4.1Backscattering geometry 109
7.4.2 Transmission geometry ….....….....110
7.4.3 Chemometric analyses ……....112
7.4.4 Model-free analysis ….....113
7.4.5 Data pre-treatment approach ….....115
7.4.6 Issues with the use of backscattering data ….....118

General Conclusion and plans for future work ….....121
References ….....122
Appendices ….....135

1 Introduction

1.1 Polymorphism

A large number of drugs are made from organic compounds which exists in different solid forms e.g. as crystalline or non-crystalline solids. A large number of these drugs are made available for use as oral dosage forms, the most popular being tablets and capsules.

The solid-state properties of a drug that is expected to be marketed as a solution may also be required to be known prior to formulation. In fact, the existence of any drug irrespective of the form by which it is finally administered is affected by the properties of the solid form, it is therefore important to find and select the solid form of any drug product with the optimal characteristic at the very early stages of drug development, in order to prevent unwanted 'surprises' in the later stages of development or after the drug has been approved for usage.

More so, pharmaceutical processes such as drying, grinding, compression and granulation can induce molecular changes in these materials, hence a good knowledge and understanding of the likely structural changes that a pharmaceutical material could likely undergo during the preparation of a new drug formulation is also very important. For example, anhydrous caffeine has been reported to change from its metastable form I to the stable form II by grinding.[1]

Polymorphs are materials with the same chemical (molecular) composition, but with different crystal structures, and therefore different physical properties, including melting point, colour, solubility, bioavailability etc.[2] Characterising polymorphs is an essential aspect of drug development in order to ensure safe and efficacious formulation and delivery, and is a regulatory requirement in getting a new medicine onto the market and thereby to patients.[2]

The type of formulations used during the various stages of drug development also determines the final properties of the drug product: for example when suspensions are used, particle size must be controlled as this can affect bioavailability. Also the solid-state properties of both the active ingredient and the excipient must be closely monitored for their chemical compatibility, which is why drugs that are expected to be poorly soluble are produced as salts while others are synthesised as hydrates for stability.

The relevance of polymorphism in the pharmaceutical industry cannot be over emphasised. This is partly due to the increased economic pressure faced by pharmaceutical companies, and the greater awareness of the effect that polymorphism may have on the bioavailability, manufacturability and stability of the drug product, as was recently evident by the recent withdrawal of neupro (a rotigotine patch used in the treatment of Parkinson's disease) from the market.[3]

The discovery of an unexpected levels of crystallisation on the surface of neupro patches resulted in a catastrophic experience for the manufacturer (UCB). Another example was when Abbott laboratories antiretroviral drug ritonavir was unceremoniously pulled from the shelves due to heterogeneous nucleation on a structurally related compound.[4]

Hence concerted efforts are made in the early stages of formulation of a drug product to isolate the polymorph with the optimal characteristics (most thermodynamically stable polymorph) under ambient conditions,[5] so as to prevent any unexpected transformation of the final drug product during or after manufacturing.

Since different polymorphs will possess different inter- and intra-molecular interactions, for example, hydrogen bonding sequences and Van der Waals forces, they will be expected to have different free energies and hence different physical properties such as solubility, chemical stability, melting point, density, etc.[6]

Solvates are obtained when solvent molecules are incorporated in the crystal lattice in a stoichiometric or non-stoichiometric way,[5] hydrates, where the solvents in this case is water, if non volatile molecules play the same role, the solids are called co-crystals.[6] While amorphous solids are defined as non-crystalline solids. They is a growing interest in studying non-crystalline solids, as studies have shown that the amorphous state can be an intermediate in some crystals prior to crystal transformations.[6] In this discussion the term 'polymorph' will only be used to refer to compounds that have similar chemical composition but different structural forms.

1.2 Relevance of solid state properties

Different solid forms have diverse physical and chemical properties that may significantly govern the performance of an active pharmaceutical ingredients and hence affect the integrity and efficacy of the final drug product.[6,7].
Examples of these properties are listed in Table 1 below;

Table 1. Physical properties that differ among various solid forms. Modified from[8]

Packing properties	Unit cell volume (crystalline forms only), density, refractive index, hygroscopicity, hydrogen bonding.
Thermodynamic properties	Melting point, enthalpy, entropy, free energy, solubility.
Spectroscopic properties	Bonding type, lattice environment, electronic transitions, colour.
Kinetic properties	Dissolution rate, rates of solid state reactions, stability.
Surface properties	Surface free energy, inter facial tensions, crystal habit, contact angles.
Mechanical properties	Hardness, tensile strength, compactibility, tableting flowability.

The difference in the mechanical properties between polymorphs can affect processing behaviour, which is the case with paracetamol polymorphs[9], where form II is suitable for direct tablet compression, but form I needs to be mixed with binding agents prior to compression.[10] Polymorphs I and II of sulfamerazine have also been reported to show different tableting properties,[11] as well as different forms of theophylline.[12] The performance of the drug in the human body can depend on the solid form, if solubility and dissolution rate are dependent on the solid state of the API. Well known examples have been found in cases involving anhydrous and dihydrate forms of carbamazepine, with the dihydrate having a higher absorption rate in vivo.[13,14] Also in ritonavir, where the metastable form I is more soluble, hence more bioavailable than the stable form II.[15]

The aim of this project, is to investigate the use of modern automated Raman spectroscopic methods (including data analysis approaches) for polymorphic screening and characterisation (with the Raman analysis complemented with other techniques such as X-ray Powder Diffraction (XRPD), Differential Scanning Calorimetry (DSC), solid state Nuclear Magnetic Resonance spectroscopy (NMR) and Scanning electron Microscopy (SEM)). This will involve in situ monitoring of pharmaceutical crystallisation using the constrained crystallisation approach (slow heating of the amorphous phase/form). Raman scattering is achieved when light is scattered inelastically, when a laser beam is used to irradiate a sample (in this case a pharmaceutical ingredient), the scattered radiation produced by the Raman effect contains valuable information about the energies of molecular vibrations and rotations, and these are directly related to the particular atoms or ions that the sample is comprised of, the chemical bonds connecting them, the symmetry of their molecular structure and the physico-chemical environment where they exist. In order words Raman spectroscopy can be employed to fingerprint different solid forms. Thus Raman spectroscopy is a unique technique for differentiating amongst the different polymorphs of the same compound as well as those of different compounds. Raman spectroscopy has the advantage of speed, no need for sample preparation and in this study we will focus on the low wave number region (4-400cm^{-1}) where inter-molecular vibrations are believed to take place. Here at the University of Nottingham, we have a modern state of the art Raman system (based in the university's nanocentre), a confocal Horiba-Jobin-Yvon LabRAM system (Horiba-Jobin-Yvon Ltd Middlesex U.K.), it has four different laser excitation capabilities i.e. UV (325nm), NIR (785nm), red (660nm) and the green laser (532nm).

It has a motorised stage that can move in the x, y and z directions and can be used to carry out fast and extensive mapping (using the SWIFT and DUOSCAN modes) and depth profiling of various samples including pharmaceuticals such as tablets.

It can be automated and can be fitted with a hot-stage and used to carry out variable temperature experiment. It is also equipped with two separate detectors, a CCD for regular Raman analysis and an EMCCD for fast mapping.

Overleaf (figure 1) is a picture of the Raman system at the Nottingham Nanotechnology and Nanoscience Centre.

A research group that also does in situ Raman spectroscopic analysis with data analysis approaches, is that based at the University of Otago, New Zealand, which comprises of Keith Gordon, Thomas Rades and Clare Strachan. They have done extensive research on the topic of polymorphic screening using Raman as well as NIR (Near infra Red) spectroscopy[16,17]. They have also done studies on crystallinity and the amorphous solid state (examples include their quantitative study of the polymorphic mixtures of ranitidine hydrochloride using Raman spectroscopy, NIR and XRPD and their study of the formation and stability of amorphous ranitide hydrochloride prepared by cryo-milling). But more recently their work has focused on the use of terahertz pulsed spectroscopy/imaging in studying pharmaceutical materials. It is worth mentioning though, that Raman spectroscopy tends to be used in a chemical engineering context rather than pharmaceutics.

As part of this study, we will also compare the conventional Raman spectroscopy with the new technique of transmission Raman spectroscopy (TRS, here Raman signal is collected on the side of the sample, in traditional Raman, signal is scattered from the surface of the sample) in quantifying polymorphic contents of a pharmaceutical formulation.

Figure 1: Picture of the Raman system at the Nottingham Nanotechnology and Nanoscience Centre

1 = laser source, 2 =sample stage, 3 = illumination source

1.3 Polymorphs/Solid state screening

A thorough knowledge of the physical/chemical properties of a compound offers varied options during the selection of the most suitable crystal form for future pharmaceutical development.[4] But more importantly, it prevents unexpected surprises during later stages of drug development, as mentioned earlier in the cases of neupro and ritonavir.
During solid state screening, different solid forms e.g. polymorphs, solvates and hydrates are identified and characterised as a knowledge of as many possible forms is needed. The optimal form is then chosen for further chemical and pharmaceutical development.[6] The thermodynamically stable form is then isolated which in the absence of solvents and humidity is not expected to transform into another polymorphic form.[6]

Aside from the the traditional thermodynamically stable form, hydrates are also very popular components of the final dosage form, as they are often the thermodynamically stable form at ambient conditions.[18]

1.4 Enantiotropism versus monotropism; Burger and Ramberger rules

Phase transitions in solids can either be thermodynamically reversible or irreversible: Polymorphic modifications which transform reversibly without passing the liquid or gaseous state, are termed enantiotropes. If the modifications are not interconvertable under the same conditions the system is monotropic.[17]

Lehmann, in 1888, coined the terms enantiotropism and monotropism to distinguish two different types of polymorphic behaviour.[6] Two types of graphs are commonly used to describe the thermodynamic behaviour of polymorphs, namely, energy-temperature diagrams and pressure-temperature diagrams.[6] In this study, emphasis will be placed only on the former (as the study will focus mainly on the temperature dependence nature of polymorphic transitions).

Energy-Temperature Diagrams

Energy-temperature diagrams were first introduced in crystallography by Burger et al in 1937.[6] These authors used schematic plots of internal energy (**U**) and Helmholtz free energy (**A**) versus temperature (**T**) to represent the phase transformations in crystalline solids. They argued that the enthalpy of crystalline solids under normal pressure conditions has negligible contribution from pressure-volume energy (**PV**).[6] Therefore, for crystalline solids at ambient pressure:

$H = U + PV \sim U$

$G = H - TS \sim U - TS = A$ (H=enthalpy, G=standard free energy, T=temperature and S=entropy)

To further understand the two concepts, let us consider a system with two polymorphs, I and II (with II being more stable at absolute zero temperature), for this system two different energy-temperature diagrams can be drawn to explain these concepts (enantiotropism and monotropism), the diagrams are as shown in figures 2a and 2b:[19]

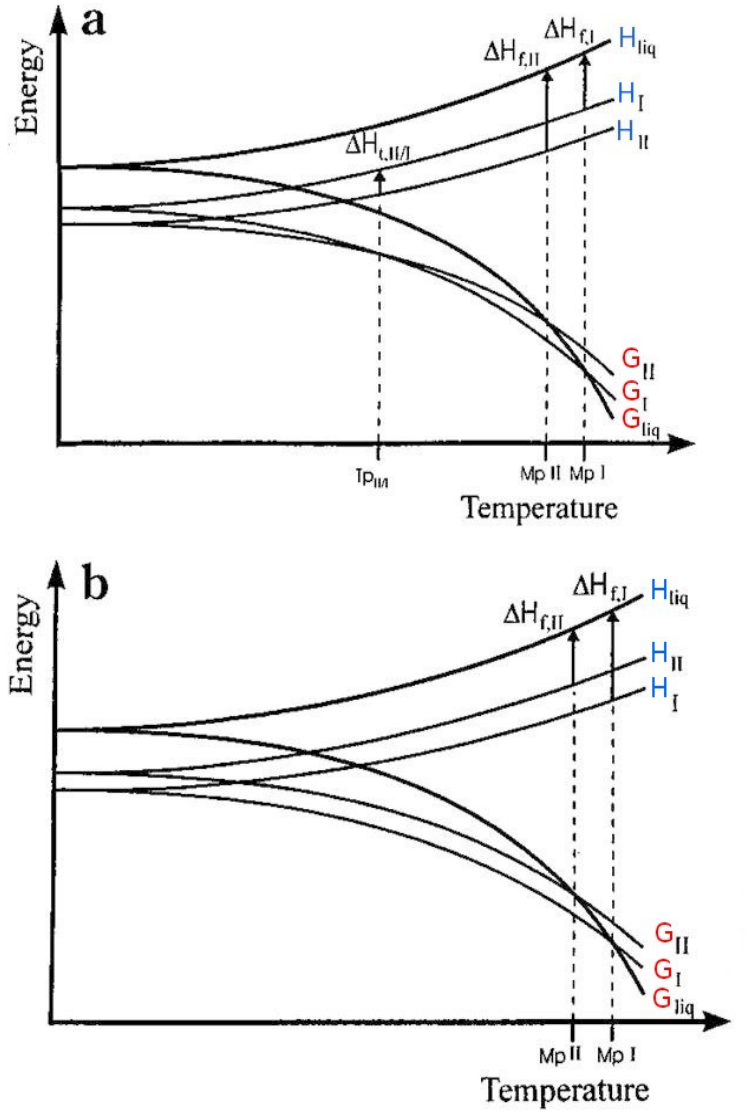

H= Enthalpy, G=free Energy, Mp=melting point, Tp=transition point

Figures 2a and 2b: Enantiotropism versus Monotropism

Figure 2a represents an enantiotropic system: the defining feature for such a system is the existence of a transition point (Tp) below the melting point of both polymorphs. In the figures 2a and 2b, the melting point of a polymorph can be defined as the temperature at which the free energy isobar of the polymorph intersects the free energy isobar of the liquid.

However, the thermodynamic transition temperature is defined as the temperature at which the free energy isobar of polymorph I intersects the free energy isobar of polymorph II, thus at Tp both polymorphs have equal free energy, i.e., G(I) = G(II) and consequently are in equilibrium with each other. Below Tp, polymorph II is the stable solid phase because the free energy of II is lower than that of I, i.e., G(II) < G(I). Consequently, below Tp, polymorph I can undergo spontaneous exothermic transformation into polymorph II. Above Tp, polymorph I is the stable solid phase because its free energy is lower than that of polymorph II, i.e., G(I) < G(II). Therefore, above Tp polymorph II can undergo spontaneous endothermic transformation into polymorph I.

Figure 2b represents a monotropic system. In general, in monotropic systems, solid-solid transformation occurs at a temperature that provides the system with sufficient thermal energy to cross the activation energy barrier, thus the transition point Tp in a monotropic system is a virtual transition point, because it lies above the melting point of both polymorphs. Hence by definition, a pair of polymorphs has a monotropic relationship if one of the polymorphs is always stable below the melting points of both polymorphs.[6]

As illustrated in figures 2a and 2b, if the free energy of polymorph I at all temperatures is below the melting point of both polymorphs, thus polymorph II can undergo a spontaneous transformation into polymorph I. For a monotropic system, this transformation is thermodynamically feasible at all temperature, because G(II) < G(I) at all temperatures.

More recently, Burger and Ramberger[20] developed rules (heat of transition and heat of fusion) which states that in the case of enantiotropism the transition of two polymorphic modifications is endothermic, whereas for monotropic forms it is exothermic.

Heat of transition rule: This rule states that if an endothermic phase transition is observed at a particular temperature (referred to as the experimental or kinetic transition temperature), the thermodynamic transition point lies below this temperature. Consequently, we can conclude that the two polymorphs are enantiotropically related.[6]

If an exothermic phase transition is observed at a particular temperature (experimental or kinetic transition temperature), there is no thermodynamic transition point below this temperature. This can occur either when the two polymorphs are monotropically related or when the two polymorphs are enantiotropically related and in addition have their thermodynamic transition temperature higher than the experimentally observed transition temperature.

Heat of fusion rule: This rule states that if the higher melting point polymorph has the lower heat of fusion then the two polymorphs are enantiotropic, otherwise they are monotropic.[6] Often, the rate of polymorphic transition is too slow to allow for an accurate measurement of the heat of transition, in which case the heat of fusion rule may be applied. This rule is based on the assumption that the heat of transition can be approximated by the difference between the heats of fusion of the polymorphs.[6]

1.5 Ostwald Rule

In 1897, a paper titled 'Studien ueber die Bildung und Umwandlung fester Koerper' (Studies of the formation and transformation of solid substances)[21] was published by Wilhelm Ostwald. The paper discussed the role of seeding of supercooled melts and supersaturated solutions, with particular emphasis on how small a quantity of seed crystal was needed to bring about crystallisation.
In conclusion, the author propounded what is now commonly known as Ostwald's rule or Ostwald's law of stages: 'When leaving a given state and in transforming to another state, the state which is sought out is not the thermodynamically stable one, but the state nearest in stability to the original state'.[22]
This implies that, in a crystallisation from the melt or from solution, the solid first formed will be that which is the least stable of the polymorphs, the one with the largest Gibbs free energy.[20]
This rule has been used extensively to explain why and how the process of crystallisation from the melt or from solution progresses, until very recently when the general applicability of the rule was queried by the discovery of a little known phenomenon, namely that it is possible to convert a stable polymorph to a less stable one by grinding.[23-26]

1.6 Characterisation of polymorphic systems

Various analytical techniques are available for the characterisation of the solid phase analysis of pharmaceutical materials, these includes thermal methods such as Differential Scanning Calorimetry (DSC) and themomicroscopy, vibrational techniques e.g. Infra red and Raman spectroscopy. Solid state Nuclear Magnetic Resonance (NMR) spectroscopy, X-ray diffraction (single crystal and powder) etc.

The method of choice would depend on factors such as: the nature of the material to be analysed, key parameters one needs to determine and the extent to which these parameters are to be investigated. Usually it is advisable to use two or more complementary methods to obtain a reliable knowledge of the forms.[27]

For the work described below five different analytical methods were employed: namely DSC (standard and temperature modulated), X-Ray Powder Diffraction (XRPD), Raman spectroscopy (traditional and transmission geometries), thermomicroscopy and solid state NMR.

1.6a Differential Scanning Calorimetry (DSC)

Differential scanning calorimetry is very useful technique for measuring heat effects (exothermic and endothermic events) associated with phase transitions and chemical reactions as a function of temperature.
In DSC the difference in heat flow to the sample and a reference at the same temperature, is recorded as a function of temperature. The reference is an inert material such as alumina, or an empty aluminium pan .
The temperature of both the sample and reference are increased at a constant rate. Since the DSC is at constant pressure, heat flow is equivalent to enthalpy changes (ΔH). DSC equipment are calibrated using the indium standard or more recently, sapphire prior to use. The advantages of DSC includes speed, minimal sample requirement and nowadays it is automated, but it is a destructive method of analysis.

Applications

DSC can be used to determine

1. Glass transition
2. Melting temperature
3. Heat of fusion
4. Percent crystallinity
5. Crystallization kinetics and phase transitions

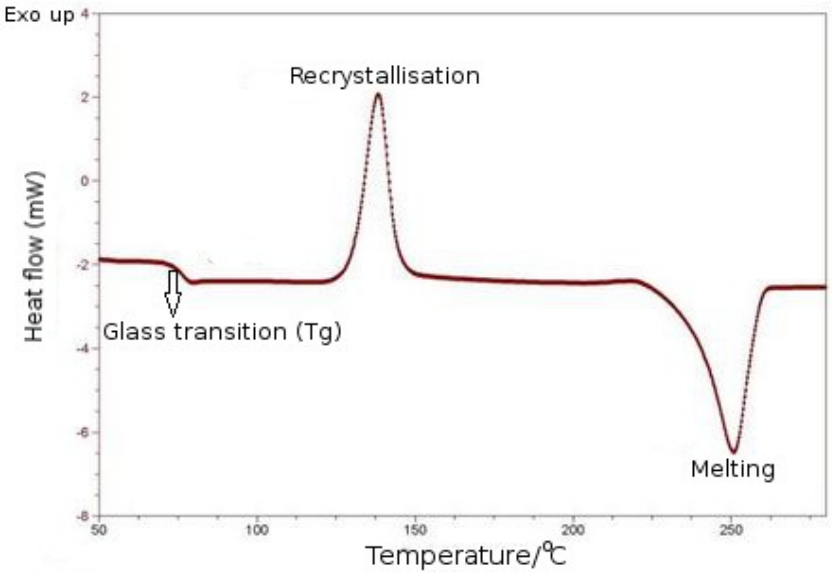

Figure 3: A typical DSC scan for an amorphous material

Types of DSC

Based on mechanism of operation DSC can be classified into two types.

1. Heat flux DSC
2. Power Compensated DSC

Heat Flux DSC

In heat flux DSC, both the sample and reference material are heated together in the same furnace, when the furnace is heated, the heat is transferred to both sample and reference pans via a thermoelectric disk. A temperature difference exists between sample and the reference owing to the heat capacity of the sample.

Power Compensated DSC

In power compensated DSC, the sample and reference pan are in separate furnaces heated by separate heaters. Both the sample and reference are maintained at the same temperature and the difference in thermal energy required to maintain them at the same temperature is measured and plotted as a function of temperature or time.

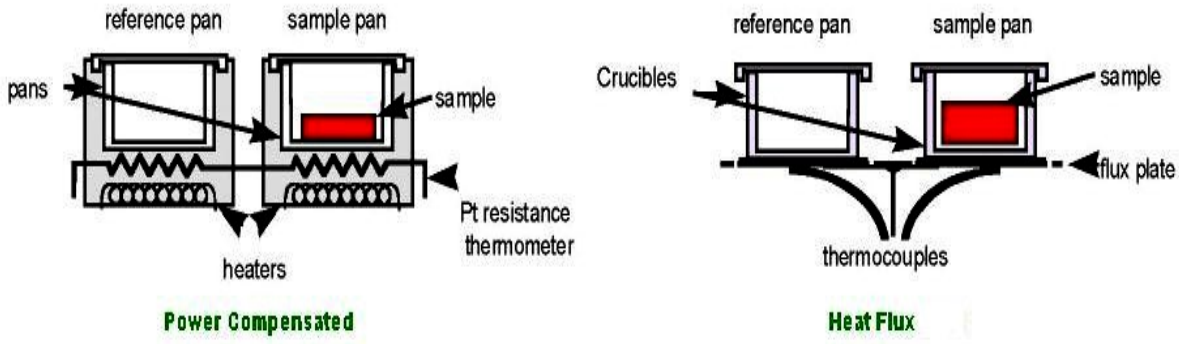

Figure 4: Schematic diagram of the two types of DSC[28]

1.6b X-Ray Powder Diffraction

X-ray powder diffraction is the 'gold standard' when it comes to the structural elucidation of different solid forms including APIs. XRPD patterns can be compared with calculated X-ray diffraction patterns obtained from crystallographic databases such as Cambridge Crystallographic Data Centre database (CCDC), from which useful information apart from unit cell dimension, such as point group symmetry and Bravais lattices can be obtained, leading to elucidation of crystal structures that where previously unknown. Below in table 2 is a list of the seven crystal systems and their corresponding Bravais lattices and symmetries, modified from.[29]

Table 2: The seven crystal systems and their corresponding Bravais lattices symmetries

			Non-centrosymmetric point groups		Centrosymmetric point groups
System	Bravais lattices	Characteristic symmetry	Enantiomorphous	Non-enantiomorphous	Non-enantiomorphous
Cubic	P I F	4 triads equally inclined at 109.47^{O}	23, 432	43m	m3, m3m
Tetragonal	P I	1 rotation tetrad or inversion tetrad	4^{P}, 422	4, $4mm^{P}$, 42m	4/m, 4/mmm
Ortho-rhombic	P I C R	3 diads equally inclined at 90^{O}	222	$mm2^{P}$	mmm
Trigonal	P R	1 rotation triad or inversion triad (= triad + centre of symmetry)	3^{P}	$3m^{P}$	3,3m
Hexagonal	P	1 rotation hexad or inversion hexad (= triad + perp. Mirror plane)	6^{P}, 622	6, $6mm^{P}$, 6m2	6/m, 6/mmm
Monoclinic	P C	1 rotation diad or inversion diad (= perp. mirror plane)	2^{P}	m^{P}	2/m
Triclinic	P	none	1P		I

Crystalline materials were discovered to interact with X-ray wavelengths in a three-dimensional format similar to the spacing of planes in a crystal lattice leading to the use of X-ray diffraction as a technique for the study of crystal structures and atomic spacing.[30]

When an X-ray beam hits a sample and is diffracted (Debye-Scherrer geometry), we can measure the distances between the planes of the atoms that constitute the sample when conditions satisfy Bragg's law (Bragg's law equates the angle (θ) between the incident and the scattered ray to (d) the spacing between the crystal planes and the wavelength (λ) of the radiation $n\lambda = 2d\sin(\theta)$.

The characteristic set of d-spacings generated in a typical X-ray scan provides a unique "fingerprint" of the material present in the sample. When properly interpreted, by comparison with standard reference patterns and measurements, this "fingerprint" allows for identification of the material.

While in the Bragg-Brentano method, the instrument uses a line focus x-ray tube, collimators and soller-slits are then used to define the divergence beam. On the diffracted beam side a (or graphite monochromator) in combination with a scintillation counter defined the energy window of the detected radiation.[30]

A receiving slit together with the step width of the diffractometer scans define the resolution of the patterns. The diffractometer uses a symmetrical beam and is operated in $\theta/2\theta$ mode for the sample and detector rotation.

XRPD can be used to analyse mixed samples e.g. a mixture of two different polymorphs, it is fast and non-destructive and can be adapted for in-situ structural determination.

But it disadvantages includes; most modern diffractometers are expensive and XRPD analysis require large amounts of sample.

1.6c Nuclear Magnetic Resonance Spectroscopy

Solid state NMR is now routinely used in pharmaceutical research for structural elucidation of compounds, investigating the chirality of drug substances, protein studies e.t.c.[31]
When a nucleus (of spin, **I**=1/2) is place in a magnetic field (figure 5 below). It spins on its axis. In the presence of a magnetic field, this axis of rotation will *precess* around the magnetic field; The nucleus can align with the magnetic field of strength $\mathbf{B_O}$ in only 2**I**+1 ways, either re-enforcing or opposing $\mathbf{B_O}$**.** The magnetogyric constant **g** relates the spin number **I** for a particular nucleus to the magnetic moment **m**; for a single nucleus with **I** = ½ and positive **g**, only one transition is possible between the two energy levels; NMR uses information about such transitions and interprets it in terms of chemical structure.[31]

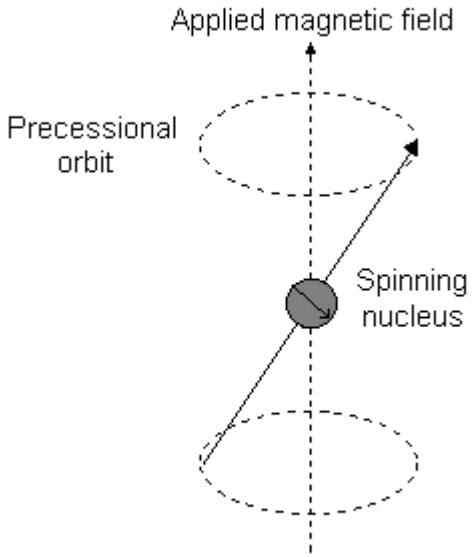

Figure 5: A nucleus precessing in a magnetic field

Cross polarization with magic angle spinning (CPMAS) is deployed when analysing pharmaceutical materials with solid state NMR, which entails spinning the sample (usually at a frequency of 1 to 70khz) at the unique magic angle θm (ca. 54.74^{O}, where $Cos^2\theta m = ⅓$) with respect to the magnetic field, this has the advantage of narrowing the usually broad lines, thus increasing the quality of resolution for better identification and analysis of the spectrum.[32,33]

NMR spectroscopy is highly selective and quantitative, it requires minimal sample preparation but it is very expensive method due to cost of instrumentation.

1.6d Raman Spectroscopy

a) Conventional/Traditional Geometry

When a sample is irradiated by a monochromatic radiation, the incident light is scattered inelastically in all directions: some are absorbed while some are reflected.

The incident photons promote the potential energy of a molecule to a higher energy virtual state, most then relax to the ground state with the emission of photons unchanged in frequency, but also, a small amount of radiation that is scattered at some different wavelength (Stokes and Anti-Stokes Raman scattering, approximately only 1 x 10^7 of the scattered light is Raman). It is the change in wavelength of the scattered photon which provides the chemical and structural information.

The uses of Raman spectroscopy includes detection of counterfeit and adulterated pharmaceutical products, mineralogy studies, biodiagnostic studies etc.[34] But in this study particular emphasis is on the phonon region (low wave number region of the the spectra), where absorption of radiation by the crystal lattice of samples is believed to occur.

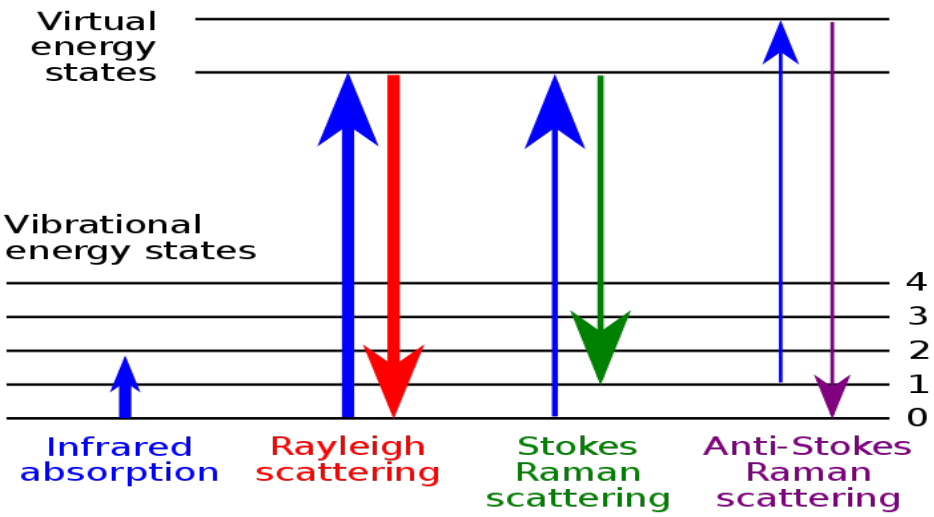

Figure 6: Schematic representation of the theory of Raman Spectroscopy

Raman spectroscopy is highly specific, fast and requiring no sample preparation. It can be carried out in solution, works with both liquids and solids, can be easily automated. It is expensive and because of the weak nature of Raman signal, its detection requires a sensitive and highly optimised instrumentation.

b) Transmission Geometry (Transmission Raman Spectroscopy, TRS)

Unlike conventional/traditional Raman spectroscopy, where the signal is collected back-scattered from the sample surface, a TRS signal is collected on the opposite side of the sample[35] (see figure 8[36]).
The additional advantages of the TRS approach over conventional Raman spectroscopy includes its ability to non- invasively probe the bulk content of turbid samples, including the elimination of sub-sampling problem and the effective suppression of surface fluorescence, which have not been recognised and exploited until recently.[37,38]
Other obvious advantages of TRS of traditional Raman spectroscopy includes: ability to provide bulk averaged information on the composition of dosage forms and its ability to penetrate coatings and capsule shells.

These new characteristics features in Raman analytical capability is particularly useful in areas such as non-invasive pharmaceutical concentration measurements and in vivo disease diagnosis.[39]

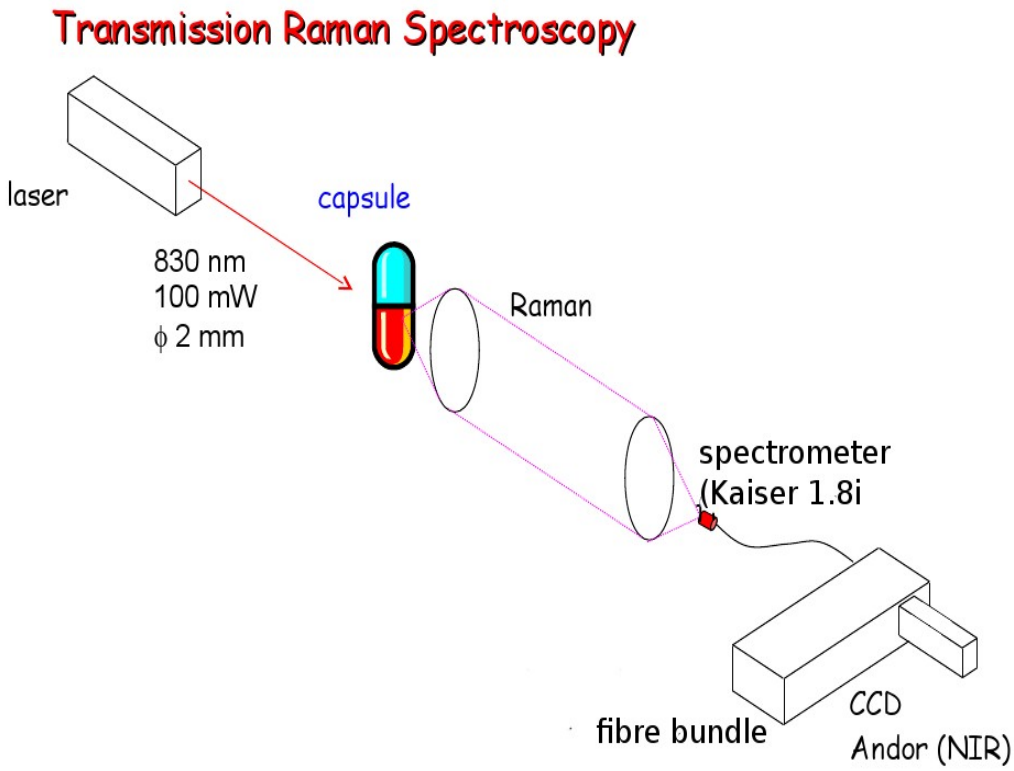

Figure 8: Schematic diagram of transmission Raman spectroscopy[36]

1.6e Thermomicroscopy

Thermomicroscopy (also known as hot stage microscopy and fusion microscopy) allows the direct observation of small samples as they are heated or cooled in a micro-furnace, or hot stage, that is placed on the specimen stage of a polarizing light microscope[6] (see figure 10).

It is the least commonly used technique for the characterisation of the solid-state properties of organic compounds, particularly the polymorphism of pharmaceutical compounds. Various authors have published books[40,41] and papers[42-47] on this unique technique.

Figure 9: Microscope heating stage (Linkam) mounted on the rotating stage of a polarizing light microscope in the Laboratory of Biophysics and Surface Analysis, School of pharmacy, University of Nottingham

Apart from complementing other thermal methods of analysis such as differential scanning calorimetry, differential thermal analysis and thermogravimetric analysis by providing a rapid and non-ambiguous method to interpret thermograms,[6] thermomicroscopy provides highly useful information about thermally induced events, such as melting, crystallisation, sublimation, desolvation and polymorphic transformations. Major drawback associated with thermomicroscopy include: image interpretation and limited chemical identification.

1.7 Data handling using principal component analysis

Principal component analysis (PCA) is a commonly used multivariate statistical technique for elucidating patterns in data of high dimension. One of its characteristic feature is the reduction of dimensionality in a given data set while keeping as much as possible of the variation originally present.[48-50]

PCA has been extensively deployed in this study because of the large volume of different data sets generated from the multiple techniques used in the probing of polymorphic behaviour in the pharmaceutical materials examined in this project.

The Raman spectra and x-ray patterns obtained were subjected to PCA analysis using 'PCA packages' within the 'R' programming suite. Raw data (variance-scaled and mean-centred before analysis) were used.

Analysis of the scores and loading for the most important principal components (PCs), as determined from percent variance plots, were used to investigate changes in the spectral features of the Raman data, as well as variations in the x-ray patterns.

This statistical approach proved to be very useful in this study as it helped to reduce data complexity and also served as a veritable tool in elucidating the different polymorphic transitions taking place in the systems that were studied.

1.8 General Introduction

Interest in polymorphism and the solid state properties of drug molecules have increased significantly in recent times, particularly in the pharmaceutical industry; apart from being a regulatory requirement for drug manufacturer's to perform polymorphic screening during the early-stage of drug development, a good knowledge of the physico-chemical properties of the various polymorphs of a drug would guarantee product quality and effectiveness.

As a result polymorphs and all other solid forms including amorphous forms, solvate and hydrates have come under intense scrutiny by regulatory bodies and agencies, and with the renewed relevance of polymorphism, polymorph screening has been moved to a much earlier stage in the drug development process.[51]

There are several techniques used for inducing polymorphic transformations e.g. Seeding,[52] addition of soluble additives,[53-57] templating,[58] solvent control,[59] mechanical grinding,[60,61] using supercritical fluids,[62-65] laser induced nucleation,[66,67] high-throughput screening[68-74] e.t.c.

While methods of polymorphic analysis includes X-ray diffraction (single and powder), DSC, Raman and Infra-Red (IR) spectroscopy, thermal microscopy/gravimetry e.t.c., of all these methods, single-crystal X-ray diffraction is the most definitive, albeit it has the disadvantage of the need to find the 'perfect' single crystal which in most cases is very difficult to obtain.

The best approach that is normally used in monitoring and analysing polymorphic transition is to use two or more complementing methods with each method offering similar perspective of the entire process.

Current state of the art polymorph screening methods can employ as little as 100 mg of sample (and a time-scale of days/weeks) for a thorough solution-state screen.[75] Reducing sample size and experimental time requirements has the potential to enable very early-stage screening of the solid-state properties of new drug molecules, and lead to a more efficient drug development pipeline.

Traditional hot-stage optical microscopy methods for investigating polymorphism can use microscopic (sub-milligram) amounts of sample,[76] but do not provide quantitative data for characterisation, patent applications, etc.

Methods to probe crystal structure or local molecular environment (as opposed to internal molecular structure) are necessary to characterise polymorphs, including X-ray single crystal diffraction, X-ray powder diffraction, thermal methods, and, more recently, THz spectroscopy.[77]

THz spectroscopy relies on detectors which are sensitive to very low wavelength infra-red radiation, including bands arising from inter- (rather than intra-) molecular vibrational (phonon) modes. The technology for detectors with appropriate low wave number sensitivity has only recently been developed.

In principle, Raman spectroscopy can offer similar phonon-mode information. Because Raman spectra are measured as a shift with respect to an incident radiation (rather than directly measuring the emitted radiation as per THz spectroscopy) conventional CCD detectors can be used, which significantly simplifies the experimental set-up.

To date, a very limited number of studies in any application area have been reported using phonon-mode Raman spectroscopy, and of these we are aware of only one report of the application of this technique to polymorphism in pharmaceuticals.[78]

We report here some early results which indicate phonon-mode Raman spectroscopy/microscopy can be a very powerful tool in investigating and characterising polymorphism in pharmaceuticals, while requiring very little sample (mg or less).

Spectra can be recorded in a matter of seconds or less on a typical modern Raman microscope/spectrometer, including bands due to both inter- (10–400 cm^{-1}) and intra-molecular vibrations (400–4000 cm^{-1}). A wealth of useful chemical information can therefore be readily accessed. The intermolecular phonon-mode vibrations are typically several times more intense than the conventional intramolecular vibrations.

For an amorphous material the intermolecular vibrations are not quantised, and thus at low wave number a broad distribution of vibrational energies ensues, whereas for a crystalline material quantisation of phonon-modes leads to a series of sharp peaks, the positions of which depend strongly on the crystal structure. Different solid forms (polymorphs, amorphous, and salts) can therefore be readily distinguished.

2.0 Polymorphism in Flufenamic Acid

2.1 Analysis and mechanistic study of a solid-solid transformation

Abstract

A solid-solid transformation between two polymorphs of Flufenamic Acid (FFA), namely forms I and III was monitored and analysed as part of a study into the rich polymorphic system of FFA. Initial results showed that FFA form III transforms to form I upon heating,with no region of co-existence of the two forms during the transformation.

The said transition was monitored using DSC (differential scanning calorimetry) and in situ confocal Raman microscopy/spectroscopy complemented with variable temperature X-Ray Powder Diffraction, while solid state NMR spectroscopy was used to distinguish between the two forms: DSC analysis showed that the transition occurred around 104°C, while results obtained from the Raman in situ experiment and VTXRPD indicated that the transformation was obtained at 114°C and 117°C respectively, the vibrationally driven nature of the transition was suggestive of a mechanism similar to the 'Lindemann melting theory'.

2.2 Review of relevant literature

Flufenamic acid (FFA), a potent non-steroidal anti-inflammatory drug (NSAID) with analgesic properties is used in the treatment of rheumatoid arthritis and osteoarthritis[36,51]. FFA, systematic (IUPAC) name, 2-[[3-(Trifluoromethyl)Phenyl] Amino] Benzoic acid belongs to a family of analgesics which also includes Mefamic and Niflumic acids, known as the fenamates.[11]

It is a crystalline powder, with its colour ranging from white to yellow, it has a molecular weight of 281.22991g/mol and a molecular formular, $C_{14}H_{10}F_3NO_2$.

Krc,[80] in 1976 had suggested the possibility of FFA having up to seven or more different polymorphs. In the paper the melting points of FFA forms I and III was estimated to be 134°C and 126.5°C respectively. Form I was reported to be the stable form above 42°C (transition temperature between forms I and III), while form III is the stable form below 42°C. Forms I and III are enantiotropically related to each other.[81]

Various other authors have published on the topic of polymorphism in flufenamic acid,[82-84] thermodynamic properties of flufenamic acid and the fenamates,[85,86] crystal structures and spectrocopic properties of flufenamic acid,[87-94] as well as the use of Raman spectroscopy/microscopy in characterizing the organic solid state and polymorphs.[95-120]

Of particular importance to this study is the reported transition temperature between the two forms of flufenamic acid, namely I and III, which was estimated to be 42°C by Krc[80] and 39°C by Yuerong et al.[90]. While these values where obtained using either solution mediated polymorphic conversions[80] or in-situ Raman spectroscopy (variable temperature) of a slurry of FFA,[90] the present study aims to estimate a transition temperature between these two polymorphs in the solid state and in the absence of solvents. Also the study will compare newly available phonon-mode Raman analysis (which has not being previously reported prior to this study) with other methods for characterising model polymorphic system i.e. Flufenamic acid, and see how many forms of FFA can be isolated.

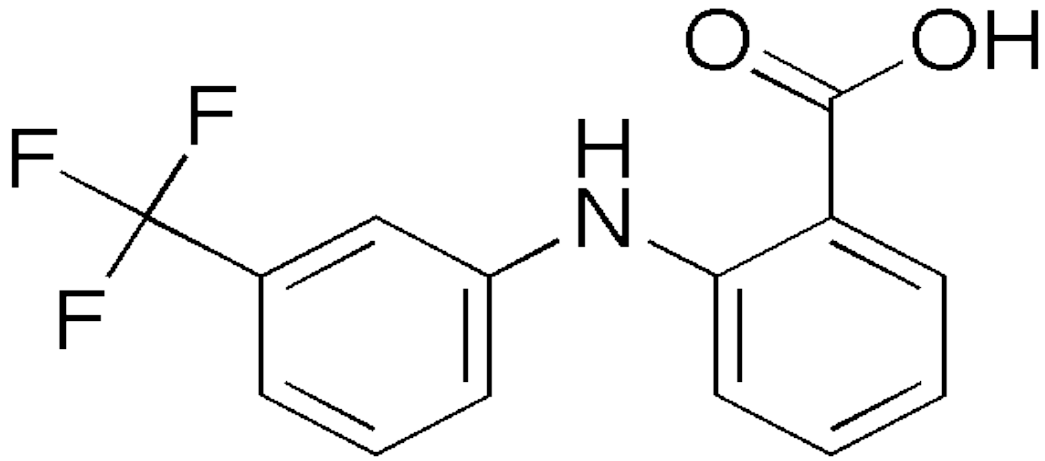

Figure 2.1: Molecular structure of Flufenamic acid

2.3 Experimental

2.3.1 Materials

Flufenamic acid was purchased from Sigma-Aldrich Dorset UK. The as-received sample was shown by comparison of its XRPD pattern with the reported crystal structure by Krishna Murthy et al.[87] to be form I. Pure form III was prepared by simple evaporative crystallisation from propanol and identified by comparison of the XRPD pattern with the reported crystal structure by McConnell.[91]

2.3.2 DSC Analysis

DSC analysis was carried out using a a DSC 2920 Differential Scanning Calorimeter (manufactured by TA Instruments LTD. Leatherhead UK) after previously calibrating the calorimeter using the indium standard.

Approximately 4mg of the sample was accurately weighed into hermetically sealed pans, and heated at various heating rates (i.e. 1, 2, 5, 10, 20, 25, 50°C) and similar cooling rates using both the standard and temperature modulated modes of the instrument. FFA form III was also subjected to the same analysis as form I.

The as received sample was also cooled isothermally for fifteen minutes over a temperature range of between -15 to -40°C and DSC (standard) experiments were carried out on all the cooled samples.

2.3.3 Ball milling experiments

100mg of both forms I and III weighed and ball-milled (dry) using the Retsch MM 400 Mill, at 30Hz over various times ranging from 30 minutes to 3 hours. The new samples resulting from the milling were also analysed by DSC (standard and temperature modulated).

2.3.4 Solubility and solvent drop milling experiments

Subsequently a basic solubility assay was carried out on both forms using solvents such as acetone, chloroform, methanol, methylated spirit, propanol, toluene, water and xylene in order to ascertain the insolubility of FFA in water and the solubility of FFA in a range of solvents.

All solvents used in the study were purchased from Fisher Scientific (UK) Limited, Bishop Meadow Road, Loughborough. Chloroform, methanol, and methylated spirit were procured as HPLC grade while ethanol, toluene, xylene and propanol were supplied as analytical grade.

Slow evaporation experiments were also carried out on both forms: saturated solutions of the samples were prepared using the solvents above and left to slowly evaporate in a watch glass under ambient conditions.

After the solubility experiments, 100mg of both FFA forms I and III were weighed and milled (using the Retsch MM 400 Mill) with two drops, approximately 2ml (from a pipette) of each solvent mentioned above and all the resulting samples from the milling experiment was analysed using DSC (standard and temperature modulated) and XRPD.

2.3.5 XRPD

In order to characterise the two forms i.e. FFA I and III, XRPD patterns were collected on a Bruker D8 diffractometer system (Bruker AXS, Madison, WI, USA), operating in a Debye-Scherrer geometry, at a wavelength (λ) of 1.54059Å, 40kV voltage, and a current of 40mA, using a LynxEye detector, samples were contained in 0.7mm borosilicate capillary tubes (Capillary tubes Ltd. UK). For the variable temperature experiment involving the heating of FFA III, a small amount of the sample was melted on a glass slide mounted on a linkam hotstage ((Linkam Scientific Instrument Ltd, Surrey U.K), the resulting molten liquid was drawn into a 0.3mm borosilicate capillary tube. The sample was heated using a Cryostream plus controller (Oxford Cryostreams Ltd. Hanborough Oxford OX29 8LN) at 3°C/minute from -10°C to 141°C and patterns were collected at each temperature step (overall accumulation time of 8 minutes) at a scan time of 0.3 second.

2.3.6 Solid-state NMR

Solid state NMR analysis of the FFA samples was carried out using the Varian Infinity Plus Spectrophotometer (at 300MHz using 7.04 Tesla magnet), manufactured by Chemagnetics, 2555 Midpoint Drive Fort Collins CO. 80525 USA., both samples were homogenised with a mortar and pestle to increase signal to noise ratio on the spectral, the samples were then filled into a rotor and spectra taken after prior calibration to a pw90H value of 2.5μs.

2.3.7 Raman spectroscopy/microscopy

Raman spectra were collected using a confocal Horiba-Jobin-Yvon LabRAM system, using a 600 lines/mm grating and a 785 nm excitation laser. A Synapse CCD detector was employed. Temperature control was achieved using a Linkam hot-stage (Linkam Scientific Instrument Ltd, Surrey U.K). Samples were heated at stepwise 1°C min^{-1} intervals, and were held at temperature during data collection (typically 10–20 s maximum). Data sets were collected every 1°C. Samples (approximately 1 mg) were contained between a glass microscope slide and cover slip.

2.4 Results and Discussion

2.4.1 X-Ray Powder Diffraction

As previously mentioned, the XRPD pattern of the as received sample of FFA showed that it is Form I[121], while the samples obtained from slow evaporation (propanol, xylene and toluene only) and solvent drop techniques (except using water) was found to be Form III[122] of FFA after calculations using mercury and comparison with single X-ray diffraction patterns downloaded from the Cambridge Structural Database (CSD), as previously obtained in literature. The XRPD patterns are shown in figure 2.2:

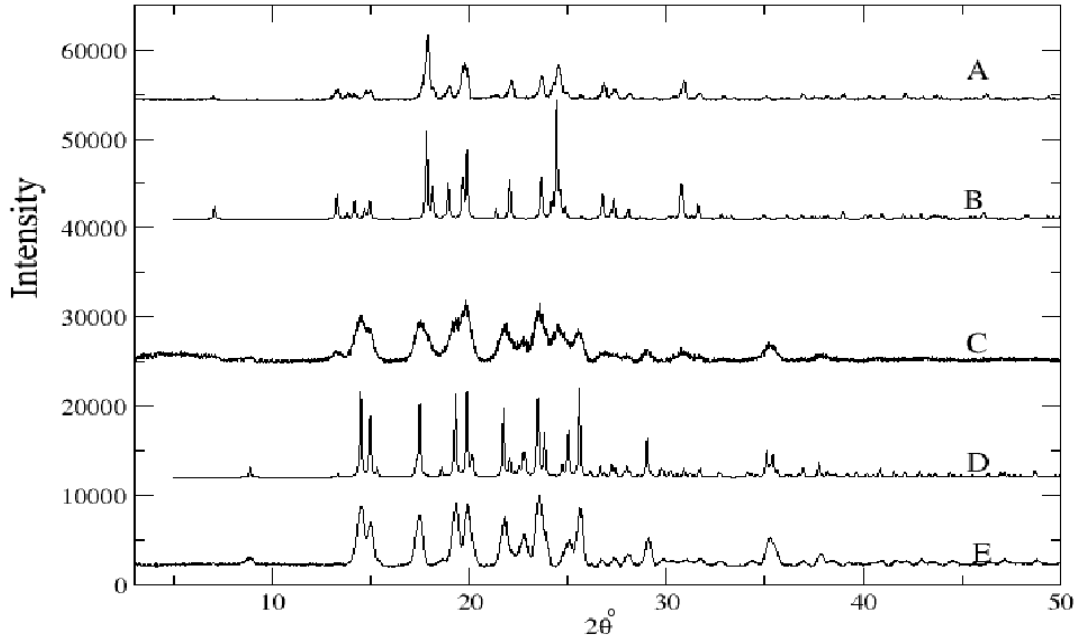

Figure 2.2: XRPD patterns of FFA

A = XRPD pattern for as received, B = Simulated FFA I, C = XRPD pattern of FFA I dry milled with FFA III, D = Simulated FFA III, E = Representative XRPD pattern for samples obtained from solvent evaporation and solvent drop milling experiments

Figure 2.3 shows a series of XRPD traces collected from samples of FFA I milled for different amounts of time, extra peaks are seen to appear after 30 minutes of milling (see left hand side of 2.3). After 40 minutes the two forms (I and III) co-exists. And after an hour of milling the pure form I is obtained after comparison with previously published data.[58] Worth noting from figure 2.3 below is the XRPD trace obtained after 50 minutes of milling which shows a pattern for pure FFA form III, this we believe is due to experimental set up (for the longer milling times i.e. 50-60mins, it becomes more difficult to remove the milled samples from the jar because the samples stick to the side of the jar, a spatula is used to scrape the samples out, this we believe could affect the molecular orientation of the samples). FFA form I does not transform into any other form upon dry milling irrespective of time of milling.

Figure 2.3 below shows the various patterns obtained as the milling experiment progressed:

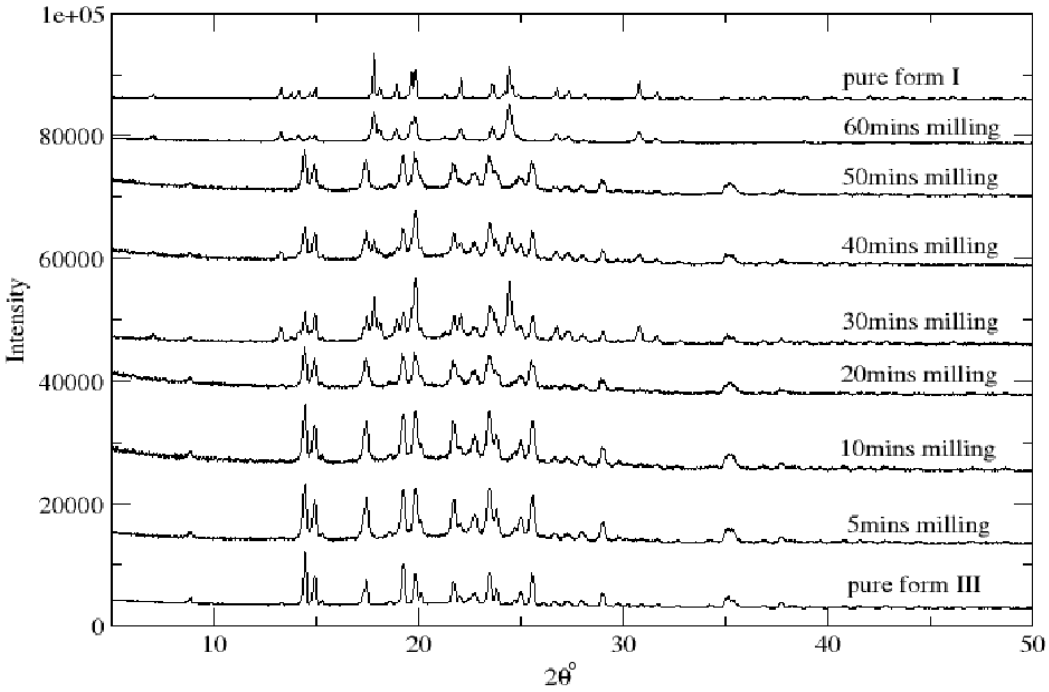

Figure 2.3: Patterns obtained from the dry milling experiment with FFA III

Figures 2.4a and 2.4b shows both the phonon-mode and molecular-mode Raman spectra of both forms of FFA, the phonon region can be easily used to distinguish between forms I and III and thus will be used to monitor how milling affects the system. The molecular-mode spectra are similar, expected as both samples contain FFA molecules.

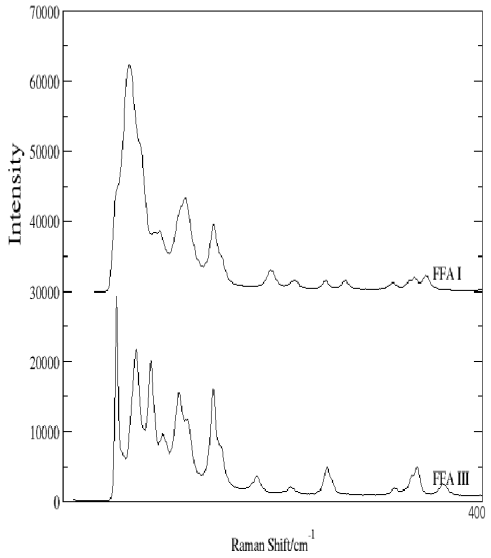

Figure 2.4a Raman spectra of the phonon-mode of both forms I and III

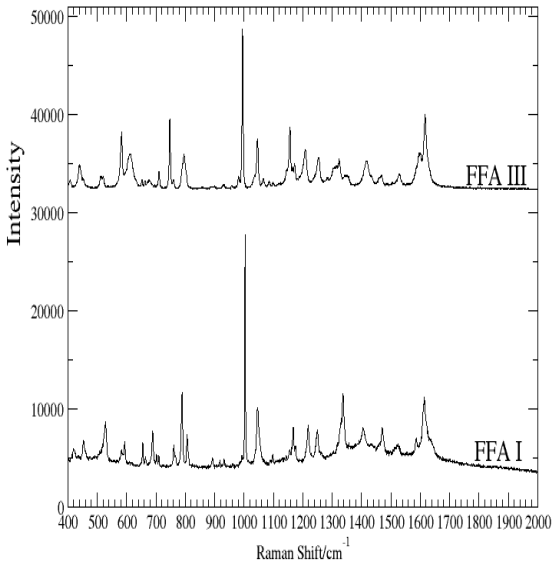

Figure 2.4b Raman spectra of the molecular-mode of both forms I and III

Figure 2.5 shows the transformation of FFA form III to I (induced by dry milling) monitored using Raman spectroscopy, thereby complementing the earlier results obtained with XRPD:

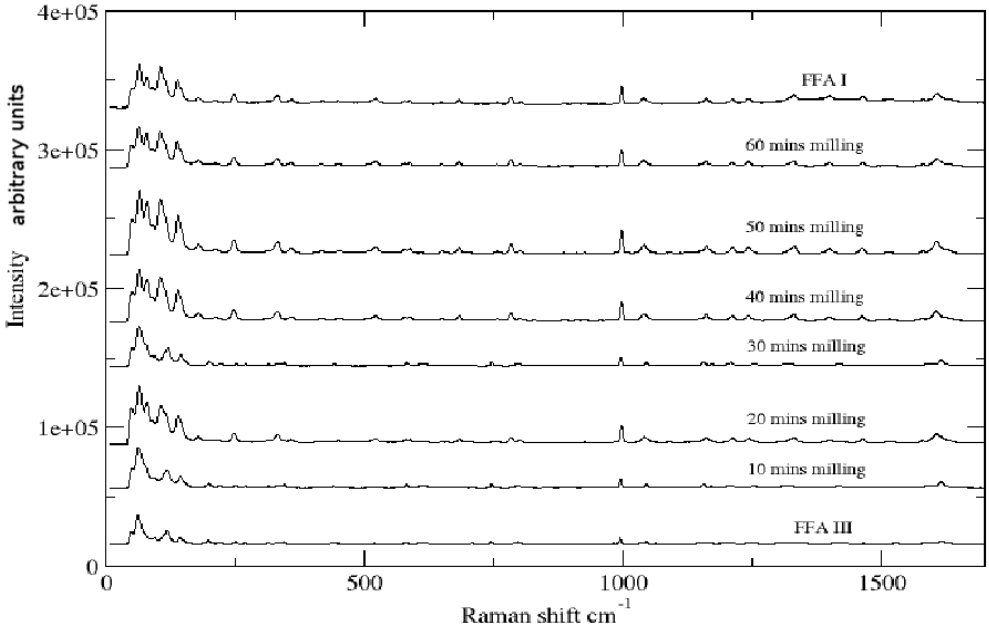

Figure 2.5: Raman spectra showing FFA III→I transformation upon dry milling

Using the phonon-mode region only, both forms I and III are easily differentiated (form I has four prominent peaks while form III has two), as the milling progresses in figure 2.5 above, after 20 minutes of milling both forms co-exists, typified by the appearance of additional peaks. These peaks continue to increase in intensity until the transformation is completed after 60 minutes of milling.

Similarly, figure 2.6 below shows the solid-solid transformation of FFA III → I (heating) monitored using variable temperature XRPD:

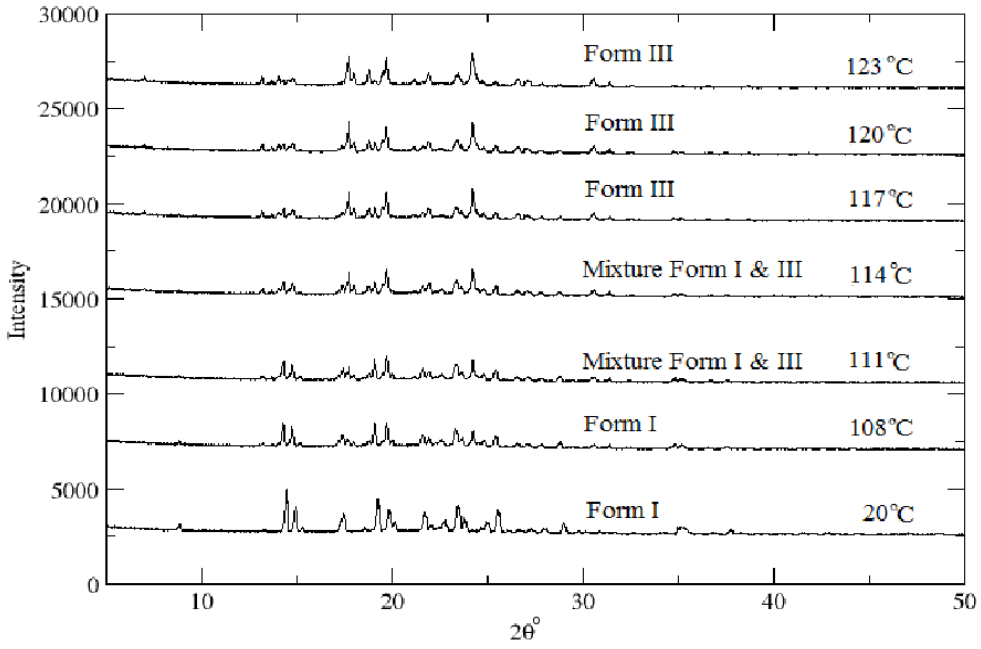

Figure 2.6: XRPD patterns of the solid-solid transformation between FFA forms I and III

As shown above the solid-solid FFA form III to I transition takes place between 110-120°C rather than at 42°C when the transformation is solvent mediated.

XRPD traces for the product of co-milling form I with a variety of solvents are given in figure 2.7a. From visual inspection of the data it is immediately apparent that form I transforms into form III in all cases expect when milled with water.

While form III remains unchanged irrespective of the solvent used as shown in figure 2.7b.

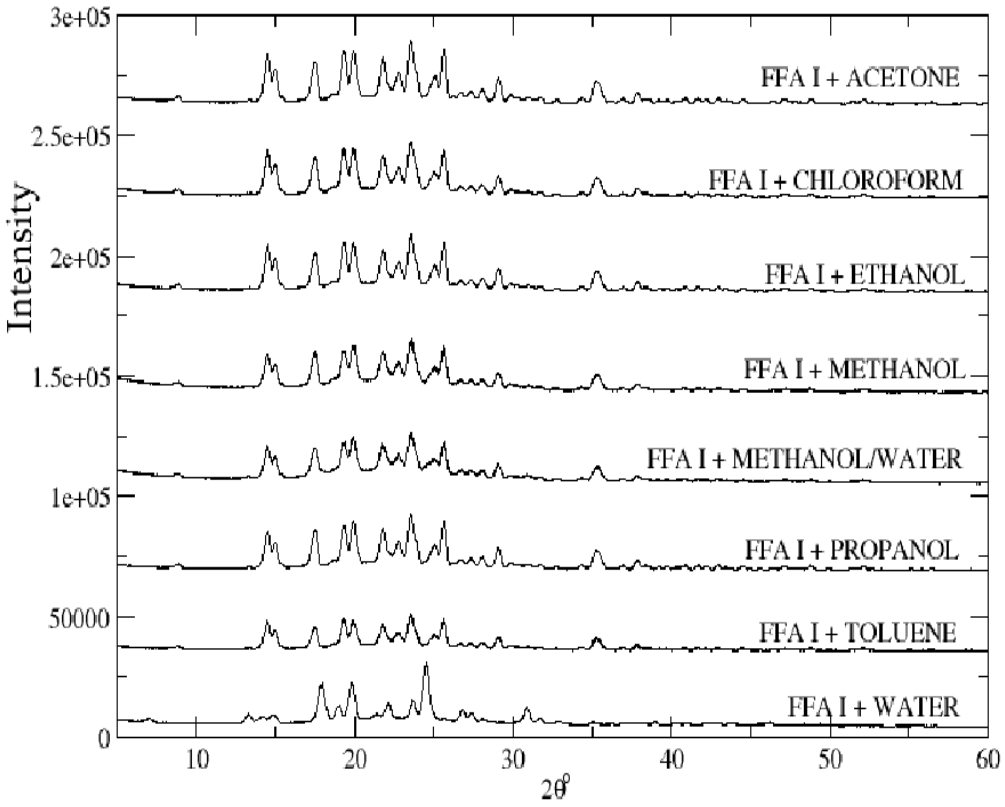

Figure 2.7a: XRPD patterns of FFA I after solvent drop milling

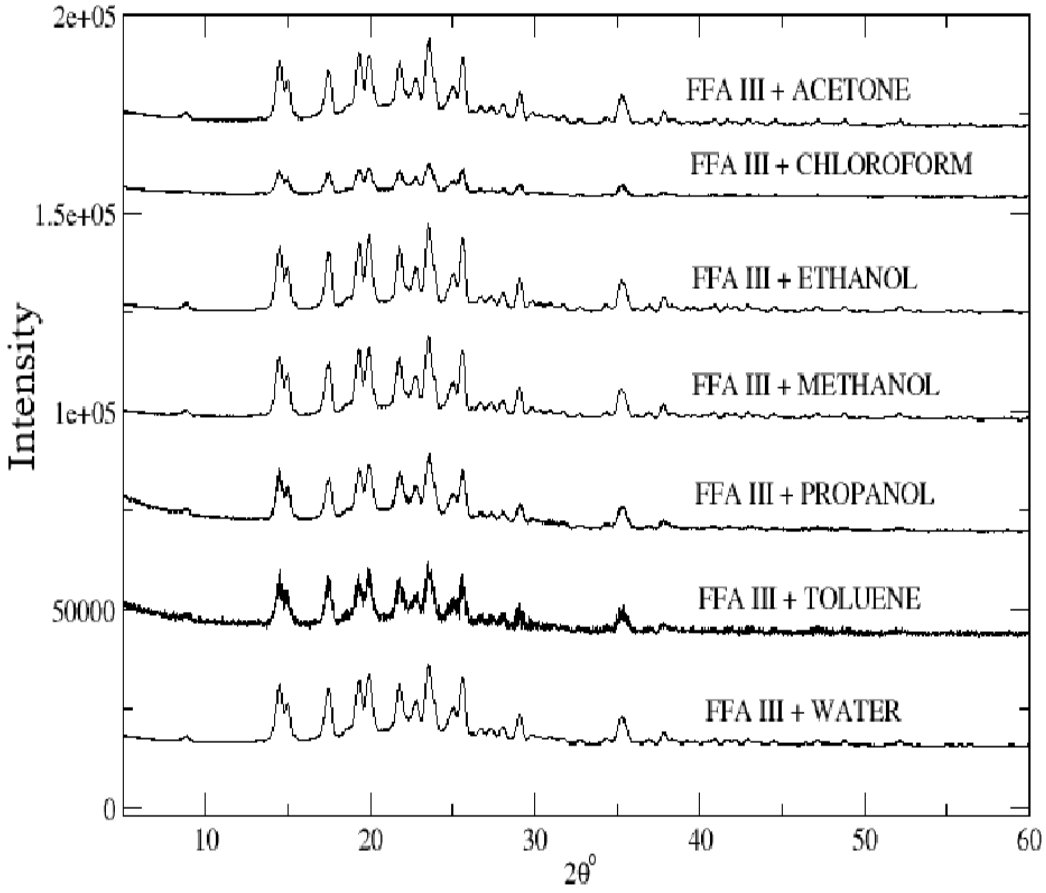

Figure 2.7b: XRPD patterns of FFA III after solvent drop milling

The above results as shown in figures 2.6, 2.7a and 2.7b respectively, clearly show that XRPD is a very effective method for distinguishing between the two forms. Also, at first glance the theory that transformations during milling are due to heat build-up seems to tie in with the results, but the effect of solvent is clearly important as well. So it is not a surprise that no transformation was observed when both forms of FFA were milled with water as they are both insoluble in water, whereas when form I is milled with all the other solvents used in the study, a transition is obtained as both forms are soluble in all the solvent used. Thus a dissolution/recrystallisation mechanism seems appropriate for the solvent-drop milling.

2.4.2 Solubility assays

Table 3 below shows the results of the basic solubility assay carried out on the as received sample.

Table 3: Solubility table for flufenamic acid as received

Solvent	Soluble
Acetone	Yes
Chloroform	Yes
Methanol	Yes
Methylated Spirit	Yes
Propanol	Yes
Toluene	Yes
Xylene	Yes
Water	No

2.4.3 Solvent milling experiment

From the solvent milling experiments, the table below was arrived at to depict the polymorphic transformations.

Table 4: Result of solvent drop milling experiments of FFA forms I and III

Form before solvent milling	Solvent used in milling	Form obtained after solvent milling
FFA I	Methanol	FFA III
FFA I	Acetone	FFA III
FFA I	Ethanol	FFA III
FFA I	Propanol	FFA III
FFA I	Toluene	FFA III
FFA I	Chloroform	FFA III
FFA I	Methanol and Water	FFA III
FFA I	Methylated Spirit	FFA III
FFA I	Water	FFA I
FFA I	None	FFA I
FFA III	None	FFA III
FFA III	Methanol	FFA III
FFA III	Acetone	FFA III
FFA III	Ethanol	FFA III
FFA III	Propanol	FFA III
FFA III	Toluene	FFA III
FFA III	Chloroform	FFA III
FFA III	Methanol and Water	FFA III
FFA III	Methylated Spirit	FFA III
FFA III	Water	FFA III

PS: Neat grinding (solvent free) of both forms I and III together yielded equimolar (approximately) amounts of both forms, this was confirmed by XRPD.

2.4.4 Molecular modelling

In order to see if a simple theoretical mechanism can explain the interconversion between the conformations I and III of FFA, molecular modelling was deployed (Monte Carlo simulation).[123,124] It must be noted however that this technique has some limitations: Solid phase packing and inter-molecular hydrogen bonding are not allowed for.

Figure 2.8a: Molecular structure of FFA

Grey atoms = Carbon

Blue atoms = Nitrogen

Red atoms = Oxygen

Green atoms = Fluorine

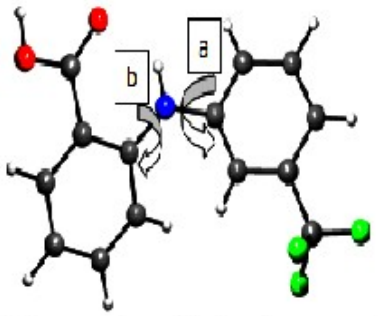

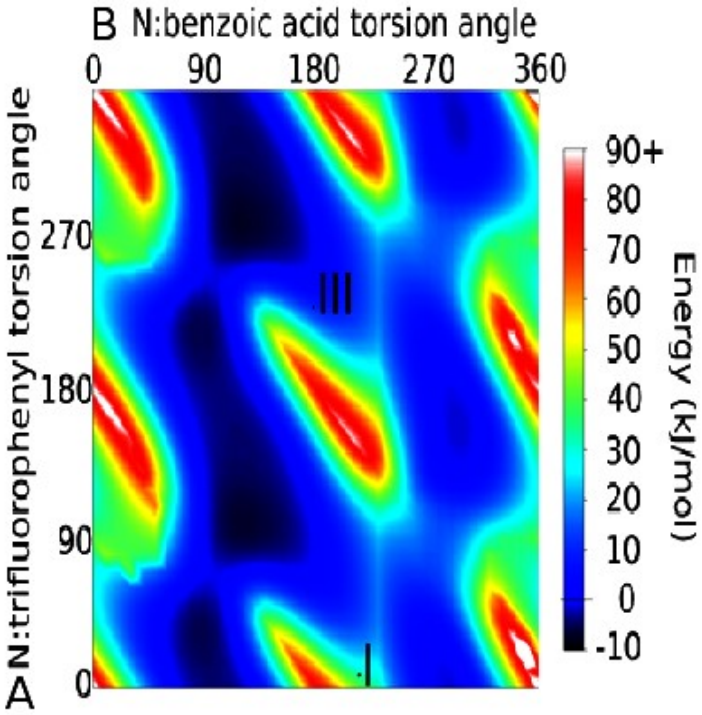

Figure 2.8b: Energy of gas-phase FFA molecule as a function of the two nitrogen-centred torsion angles

The molecular structure and the calculated gas-phase energies of the FFA molecule are presented in figure 2.8a and 2.8b respectively and compared with the molecular conformations in the polymorphs I and III. The molecule exhibits nearly free rotation about the N:m-trifluoromethylbenzene bond (direction indicated by arrow a). Rotation about the N:o-benzoic acid bond is sterically hindered (direction indicated by arrow b). In neither polymorph do the molecules adopt a gas-phase energy minimum conformation. From these calculations (which assume an isolated molecule in the gas phase), the molecular conformation of form III is of lower enthalpy than that of form I.

It should be noted that in the solid state effects like lattice energy and non-bonded interactions are likely to have a very significant effect on the relative energies of the two forms.

2.4.5 Solid-state NMR

In order to further distinguish between the two forms of FFA, solid-state NMR was employed, and despite the obvious advantages of this technique (e.g. over other methods such as XRPD and Raman) which include: its non-invasiveness, minimal sample requirement/preparation, it is also highly quantitative and selective, it also has its own draw-backs: it is very expensive, it often requires a lot of expertise in the technique to run it properly, automation is difficult and experimental parameters need to be pre-determined for every experiment.
Although the assignment of the various peak positions are non-trivial, the NMR spectral in figure 2.9 below also showed that the two forms are different.

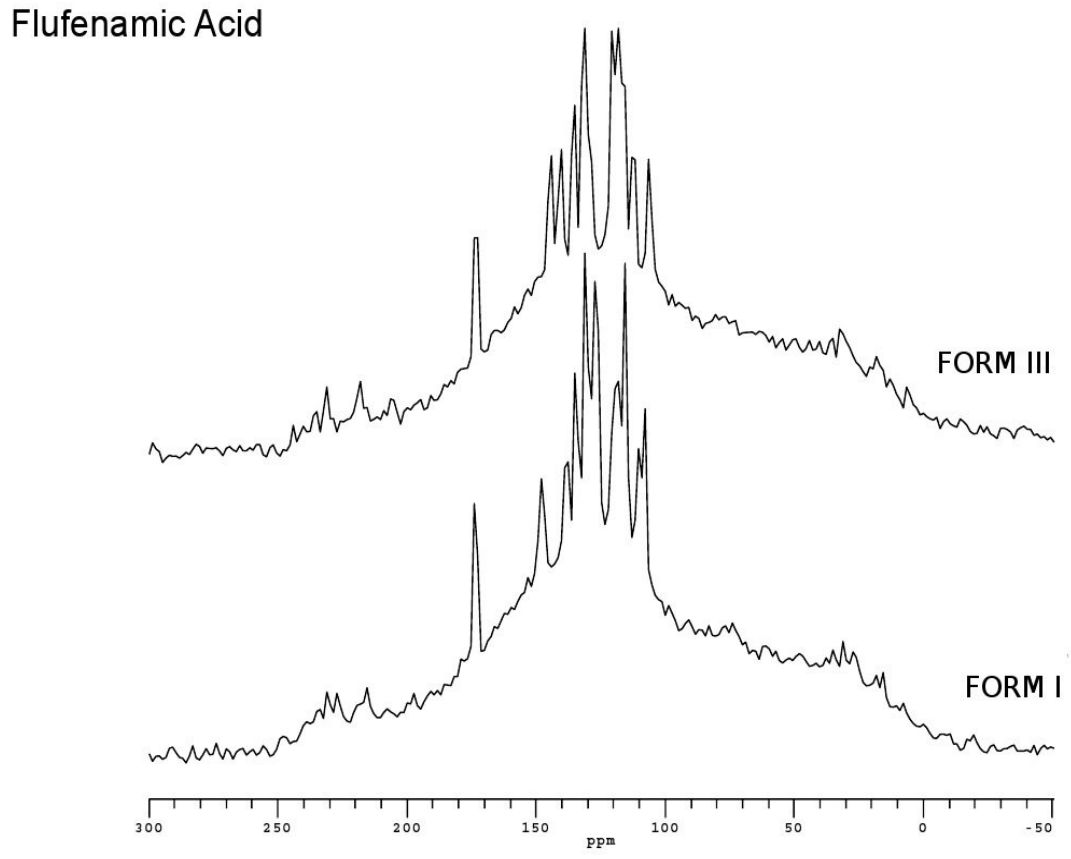

Figure 2.9: Solid-state NMR spectral of FFA I and III

2.4.6 Differential Scanning Calorimetry (DSC)

Representative DSC data for FFA forms I and III (10˚C heating rate) are presented in figure 2.10 below:

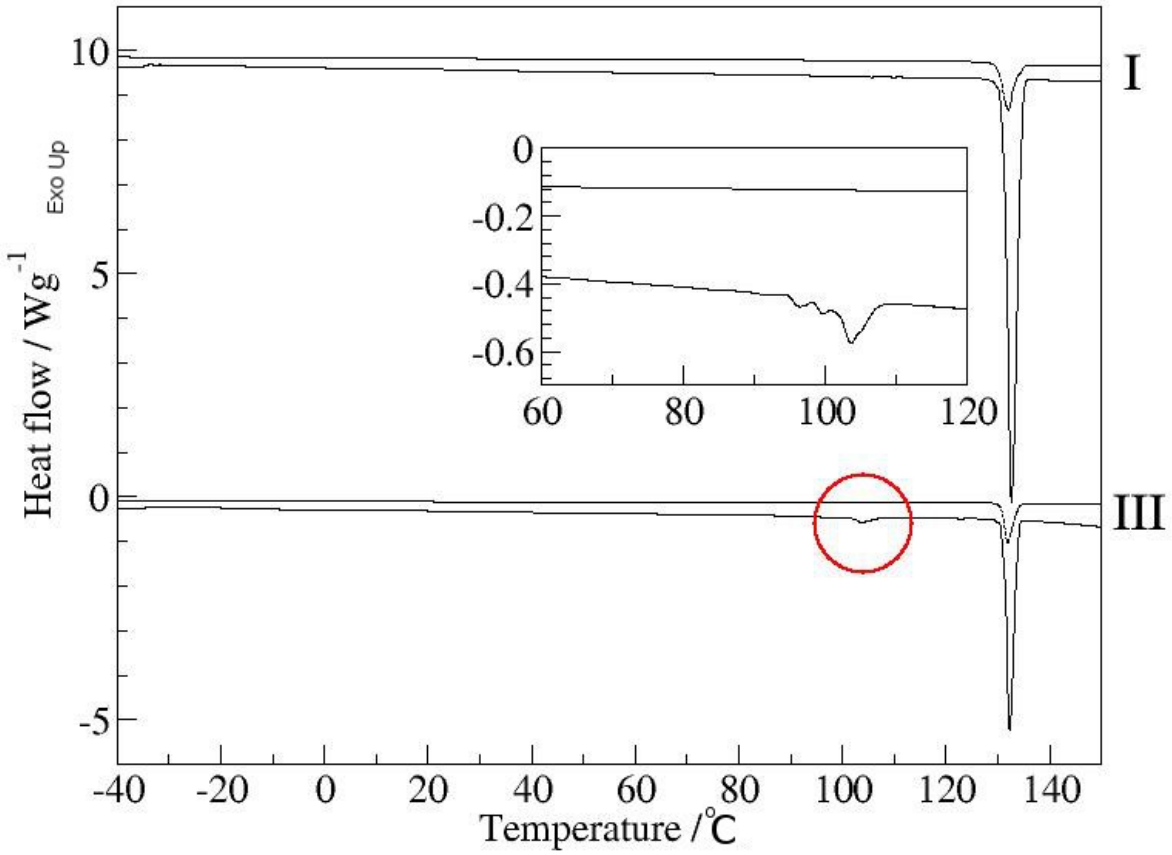

Figure 2.10: DSC plots for both FFA forms I and III

The two DSC traces appear broadly similar: both exhibit a large endothermic event with an onset temperature of 132.2˚C and an enthalpy of 95.8kJ/mol (data for both I and III being the same within experimental uncertainty). The temperature of this event corresponds well with the reported melting temperature of FFA.[80] However, on closer inspection of the two traces (inset, figure 2.10) a clear difference becomes apparent: form III, but not form I, exhibits a weak endothermic transition with an onset temperature of 104˚C and an enthalpy of 4.3 kJ/mol. This value corresponds to the enthalpy difference between forms I and III, and the endothermic nature of the transformation indicates that the driving force for the transformation is an increase in entropy on moving from form III to form I. These data therefore suggest that under these experimental conditions form I remains stable until 132.2˚C, at which it melts, whereas form III transforms into form I at 104˚C, with the newly crystallized form I melting at 132.2˚C.

From figure 2.10 the III to I transition is endothermic, and application of the rules for polymorph stability outlined by Burger and Ramberger[20] suggests that the relationship between forms I and III is enantiotropic, i.e. the free energy versus temperature curves of the two solid forms cross, and the transformation is reversible.

A number of experiments were performed in order to probe the enantiotropic nature of this transition, including heating a sample of form III until it melt, cooling the melt down to -20°C and reheating again, this was done four times using the initial starting sample, it was observed that only on the first heating was the event at 104°C evident. We therefore conclude that either: (a) the FFA III to I transition is in fact monotropic and that the Burger and Ramberger rules are not applicable in this case; or (b) the reverse transformation is kinetically hindered.

We are unable to determine which of these is the case, as it seems reasonable to suppose that a solid-state transition between two conformational polymorphs such as FFA I and III would be highly sterically hindered and therefore kinetically hindered as well as earlier depicted from the molecular modelling results.

2.4.7 *In situ Raman spectroscopy/microscopy*

The data in figure 2.11a and 2.11b shows the phonon-mode and molecular-mode Raman spectra of both FFA forms I and III

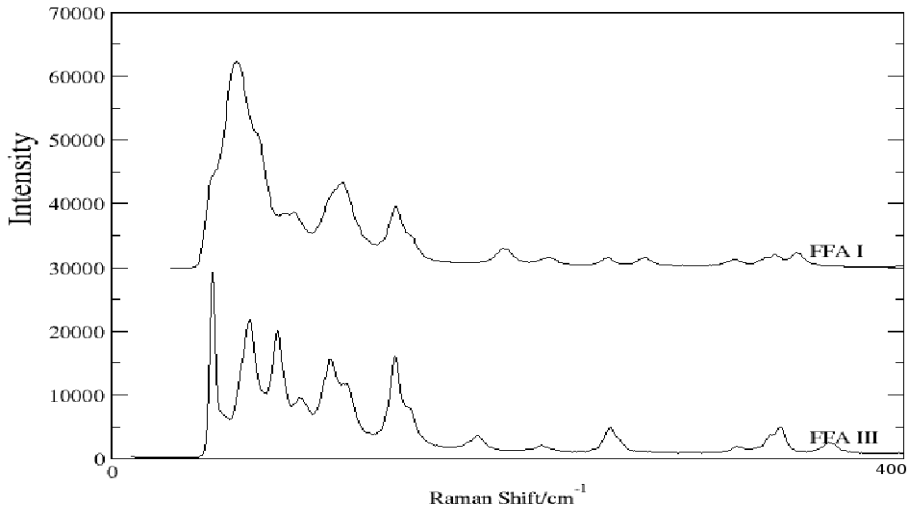

Figure 2.11a: Phonon-mode Raman spectra of FFA forms I and III

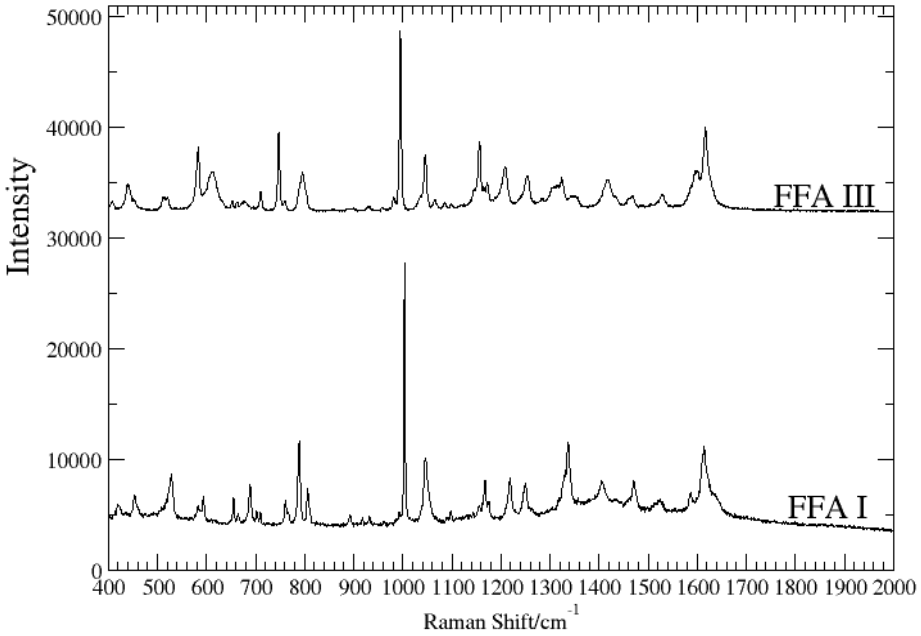

Figure 2.11b: Molecular-mode Raman spectra of FFA forms I and III

At room temperature the two polymorphs, forms I and III, exhibit markedly different Raman spectral (figure 2.11a and 2.11b).
The two spectra from the two solids forms of FFA are readily distinguished by eye, with peaks at 1003.8(995.1), 1046.9 (1045.6), 1253.1 (1249.3), 1596.4 (1586.7), 1617.3 (1615.1) cm^{-1} for form I (and III) respectively, etc. As forms I and III are conformational polymorphs, the different molecular arrangements in the crystal structures lead directly to these strong differences in molecular vibrational bands (400-4000cm^{-1}).
The Raman spectra (2.11a) show the low wave number bands (40-400cm^{-1}) due to lattice vibrational modes (this region provides useful information about lattice environment), this is the first time that these data have been presented for this system, and one of a very limited number of phonon-mode data sets collected to date on pharmaceutical systems (emphasis in previous publications[51, 53-70] were placed on the fingerprint region 500-2000cm^{-1}, where intra-molecular vibrations dominates), absorptions in the low wave number region are also more intense than the bands due to intra-molecular vibrations which makes it useful in distinguishing between crystalline as well as amorphous materials.
While 2.11b, the high wave number bands can be used to deduce information about the molecular vibrations in the molecule : as expected for two polymorphs (necessarily having different crystal structures), the lattice modes are extremely different for the two forms. The same differentiation in peak widths is observed for the molecular stretches, for example the phenyl symmetric breathing mode at 1003.8(995.1) cm^{-1} has a width of 2.98(4.33) cm^{-1} in form I (and III). The bands for form I appear sharper and therefore better-resolved than those of form III.

In order to investigate the transformation between form I and III suggested from the DSC experiments (to further investigate the nature of the solid-solid transition i.e. whether it is abrupt or not), in-situ experiments were performed in which the samples were heated at 1°C/min from -45°C to 145°C, with a Raman spectrum being collected every 1°C for the representative spectral window 40-2000 cm^{-1}. A total of 153 spectra were collected for each of the two samples.
Pertinent data from these experiments are presented in figure 2.12a and 2.12b (intensities in colour):

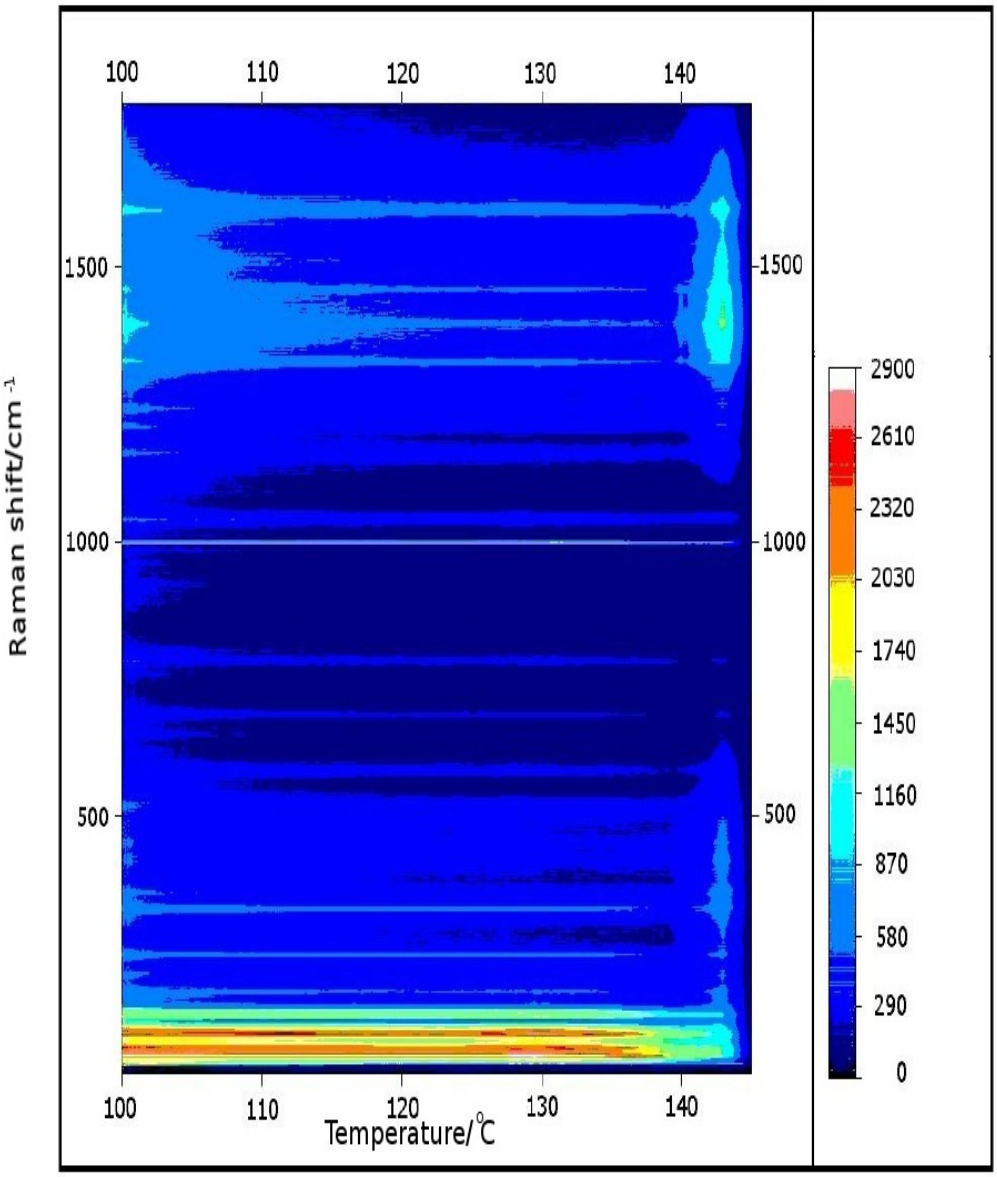

Figure 2.12a: Variable temperature Raman Spectroscopy experiment of FFA form I

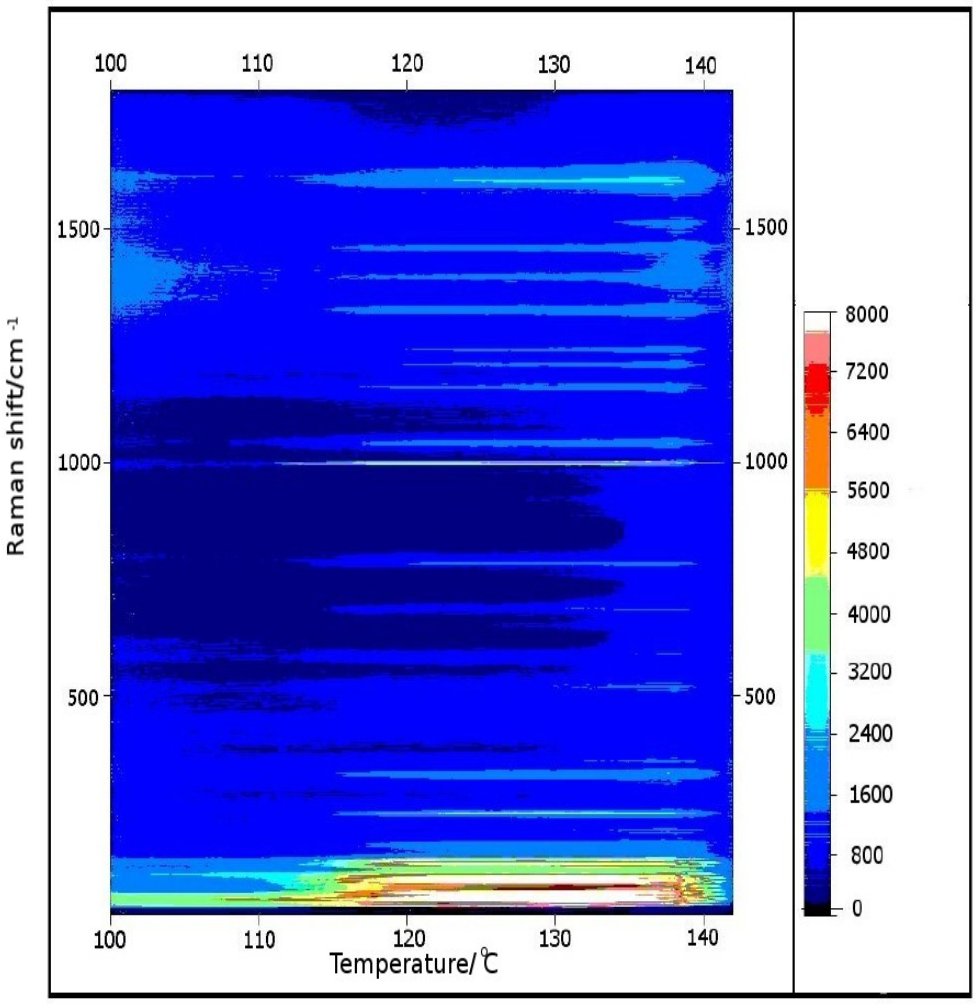

Figure 2.12b: Variable temperature Raman Spectroscopy experiment of FFA form III

On heating form I (figure 2.12a), no changes are apparent until 135-145°C, at which point a major change in spectra occurs. Many of the peaks decrease in intensity and increase in width, including the lattice vibrations (40-400cm^{-1}). Optical inspection of the sample before and after this transition confirms that this corresponds to the sample melting.
The melting point is slightly higher, and broader, than that from the DSC experiments, and this is almost certainly a result of the different sample configurations employed in the two methods. The DSC data were recorded in a small aluminium pan heating at 1°C/min, where as the Raman data were collected on a sample contained in a microscope hot-stage, supported on a glass microscope slide and under a cover slip.

The heat transfer is expected to be more efficient in the DSC than in the microscope hot-stage, and this explains both the greater width and the slightly higher temperature of the transformation in the Raman experiments.

In contrast to the simple behaviour exhibited by form I, the spectra for form III change abruptly between 114 and 115°C (figure 2.12b). Visual inspection of the spectra, and comparison with room temperature data from the two polymorphs, indicates that below this temperature (114-115°C) form III is present, and above that form I. No region of co-existence of the two phases is apparent (as depicted in figure 2.13 below).

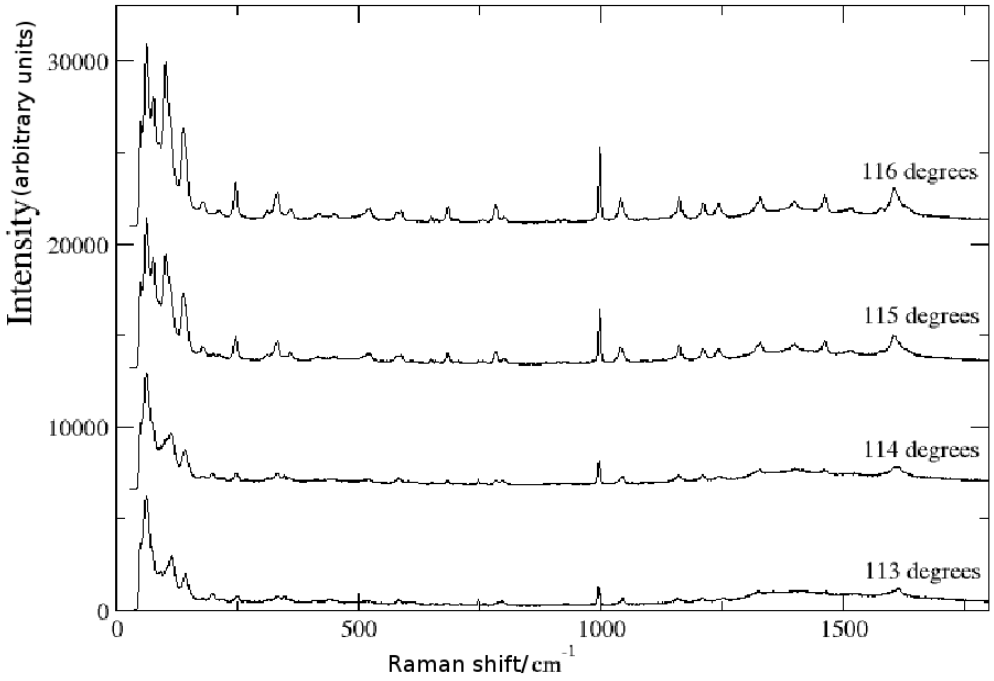

Figure 2.13: Representative Raman spectra from the heating FFA form III taken between 113-116°C

The change in peak position and peak width (using a Gaussian fit) of the symmetric phenyl breathing mode around 1000cm^{-1} (this peak was chosen because of its high intensity and the unique molecular structure of FFA ; made up of two phenyl rings) on heating across the transition is reported in figure 2.14 below:

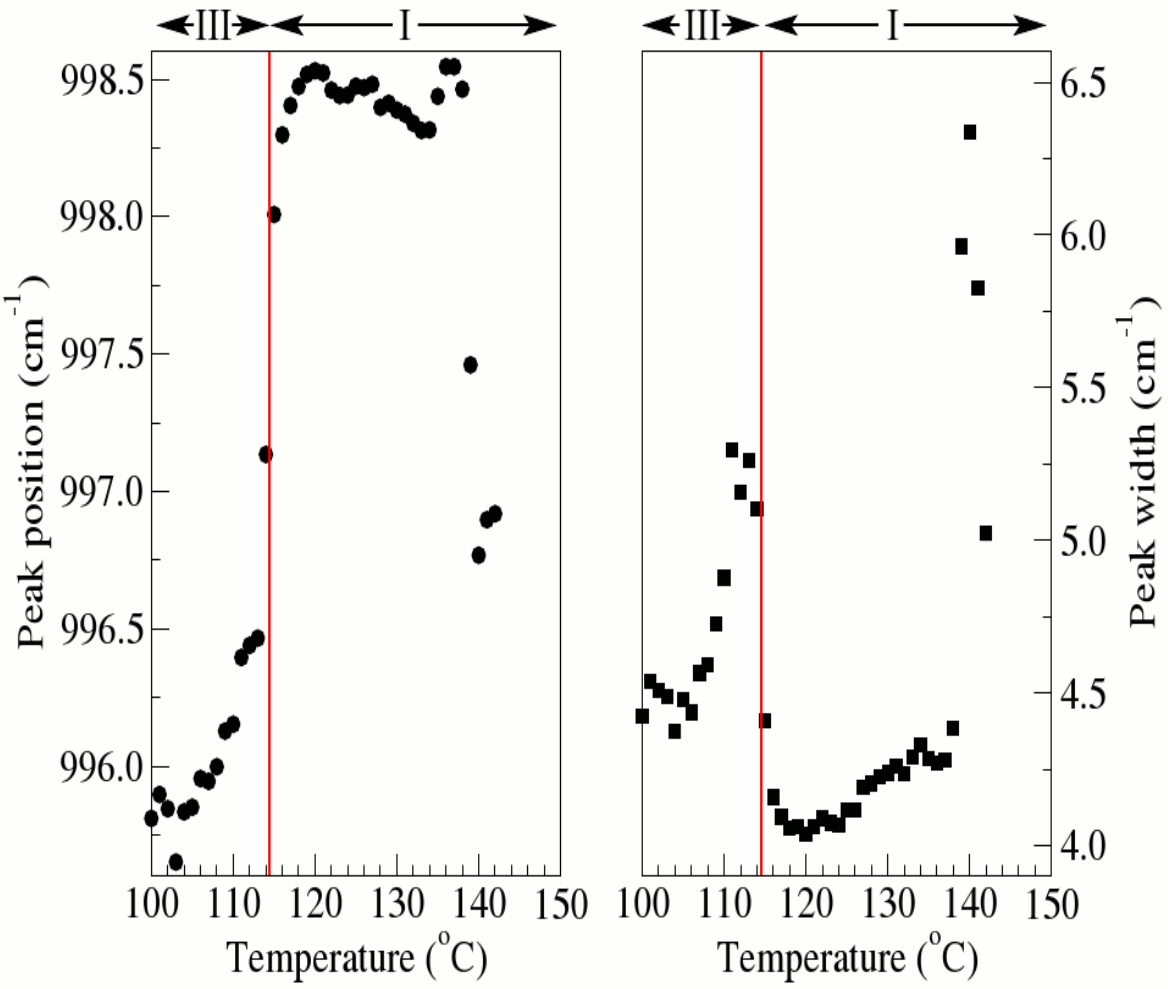

Figure 2.14: Plot of peak width and peak position as a function of temperature

On approaching the transition from below, the peak position exhibits a gradual increase from ca. 995 cm^{-1} at 100˚C, to 996.5 at 113˚C. It then jumps to 997.1 at 114˚C, 998.0 at 115˚C, and then levels off to 998.3-998.5cm^{-1} until the melting point.
The higher peak position for form I (above the transition temperature) is in full agreement with the data from room temperature. The variation in peak width is also presented in figure 2.14.
The peak width below the transition is greater than that above the transition, which again is in full agreement with the room temperature data on forms I and III. Despite the decrease in peak width on transforming from form III to I, as the transition is approached the peak width increases from ca. 4.5cm^{-1} to ca. 5.3cm^{-1}, before decreasing to ca. 4.1cm-1 after the transition.

Note again that no region of co-existence of forms I and III is apparent in Raman, and that this peak broadening therefore has its origin purely in the molecular motion in form III.
The increase in peak width over several degrees Celsius as the transition is approached indicates that (averaged over the experimental time scale of ca. 4 seconds) the FFA molecules in form III can adopt a wider range of vibrational energies (and hence local molecular environments for the phenyl ring) as the transition is approached. This observation further shows the unique advantage of Raman spectroscopy over the other techniques used in polymorphic identification/characterisation as it allows us to explore molecular changes as a function of temperature.
A possible mechanism for the transformation can be envisaged, using vibration of atoms in the crystal to explain the melting transition, this resembles the so-called Lindemann vibrational catastrophe (in its simplest form suggests that melting is a spontaneous process i.e. the solid and the liquid phase does not co-exists at any time during the melting process) in melting theory.[125-134] In this mechanism, melting is assumed to occur when the amplitude of vibration of the atoms reaches a certain fraction of the equilibrium atomic spacing, Lindemann's model assumes that the vibrations of the atoms are harmonic, with a common frequency. Quantitative calculations based on the model are not easy, hence Lindemann offered a simple criterion: melting might be expected when the root mean vibration amplitude $\sqrt{<u^2>}$ exceeds a certain threshold value (namely when the amplitude reaches at least 10% of the nearest neighbour distance).

The average amplitude of thermal vibrations increases when the temperature of the solid increases, at some point the amplitude of vibration becomes so large that the atoms start to invade the space of their nearest neighbours and disturb them and the melting process initiates. The sudden surge in peak width (suggesting rather rapid increase in disorder) is a further pointer towards the assumption of the Lindemann model.

Conclusions

It is clear from the above study that FFA I and III are both conformational polymorphs.

Above the thermodynamic III ->I transition temperature we see III -> I (using Raman hot-stage), whereas below it (as seen from the room temperature solvent drop milling and slow evaporation results) we tend to see I -> III. i.e. we tend to see the thermodynamically most stable form at ambient temperature.

FFA III transforms to FFA I on heating, the transition is vibrationally driven, with both forms easily distinguishable by Raman spectroscopy, with the low wave number region or phonon-mode region being highly valuable for studying polymorphs.
While the transition is abrupt with no co-existence of the two forms in the Raman analysis, this is not so with XRPD where the transformation proceeds via a mixture of the two forms, this is because the Raman experiment involved only a microscopically small amount of sample (as it uses a microscope) whereas the XRPD looks at significantly more sample.

The mechanism of the transition is similar to the 'Lindemann melting theory' as indicated by the rapid increase in disorder during the transformation.

The large number of polymorphs of FFA is thought to arise from a delicate balance between molecular conformation, hydrogen bonding and crystal packing.

3.0 Polymorphic Transformations in Flufenamic Acid

3.1 Monitoring polymorphic changes in flufenamic acid using variable temperature X-ray powder diffraction and in situ Raman spectroscopy

While in the last chapter (2), the study focussed on the transitions between two crystalline forms of FFA (i.e. I and III), this chapter (3) looks at the amorphous form and what happens when we heat it. A previous study has shown that the amorphous can be an intermediate in some crystals prior to crystal transformations.[6] The main purpose of this study is to show that the method of constrained crystallisation (slow heating of the amorphous state/form) can be a veritable tool for studying polymorphism.

Abstract

The aim of this study was to use variable temperature X-Ray Powder Diffraction (VTXRPD) and in situ Raman spectroscopy to monitor the polymorphic transformations in flufenamic acid (FFA) forms I and III using the constrained crystallisation approach.

Initial results from the VTXRPD experiments using FFA form I showed a transformation to a new form at 50°C, this then transforms into form II (70°C) and then back to form III at 90°C before melting at 140°C. While heating form III produced only a transition back to form I.

In situ data from the Raman experiments revealed that FFA form I, changed first to form III and then back to its original form (I) before melting, while the same transformation as obtained with the VTXRPD experiment on form III (form III →form I) was observed also with the Raman experiment.

Differential Scanning Calorimetry (DSC) was also used similarly to support the findings observed above from the VTXRPD and Raman experiments. Principal component analysis was used in analysing the data obtained from the in situ Raman experiments.

3.2 Experimental

3.2.1 Materials

Flufenamic acid form I (confirmed using DSC, XRPD and Raman spectroscopic analysis and results compared with already published data[40,41]), was purchased from Sigma-Aldrich Dorset UK was used in all experiment as received.

Pure flufenamic acid form III was prepared by simple evaporative crystallisation (of FFA I) from propanol and its spectroscopic data confirmed like in the case of form I.

3.2.2 DSC

A Q2000 series differential scanning calorimeter, manufactured by TA Instrument, Crawley, England, was used for the DSC analysis. Approximately 4mg of both forms were first heated at 1°C/minute to 150°C, cooled down to -100°C at 1°C/minute before subsequently heating the supercooled sample slowly at a heating rate of 1°C/minute back to 150°C.

3.2.3 XRPD

XRPD patterns were collected on a Bruker D8 diffractometer system (Bruker AXS, Madison, WI, USA), operating in a Debye-Scherrer geometry, at a wavelength (λ) of 1.54059Å, 40kV voltage, and a current of 40mA, using a LynxEye detector. The sample was heated using a Cryostream plus controller (Oxford Cryostreams Ltd. Hanborough Oxford OX29 8LN) at 3°C/minute from -10°C to 150°C and patterns were collected at each temperature step (overall accumulation time of 8 minutes) at a scan time of 0.3 second.

3.2.4 Raman

Raman spectra were collected using a confocal Horiba-Jobin-Yvon LabRAM system (Horiba-Jobin-Yvon Ltd Middlesex U.K.), using a 600 lines/mm grating and a 785 nm excitation laser. A Synapse CCD detector was employed. Temperature control was achieved using a Linkam hot-stage (Linkam Scientific Instrument Ltd, Surrey U.K).

Flufenamic acid samples were first heated to 150°C, held at this temperature for 2 minutes and quenched on a surface that had been pre-cooled to -100°C with liquid nitrogen.

The super-cooled samples were then heated at stepwise 1°C/ minute intervals, and were held at temperature during data collection (typically 10–20 seconds maximum). Data sets were collected every 1°C. Samples approximately 1 mg were placed on a microscope slide without a cover slip.

3.2.5 Data Analysis

The Raman spectra obtained were subjected to PCA analysis using 'PCA packages' within the 'R' programming suite. Raw spectra were used, the phonon spectra range/mode (30-400cm^{-1}) and molecular fingerprint range/mode region (500-2000cm^{-1}) were used for the analysis.
The most important principal components (PCs) were determined from percentage variance plots and were used to investigate trends in the spectra features of the Raman data. PC1, PC2 and PC3 were selected as they accounted for over 90% of the variance.

3.3 Results and Discussion

3.3.1 X-ray powder diffraction

The powder patterns obtained from the heating of amorphous samples prepared from FFA form I are shown in figure 3.1 below:

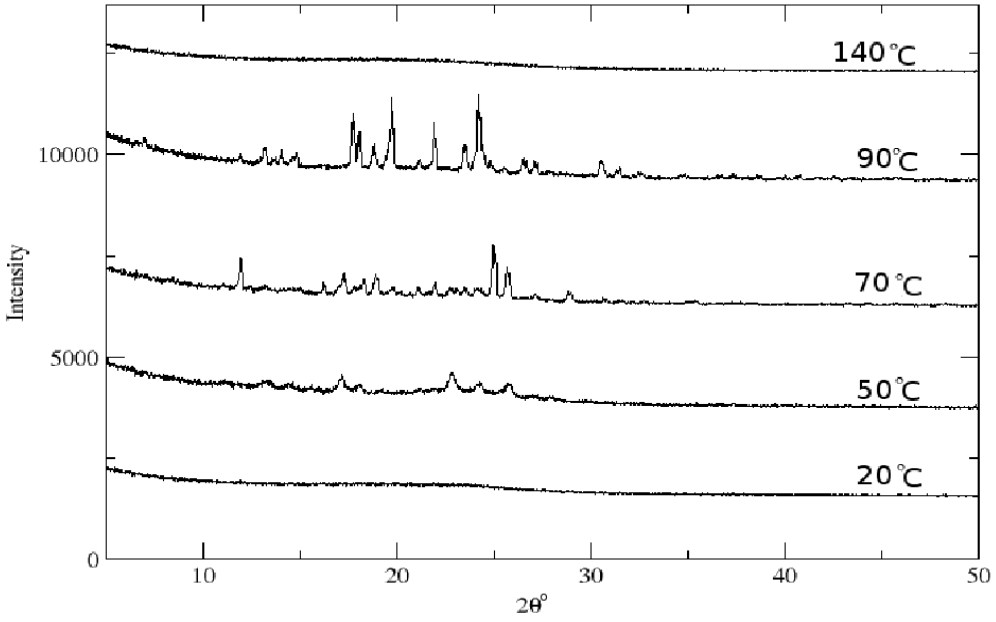

Figure 3.1: In situ XRPD pattern from the heating of the amorphous form prepared from FFA I

The pattern (figure 3.1) shows a transformation to a new form[135] at 50°C, which transforms into form II (70°C) and then to form III at 90°C before melting at 140°C. The XRPD pattern of Form II has not yet been published (its structure was determined from single crystal X-ray at a synchrotron).

3.3.2 Confocal Raman spectroscopy

The in situ Raman spectra of the slow heating of the amorphous samples obtained from FFA forms I and III are presented in figure 3.2a (left hand side) and 3.2b (right hand side, intensities in both cases are in colours, PC1 is black and PC2 is red): the amorphous form obtained from either forms are expected to be the same, therefore forms I and III refer only to the crystalline forms.

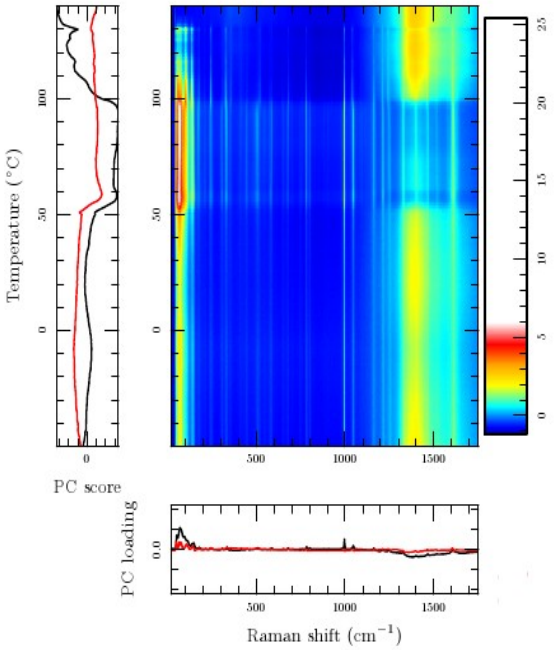

Figure 3.2a: Variations in the Raman spectra (top right), PC1, PC2 (top left) with temperature and loadings (bottom), for the slow heating of the amorphous form obtained from FFA I

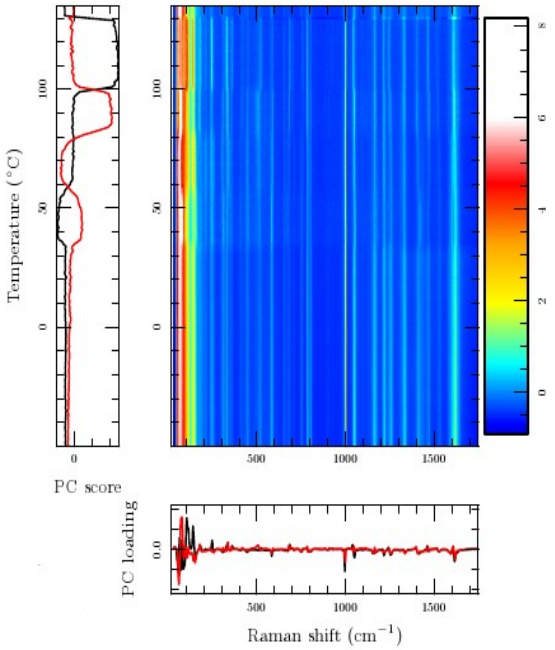

Figure 3.2b: Variations in the Raman spectra (top right), PC1, PC2 (top left) with temperature and loadings (bottom), for the slow heating of the amorphous form obtained from FFA III

Visual inspection of figure 3.2a shows two separate events occurring as the amorphous sample (prepared by melting FFA I) is being heated: at 50˚C and 100˚C respectively (see left hand side panel i.e. scores). While the lower panel (loadings) only shows significant changes in the phonon-mode region as the sample is being heated.

While in figure 3.2b, four separate events are observed (see left hand side panel): at ~ 34˚C, 59˚C, 80˚C and at 100˚C respectively during the heating of the amorphous sample (obtained by melting and quenching FFA III) . Similarly the phonon-mode region as seen in the lower panel of figure 3.2b undergoes noticeable changes in the course of the experiment.

Further data treatment using principal component analysis (PCA), enumerates the transition observed from the in situ Raman experiments. Figures 3.3a and 3.3b, shows the principal component projections for the phonon-mode as well as molecular-mode region for the slow heating of amorphous form obtained from melting FFA I:

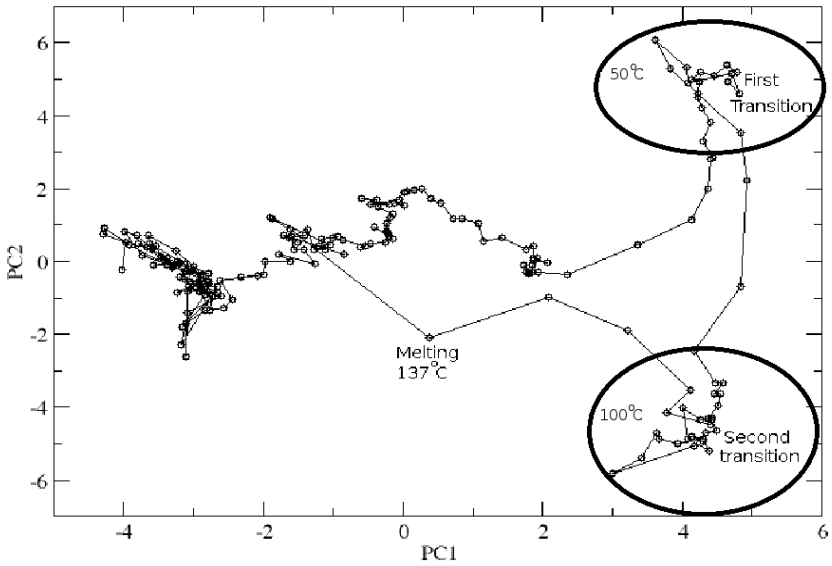

Figure 3.3a: Phonon-mode projection of the heating of amorphous form (prepared by melting FFA I)

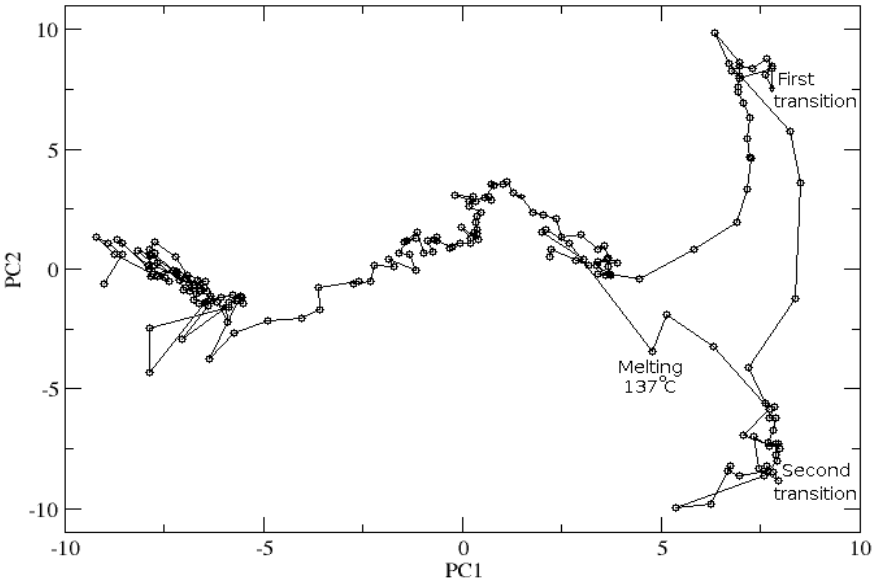

Figure 3.3b: Molecular-mode projection of the heating of amorphous form (prepared by melting FFA I

While figures 3.4a and 3.4b show a similar principal component projection for the in situ experiment involving the amorphous form (obtained by melting FFA III), here the phonon-mode projection better describes the transition than the molecular-mode. These plots i.e. 3.2a, 3.2b, 3.3a, 3.3b, 3.4a and 3.5b shows that the PCA highlights transformation, scores allows temperature of transitions to be picked, while loadings tells us about peak changes.

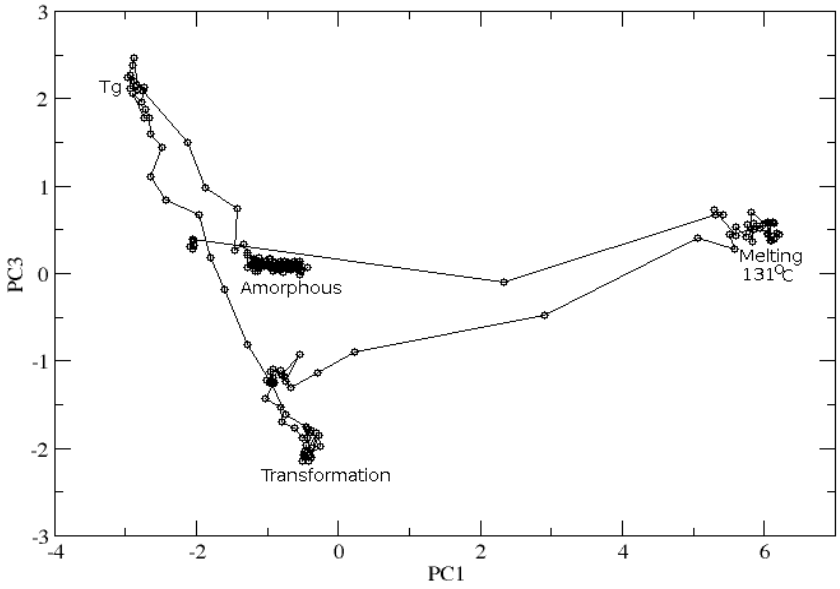

Figure 3.4a: Phonon-mode projection of the heating of amorphous form (obtained by melting FFA III)

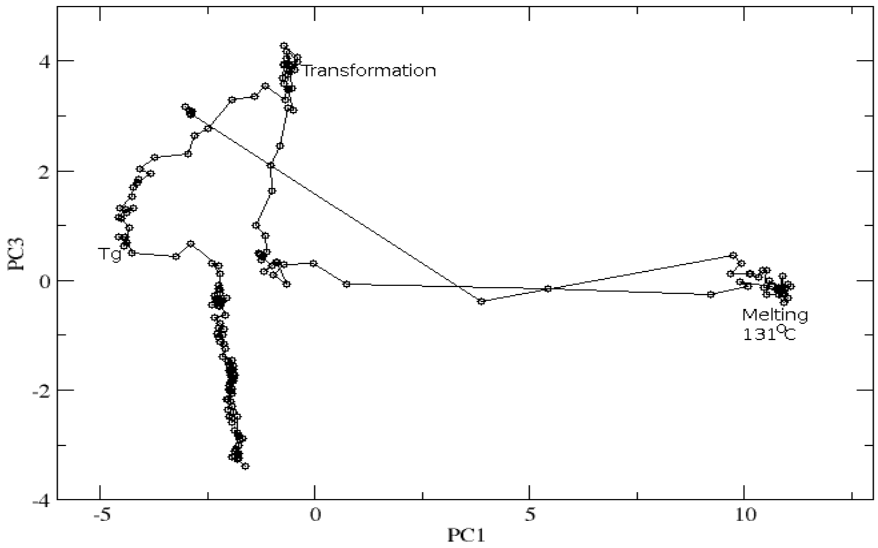

Figure 3.4b: Molecular-mode projection of the heating of amorphous form (obtained by melting FFA III)

3.3.3 DSC Analysis

Figure 3.5a below shows the DSC trace obtained from the slow heating of the amorphous sample prepared by melting and quenching FFA I (1°C heating rate): further analysis revealed an exotherm at ~ 39°C, followed by two weak endotherms at approximately 126.4°C and 128°C (inset, figure 3.5a) respectively, before the final melting of the sample at 133.4°C.

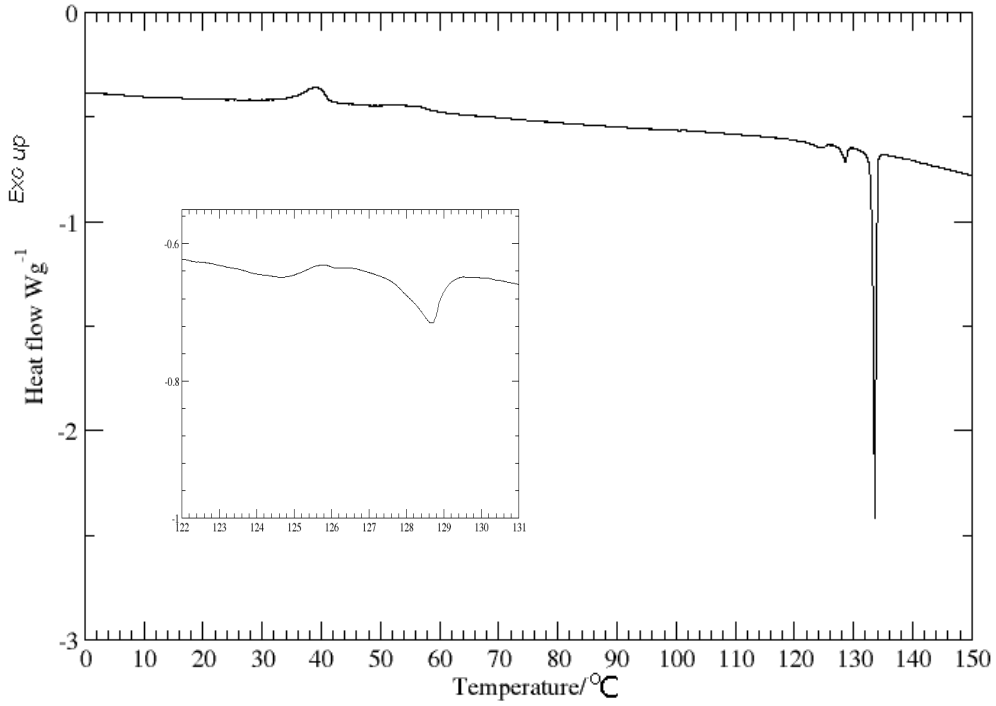

Figure 3.5a: DSC trace of the slow heating of amorphous sample prepared by melting and quenching FFA I: inset are the two weak exotherms

The representative DSC trace from the heating of the amorphous sample prepared by melting and quenching FFA III is shown in figure 3.5b below: two exotherms at 38.7°C and 54.7°C were observed before the final melting at 133.4°C.

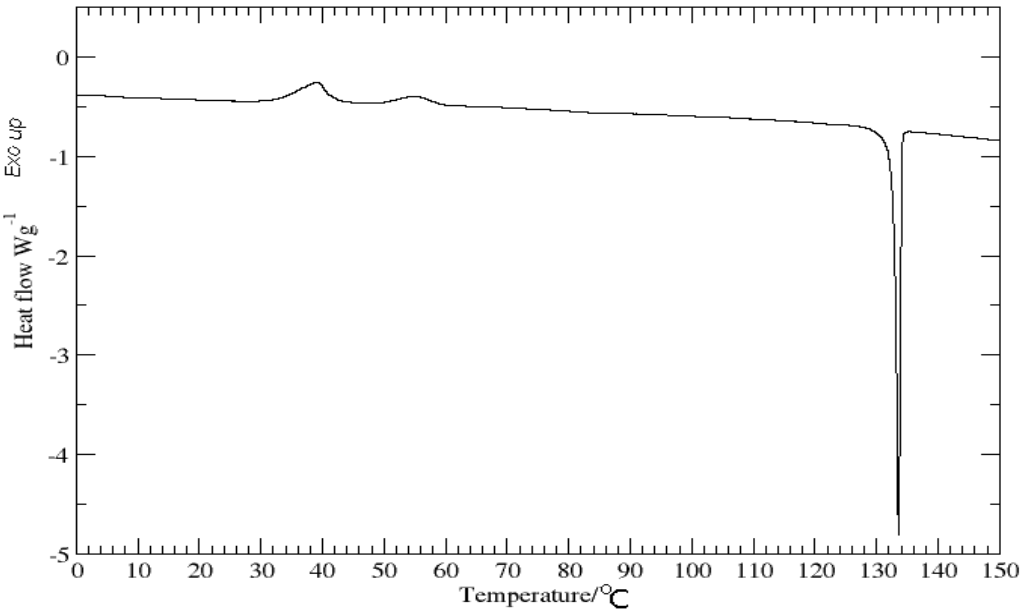

Figure 3.5b: DSC trace of the slow heating of amorphous sample prepared by melting and quenching FFA III

Figure 3.5a shows a glass transition (at ~ 39°C), followed by two successive melting events before the final melting event (at 133.4°C) suggesting that two separate forms of FFA could be obtained from the slow heating of its amorphous form (prepared from FFA I). While figure 3.5b; shows two separate recrystallisation events, an indication that has the heating progresses two different polymorphic transformation occurs.
This rich display of polymorphism by FFA as seen in the DSC traces (figures 3.5a and 3.5b) is in agreement with previous publication by J. Krc Jr.,[80] who suggested that FFA could adopt several polymorphic transitions as a result of an interplay of both its molecular conformation, hydrogen bonding sequence and its unique crystal packing.

Conclusions

In concluding, the use of the constrained crystallisation approach in inducing polymorphic transformation is a veritable tool for monitoring polymorphism as shown in this study: especially when monitored using a combination of in situ Raman spectroscopy and variable temperature XRPD. The results obtained in the study compares favourably well with those obtained using other techniques traditionally used to induce polymorphic transitions. Two new powder x-ray patterns of FFA were also uncovered in the study. The use of PCA in analysing the data obtained from the study was very helpful, allowing for easy visualisation of not only the transformations but also the temperature at which these transformations occurs as well as changes in peak positions as the experiment progressed. The differences in the transformation temperature observed in the DSC experiment as compared to the Raman analysis we adduce to the slightly different experimental set up in the two techniques: In DSC the samples are heated inside aluminium (covered) pans while they are heated on a microscope slide during the Raman experiment.

4.0 Polymorphism in Nifedipine

4.1 In situ investigation of the polymorphic transformations from amorphous nifedipine using Raman spectroscopy

Abstract

We report a novel investigation into the polymorphic transformations of nifedipine (a calcium-channel blocker) from its amorphous form using in situ variable temperature Raman (confocal) spectroscopy, by employing the constrained crystallisation approach (heating of the amorphous form). Our results were complemented with Differential Scanning Calorimetry (DSC) and variable temperature X-Ray Powder Diffraction (XRPD).

Initial visual analysis of the Raman spectroscopic data from the slow heating experiments showed that amorphous nifedipine transforms into form II at approximately 52°C and back to the as received form I at 75°C before finally melting at 175°C. While heating the amorphous sample first to 180°C and cooling to room temperature, before slowly reheating back to the melting point gives form II at room temperature, form III at ~28°C and form I at 75°C. Forms II and III are endothermically related (by applying the Burger and Ramberger rule) as previously reported.[136]

DSC analysis of the melt and quenched sample of the as received (form I) showed a glass transition (Tg) at ~ 43.3°C, followed by two exotherms (98.7°C and 112.6°C) and an endothermic event (melting) at 170.5°C.

While patterns obtained from the in situ XRPD analysis of the melt and quenched sample of nifedipine form I, identified that amorphous nifedipine transformed to form II and then back to form I.
The diffraction patterns obtained from the reheat of form II (prepared by cooling the melt and quenched sample of form I to room temperature), showed the presence of two intermediates which appears to be a mixture of both forms I and II before transformation back to form I .
A multivariate approach was adopted for a more detailed analysis of the Raman data by using Principal Component Analysis (PCA).

4.2 Introduction

Nifedipine (dimethyl-1,4-dihydro-2,6-dimethyl-4-(2-nitrophenyl)pyridine 3,5-dicarboxylate), shown below is known to exhibit polymorphism, a fact that has been well documented in literature.136-147

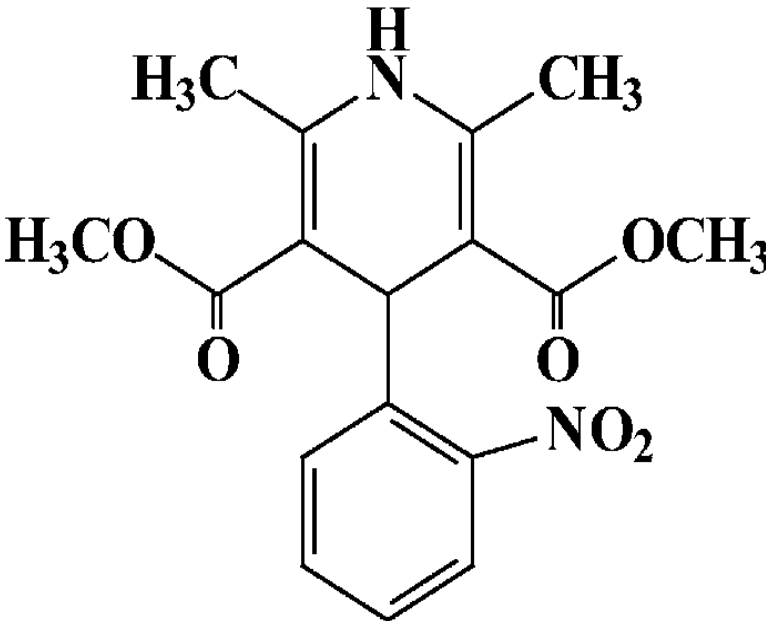

Figure 4.1: Molecular structure of nifedipine

Using DSC and thermomicroscopy, Eckert and Muller[137], concluded that two modifications i.e. form II (fine ray-shaped aggregates) with melting point between 162°C and 164°C and form III (beam shaped) with melting range 134°C to 137°C can be obtained from the supercooled melts of nifedipine (most thermodynamic stable form I), with melting point between 172-172.5°C.

While Burger A. and K.T. Koller[138] monitored the crystallisation of the supercooled melt of nifedipine using Infra-Red (IR) spectroscopy, findings were similar to that of Eckert et al. They summarised their results by claiming: nifedipine exists in three monotropically related modifications. Form I (melting point. 169 to 173°C) is the thermodynamically stable modification at room temperature. The two unstable modifications form II (melting point. 161°C to 163°C) and form III (melting point. 135°C) could only be obtained from the melt on a object slide.
They were the first to present the IR spectra of nifedipine forms II and III, they also prepared four different solvates (A,B,C and D) of nifedipine by crystallisation from 1,4-dioxane.

Hirayama[139] et al. studied the crystallisation of amorphous nifedipine with and without a cyclodextrin derivative added, and confirmed that supercooled nifedipine in the absence of the derivative crystallises first to a metastable form II around 110°C , which then reconverts to the thermodynamically stable form I at 125°C using (XRPD). The presence of the derivative was reported to slow down the rate of crystallisation of amorphous nifedipine to form I and a form II melt was obtained at 163°C.

The results published by Aso[140] et al. showed that the supercooled melt of nifedipine crystallised from the amorphous state to a metastable form II at 90°C which then enantiotropically reconverted to the thermodynamic stable form I around 110°C.

Bram Keymolen[143] et al. reported that recrystallisation, solid-solid and solid-liquid-solid transformations processes occurred in glassy nifedipine when heated from 45°C to its final melting point of 172°C, including a glass transition ~48°C. They concluded that there are probably four polymorphic forms of nifedipine.

D. Grooff[144] et al. monitored the thermal behaviour of nifedipine with the view to understand the various phase transitions between its polymorphs using a combination of DSC, MTDSC, TG, HSM, PXRD and VTPXRD. They concluded from their results that the metastable form II, melting point ~163°C, was enantiotropically related to a third modification, form III, which existed at a lower temperature. Form III converted endothermically to form II at ~56°C on heating and was shown by HSM to be accompanied by morphological changes. Discontinuities in the reversing heat flow signal during crystallisation of amorphous Nifedipine (from ~92°C) to form II, suggested that a number of polymorphs may nucleate from the melt prior to form II formation.

Chan[145] et al. reported on polymorphism in nifedipine under controlled humidity, their results showed that glassy nifedipine crystallises to the thermodynamically stable α-polymorph (form I) via a transient metastable β-nifedipine (form II) phase. Increasing relative humidity in the range 20-60% is found to favour the surface crystallisation of the glass β-nifedipine while at high relative humidity (80%), β-nifedipine is rapidly converted to α-nifedipine.

D. Zhou[136] et al. reported their study on the crystallisation of amorphous nifedipine using hot-stage microscopy (HSM), (PXRD), and (DSC). The kinetic data obtained from DSC studies under isothermal and non-isothermal conditions were examined using both model-fitting and model-free approaches.

Their results concluded that amorphous nifedipine transforms into form II upon heating at around 105°C, which then undergoes a solid-solid transformation back to form I at ~145°C, they also found out that by cooling the sample of form II back to room temperature, a small exotherm appeared at 30°C during cooling and a small endotherm appeared at 60°C during subsequent heating, they then concluded that this shows the presence of a polymorphic transformation between form II and another form. The reverse event occurs during the cooling process, thus indicating that forms II and this third form are related enantiotropically.

Caira[148] et. al. reported for the first time the single-crystal structure of the solvated species $(nifedipine)_2$. 1,4-dioxane. They also showed that desolvation of these species involves complete disruption of the crystal structure at the relatively high temperature of 150°C-153°C, i.e., 50°C above the boiling point of 1,4-dioxane, and yields a monoclinic polymorph (modification I) with a melting point of 174°C. When exposed to an aqueous medium for 48 hours, the solvate transforms into a dihydrate.

It is also worth mentioning that the crystal structure of nifedipine (modification I) was first reported by Triggle et al.[148]

Table 5 Below summarises the results obtained by the various authors previously mentioned.

Authors and year of publication	Analytical methods/techniques used	Form(s) of nifedipine obtained/isolated
T. Eckert and J. Muller (1976)[137]	DSC and thermomicroscopy	Forms II and III (from form I)
A.M. Triggle et. al. (1980)[163]	XRPD	Crystal structure of form I
Hirayama et. al. (1994)[139]	XRPD	Forms II and III (from form I)
Aso et. al. (1995 & 2001)[140]	Microcalorimetry	Form (II from form I)
Keymolen et. al. (2003)[143]	Thermomicroscopy	Suggested the possibility of four different forms
Zhou et. al. (2003)[136]	HSM, XRPD and DSC	Form II and a 'possible' third form (from form I)
Caira et. al. (2003)[147]	Single-crystal XRD	Nifedipine dihydrate
Chan et. al. (2004)[146]	FT-IR, FT-Raman and Raman microscopy	Forms I and II (from form I)
Burger et. al. (2006)[138]	IR	Forms II and III (from form I), solvates A, B, C, & D
Grooff et. al. (2007)[144]	DSC, MTDSC, TG, HSM, PXRD and VTPXRD	Forms II and III (from form I), and suggests the possibility of the existence of some other forms

Table 5: Summary of previous publications on the polymorphic modification of nifedipine

The crystal structure of nifedipine first reported by A.M. Triggle et. al. (1980),[148] was found to be similar to that described by Caira et al.[147] crystallizing in the space group $P2_1/c$ with Z¼=4; the structural arrangement clearly favouring the emergence of likely hydrogen bonding between molecules of nifedipine leading to different structural possibilities.

Polymorphic transformations can be studied in situ by infra-red and Raman micro-spectroscopy combined with a controlled environment unit.[143,149,150] Compared to DSC and XRPD, Raman spectroscopy does not require sample isolation and invasive preparation before data acquisition.[162]

This study will focus on monitoring the polymorphic modifications from the melt quenched sample of the commercially available form (form I) of nifedipine, this will involve applying chemometric methods and in-situ Raman, including phonon-mode data, to a controversial system (Bram Keymolen et.al. found out that the order of transitions (using DSC) from the amorphous form was not as previously reported by[143] by Hirayama et. al.,[139] this they postulated could be dependent on heating rates). We will also compare the results obtained from the Raman analysis with data from similar experiments using DSC and in situ XRPD.

We will adopt the nomenclature used by Eckert and Muller,[137] in identifying the various form of nifedipine in this study. Because of the usefulness of PCA in data classification,[151-153] it was employed in this study to explain trends in the data acquired from the in situ experiment (Raman spectroscopy).

4.3 Experimental

4.3.1 Material

Nifedipine, was purchased from Sigma-Aldrich CO, 3050 Spruce Street, St. Louis, MO 63103 USA and used in all experiment as received. The as received sample was identified as nifedipine form I by DSC and XRPD analyses after comparison with previous results published by Zhou et. al.[136] and Groof et.al.[144]

4.3.2 DSC

A Q2000 series differential scanning calorimeter, manufactured by TA Instrument, Crawley, England, was used for the DSC analysis. Approximately 4mg of the as received sample was accurately weighed and was first heated at 1˚C/minute to 180˚C, above the melting point, cooled down rapidly to -40˚C at 40˚C/minute before subsequently heating the supercooled sample slowly at a heating rate of 1˚C/minute back to 180˚C. For the reheat of nifedipine form II (obtained by cooling a melt quenched sample of form I to room temperature), 2.77mg of the as received sample was weighed, heated at 10˚C/minute to 180˚C, and subsequently quenched at 40˚C/minute to room temperature (20˚C), before a slow reheat was performed at 1˚C/minute to 180˚C.

4.3.3 Raman spectroscopy

Raman spectra were collected using a confocal Horiba-Jobin-Yvon LabRAM system (Horiba-Jobin-Yvon Ltd Middlesex U.K.), using a 600 lines/mm grating and a 785 nm excitation laser. A Synapse CCD detector was employed. Temperature control was achieved using a Linkam hot-stage (Linkam Scientific Instrument Ltd, Surrey U.K).

Nifedipine samples were first heated to 180˚C above the melting point, held at this temperature for 2 minutes and quenched on a surface that had been pre-cooled to -100˚C with liquid nitrogen.

The super-cooled samples were then heated at stepwise 1˚C/ minute intervals, and were held at temperature during data collection (typically 10–20 seconds maximum). Data sets were collected every 1˚C. Samples (approx. 1 mg together with ~ 0.5mg of ground glass needed to initiate nucleation) were contained inside unsealed hermetic DSC pans (T080723) supplied together with the Q2000 series differential scanning calorimeter.

4.3.4 XRPD

XRPD patterns were collected on a Bruker D8 diffractometer system (Bruker AXS, Madison, WI, USA), operating in a Debye-Scherrer geometry, at a wavelength (λ) of 1.54059Å, 40kV voltage, and a current of 40mA, using a LynxEye detector. The sample was heated using a Cryostream plus controller (Oxford Cryostreams Ltd. Hanborough Oxford OX29 8LN) at 3˚C/minute from -10˚C to 175˚C and patterns were collected at each temperature step (overall accumulation time of 8 minutes) at a scan time of 0.3 second.

4.3.5 Data analysis

The Raman spectra obtained were subjected to PCA analysis using 'PCA packages' within the 'R' programming suite. Raw spectra (variance-scaled and mean-centred before analysis) were used, the entire data range as well as the phonon spectra range/mode (30-400cm^{-1}) and molecular fingerprint/mode region (500-2000cm^{-1}) were used for the analysis.
The most important principal components (PCs) were determined from percentage variance plots and were used to investigate trends in the spectra features of the Raman data. PC1 and PC2 were selected as they accounted for over 99% variance.

4.4 Results and discussion

4.4.1 DSC

The DSC trace for the slow heating (heating rate 1˚C) of the amorphous form of nifedipine (figure 4.2a below), showed a weak glass transition, Tg (inset) at ~ 43.4˚C, a sharp exotherm at 98.7˚C (II) followed by another exotherm at 112.6˚C (I) and an endotherm at 170.5˚C (melting).

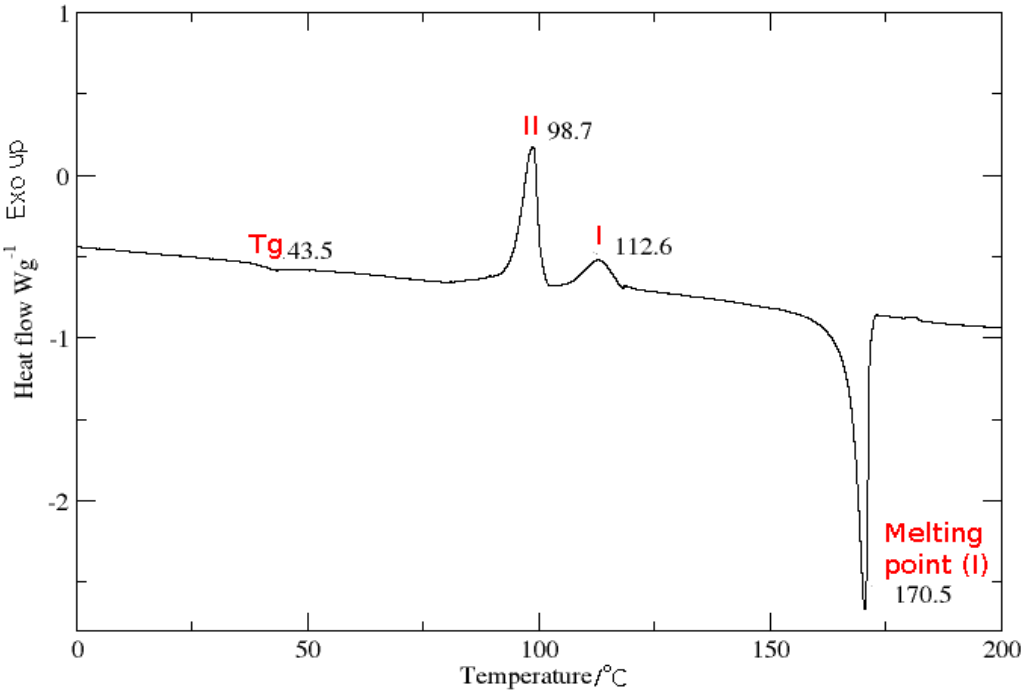

Figure 4.2a: DSC trace of the slow heating of amorphous sample prepared from nifedipine form I

These data is consistent with the following transformations: amorphous → form II (98˚C) → form I (112˚C) → melt (170˚C) and compares favourably well with those reported by Eckert and Muller.[137]

Figure 4.2b below shows the DSC plot obtained from the slow heating of nifedipine form II (prepared by cooling a melt and quenched sample of nifedipine form I to room temperature, i.e. 20°C in this case), as described by D.Zhou et. al.[150]. This was done so as to explore other methods of inducing polymorphic transformations in nifedipine for data comparison purposes.
A gradual exothermic event at 92.88°C was followed by the final melt at 172.50°C (see fig. 4.2b below). Thus suggesting one polymorphic transition during the heating of nifedipine form II prior to melting.

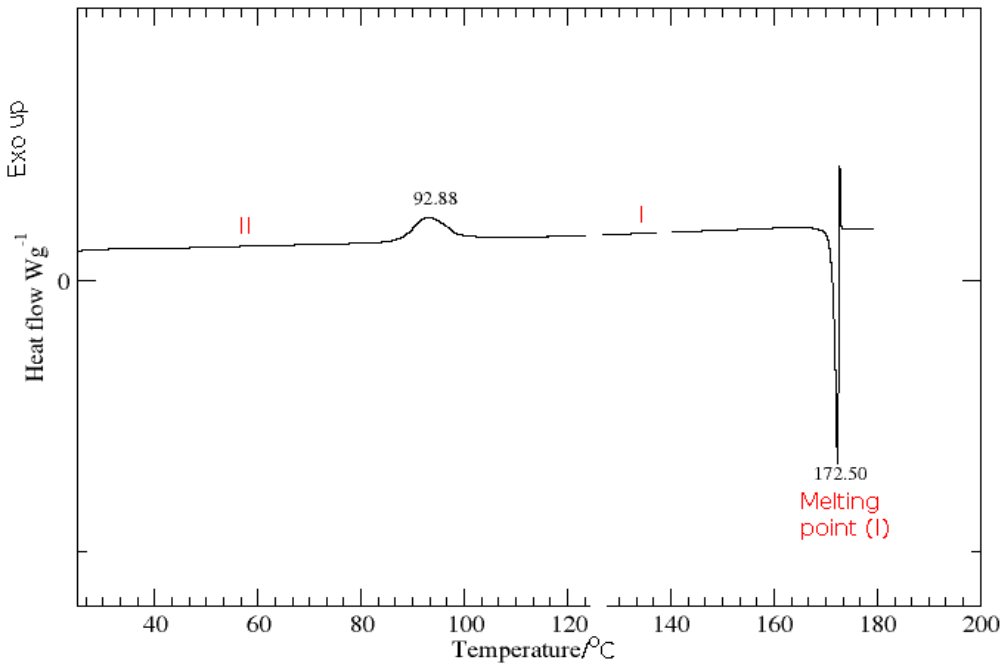

Figure 4.2b: DSC plot of the slow heating of nifedipine form II

4.4.2 Confocal Raman spectroscopy

Visual inspection of the in situ Raman spectra from the slow heating of the amorphous form of nifedipine (figure 4.3a below, intensities is in colours, PC1 is black, PC2 is red), shows three events at 25°C (the Tg), 55°C and 150°C respectively (amorphous → form II → form I) as previously reported using thermal methods.[138]

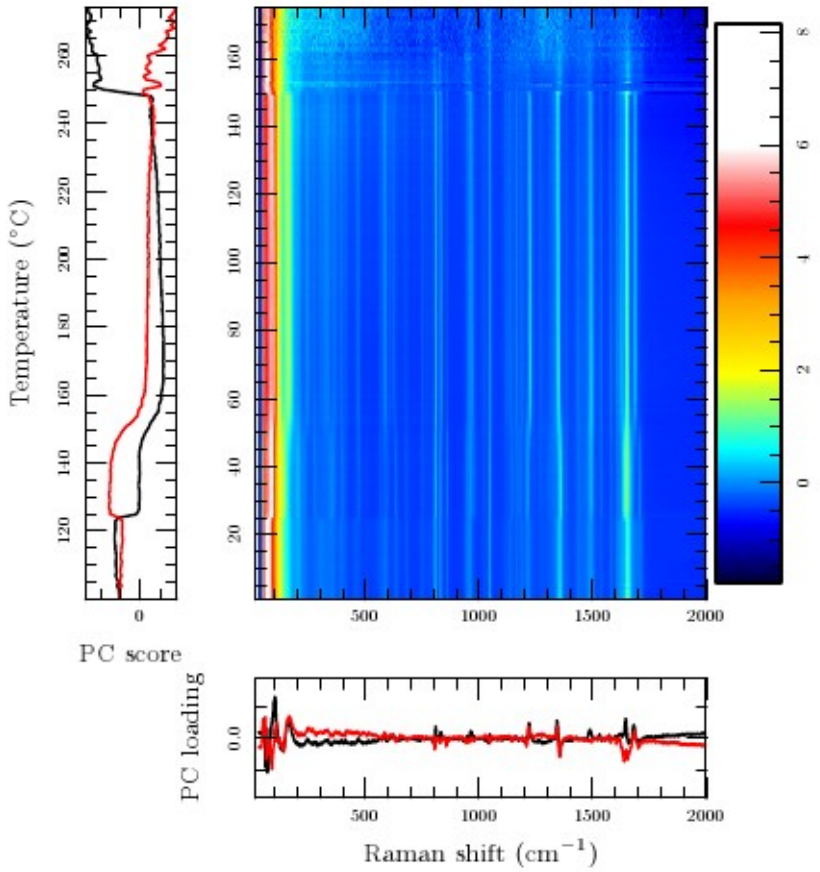

Figure 4.3a: In situ Raman spectra from heating amorphous form of nifedipine

Its worth mentioning here that the above transitions (i.e. amorphous → form II → form I) were obtained only when ground glass was added to the nifedipine sample before quenching to the amorphous form and the subsequent slow heating in order to induce nucleation.

This in essence further shows the robustness of the in situ Raman spectroscopic experimental set up used in this study as compared to DSC and VTXRPD where the introduction of the grounded glass cannot be achieved without further complications.

While figure 4.3b below, is the Raman spectra (phonon-mode only) obtained by using the method described by Zhou[136] et al. i.e. isolating form II by rapidly cooling the melt quenched sample of form I below 30°C (the sample was cooled down to 20°C in this study) before slowing reheating it back to the melting temperature. One major transformation were observed at 75°C (suggesting the following transition form II → form I).
This result is in agreement with the data obtained from the DSC experiment shown in figure 4.2b.

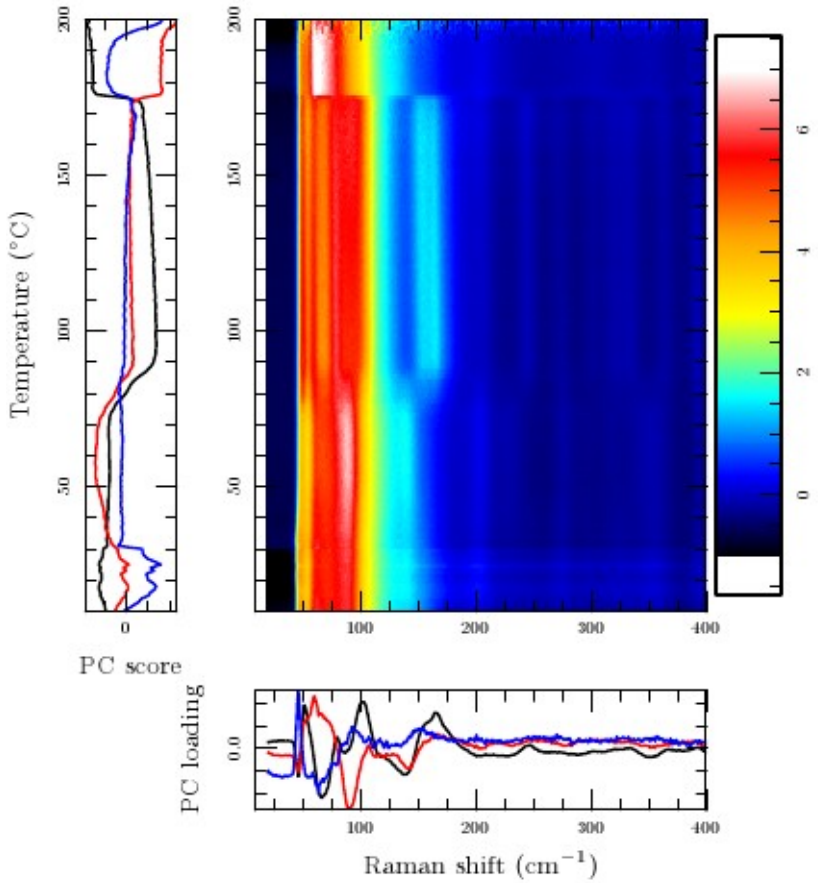

Figure 4.3b: In situ Raman spectra of reheating nifedipine form II (phonon-mode only)

Figure 4.3c below shows the Raman spectra of the molecular-mode region obtained from the same experiment (reheat of nifedipine form II).

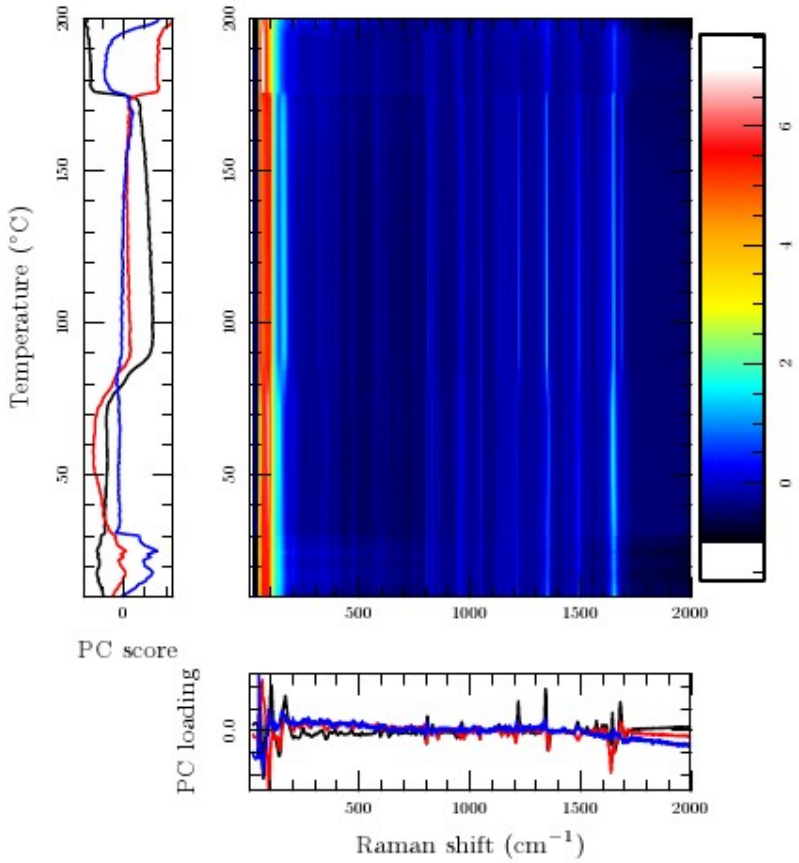

Figure 4.3c: In situ Raman spectra of nifedipine (molecular-mode region only)

While the changes are easily discernible by visual inspection in figure 4.3b, it is not so clear in the figure above (4.3c). Further showing the advantages of the phonon-mode in monitoring polymorphic transformation over the traditional fingerprint region.

Figures 4.4a and 4.4b below and overleaf shows the changes in the symmetric NO_2 stretching mode and the υ(C=O) vibration as the nifedipine sample is being heated respectively, showing the temperature dependent nature of the transformation.

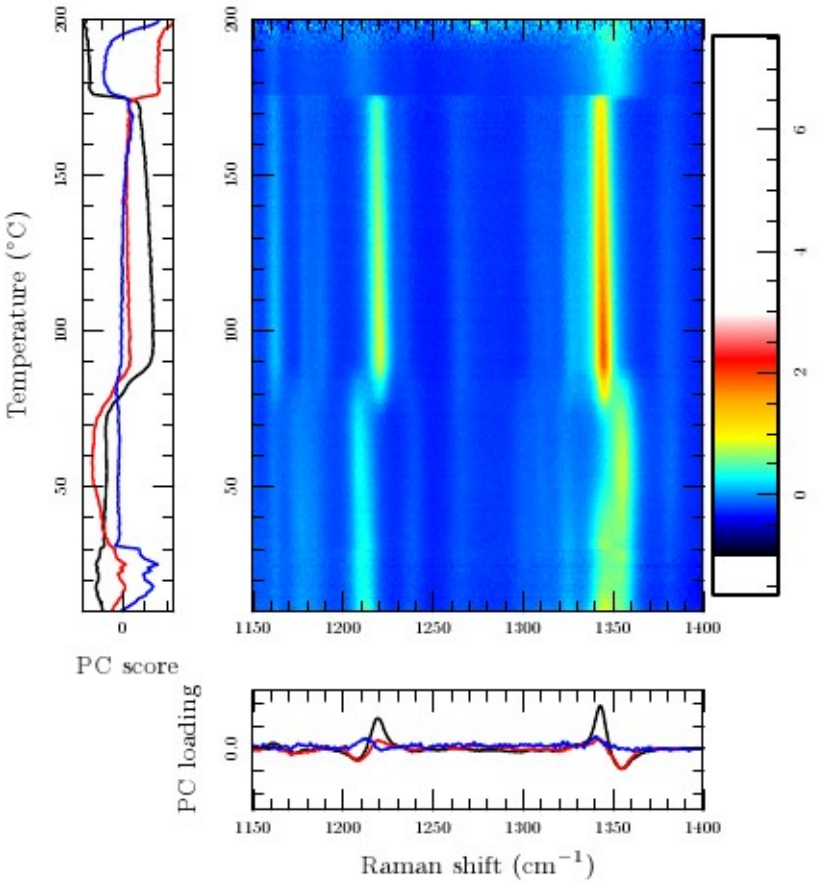

Figure 4.4a: Raman spectra showing changes in the symmetric NO_2 stretching mode

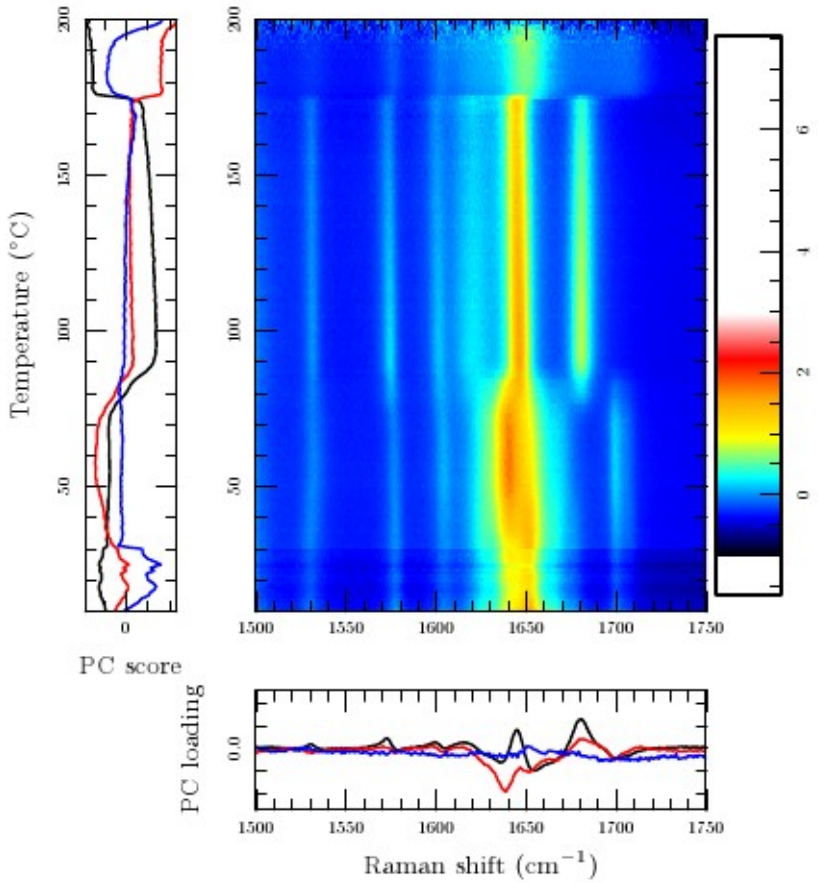

Figure 4.4b: Raman spectra showing changes in the υ(C=O) vibration stretching mode

These plots (figures 4.4a and 4.4b), seem to suggest that the hydrogen bonding motifs change between forms I and II.

Figure 4.5a (phonon mode, 30-400cm^{-1}) and figure 4.5b (molecular mode, 500-2000cm^{-1}) shown overleaf are the representative Raman spectra for the amorphous and crystalline forms of nifedipine obtained from both (heating the super-cooled melt and reheating form II) in situ experiments.

For the first time we report the low wave number (phonon-mode) Raman spectra of the different forms of nifedipine, emphasis in previous publications were placed on the fingerprint region (molecular mode). Absorptions in the phonon region are are very useful and more intense than the bands due to intra-molecular vibrations as they provide useful information about the lattice environment and as such this region is very useful in distinguishing between both amorphous and crystalline forms of nifedipine as clearly evident in the two figures.
While the different forms are easily distinguishable by visual inspection using the phonon-mode spectra (see figure 6a) the difference is not that obvious in the fingerprint region except for the peaks around 1600 -1620 cm^{-1}.

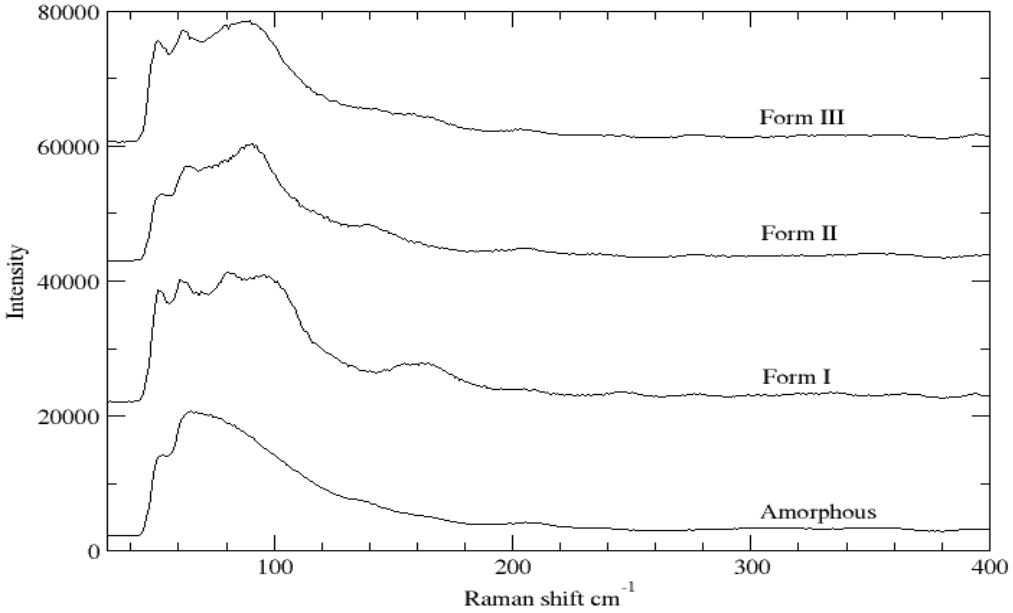

Figure 4.5a: Phonon mode Raman spectra of nifedipine

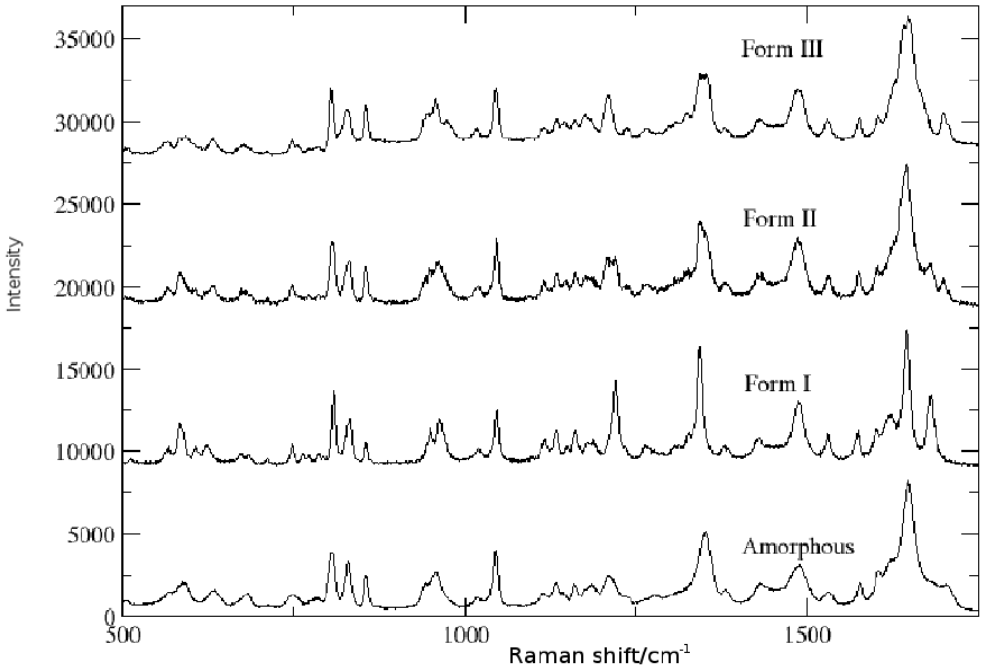

Figure 4.5b: Molecular mode Raman spectra of nifedipine

To further clarify the changes in the Raman spectra as the transition progresses during the heating of the amorphous form of nifedipine as well as the reheat of form II, we present a series of principal component projections obtained from the analysis of data from the in situ experiments.

Figures 4.6a (below) and 4.6b (overleaf) shows the projections of the entire spectral window (30-2000cm^{-1}) for the slow heating of the amorphous form (prepared from form I) and the reheat of form II respectively:

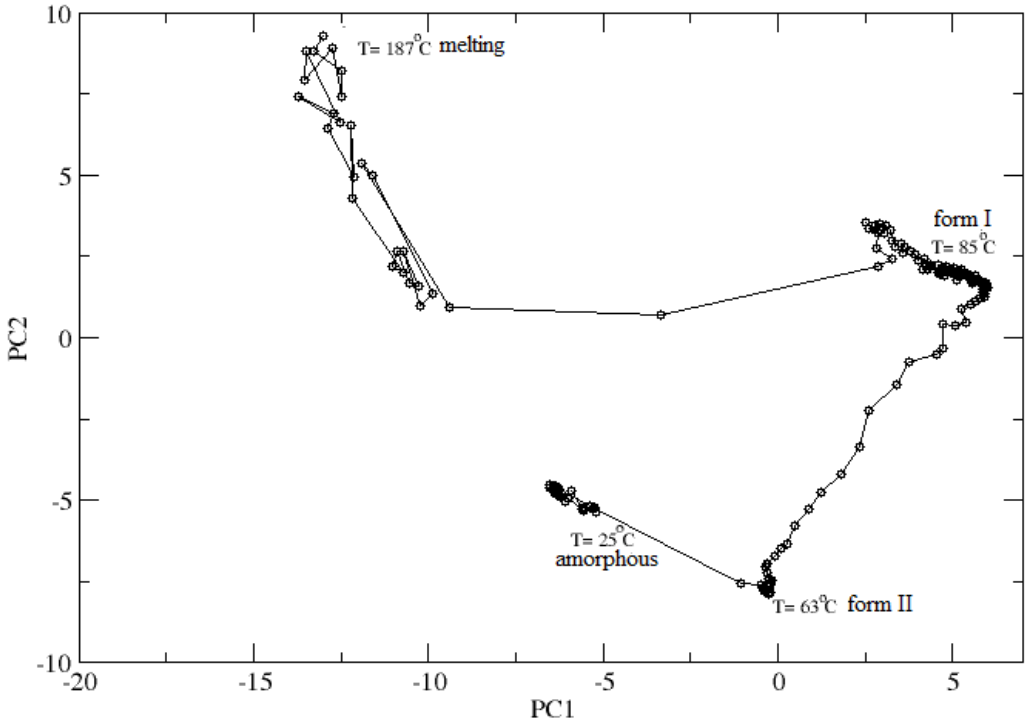

Figure 4.6a: Principal component projection of the heating of amorphous form of nifedipine

From figure 4.6a above, the PCA clearly shows three distinct cluster regions as the heating progresses, clearly supporting the observation from the inspection of the in situ experiment that amorphous nifedipine goes through an intermediate (form II) before transforming to the stable form I.

This is in agreement with results by other authors[137,138,144] and compares positively with the results that was obtained with the DSC analysis in this study.

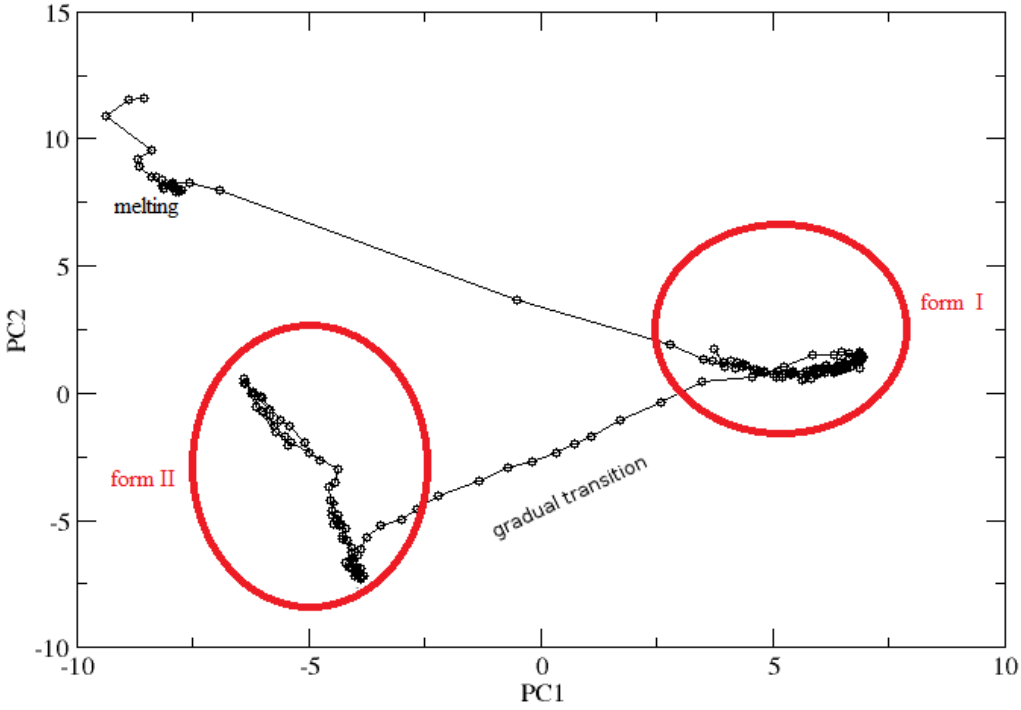

Figure 4.6b: Principal component projection of the reheating of nifedipine form II

Figure 4.6b shows the directionality of the experiment, particularly showing that there is a gradual rather than abrupt transformation before form II reverts back to form I.

Figures 4.7a (phonon region) and 4.7b (molecular region) below both provides a more precise representation of the spectra changes in the Raman data during the transition of the amorphous form nifedipine to form I via form II.

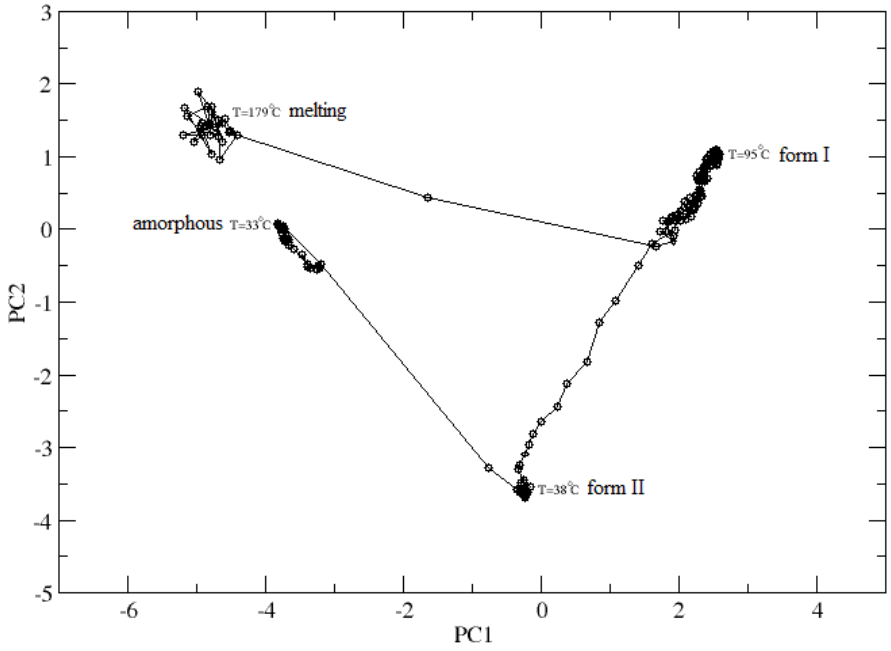

Figure 4.7a: Phonon-mode projection of the heating of amorphous form of nifedipine

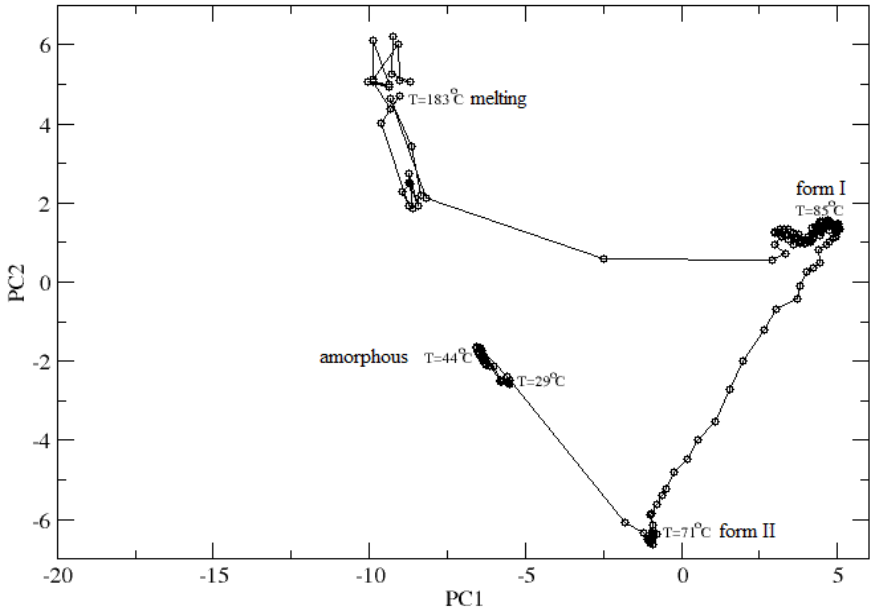

Figure 4.7b: Molecular-mode projection of the heating of amorphous form of nifedipine

As would be expected figures 4.8a and 4.8b (below) both projections of the reheat of nifedipine form II using the phonon-mode and molecular-mode regions respectively also shows a better interpretation of the transformations previously depicted in the in situ experiment, with the latter showing a smoother trend across the transitions.

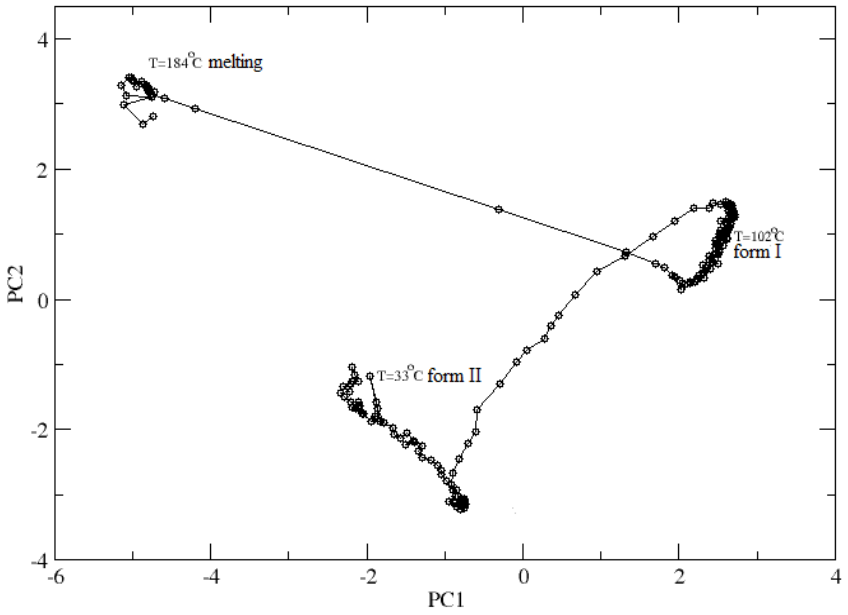

Figure 4.8a: Phonon-mode projection of the reheat of nifedipine form II

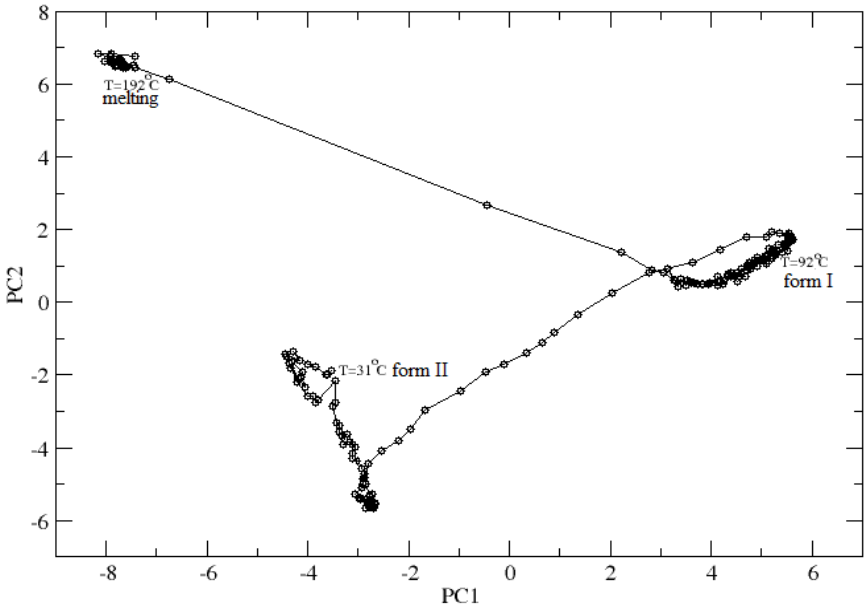

Figure 4.8b: Molecular-mode projection of the reheat of nifedipine form II

4.4.3 Variable temperature XRPD

The pattern obtained from the in situ XRPD analysis is shown below in figure 4.9a, two crystalline transformations at 90°C and 140°C were also observed upon heating the amorphous form (amorphous → form II → form I). Similar to what was obtained in the Raman experiments and in agreement with previously published results by Hirayama.[139] The difference in the transformation temperature we ascribed to the slightly different experimental conditions employed in the two techniques.

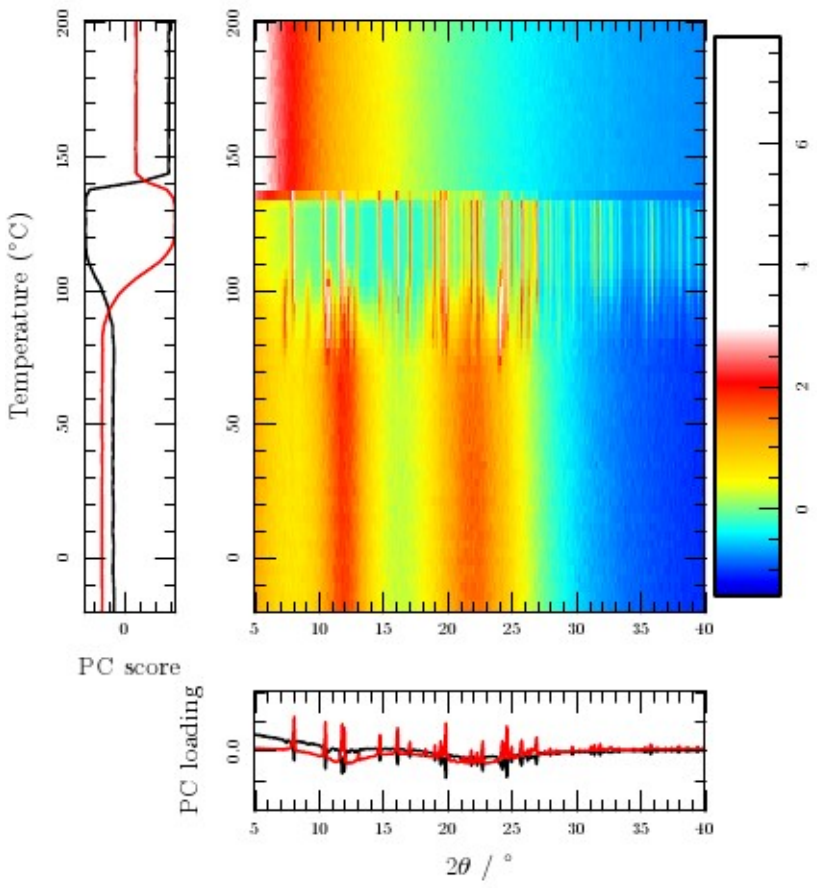

Figure 4.9a: In situ XRPD pattern showing the crystallisation of amorphous nifedipine

The pattern obtained from the slow heating of nifedipine form II using the method described by Zhou et al,[136] is shown in figure 4.9b below: with two transformations at 55˚C and 110˚C respectively (see left hand side of figure 4.9b).

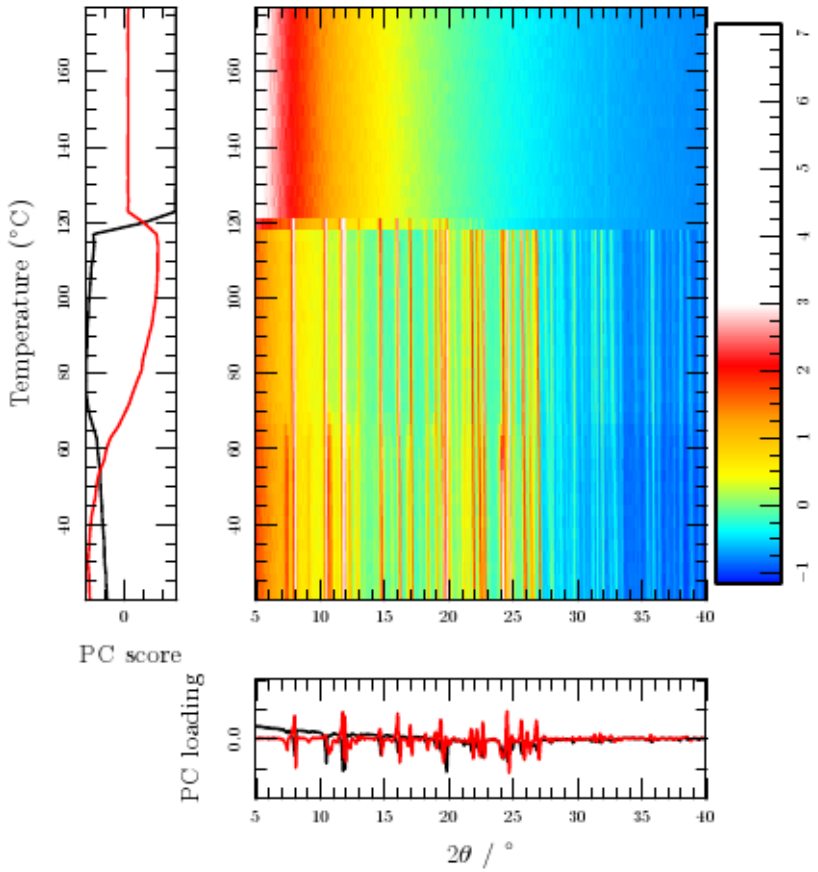

Figure 4.9b: In situ XRPD pattern from the reheating of nifedipine form II

Further analysis of the pattern above showed that nifedipine form II undergoes a slow transformation with co-existence of two forms as highlighted by the PCA back to form I via two similar 'intermediates' (60˚C and 66˚C, see appendix). These intermediates appear to be a mixture of both forms (1 and II), we suggest here that the inability of these intermediates to differentiate into distinct crystal patterns might be do to incomplete nucleation, a problem we initially encountered in the in situ Raman experiment but was remedied by the addition of ground glass (see experimental section). While this is easily achievable in the experimental set up for the Raman, it is not easily applicable with variable temperature XRPD experiment without introducing complications.

But it is also worth mentioning that while these intermediates occur with the heating of form II, it was not observed in the heating of amorphous nifedipine, thereby suggesting that there could be new form(s) present in between forms II and I as previously reported.[137,141,144]

Principal component analysis was further deployed to differentiate between the patterns as the experiments (in situ XRPD) progresses in both case i.e. heating amorphous nifedipine and the subsequent reheat of form II. The results are shown in figures 4.9c and 4.9d below.

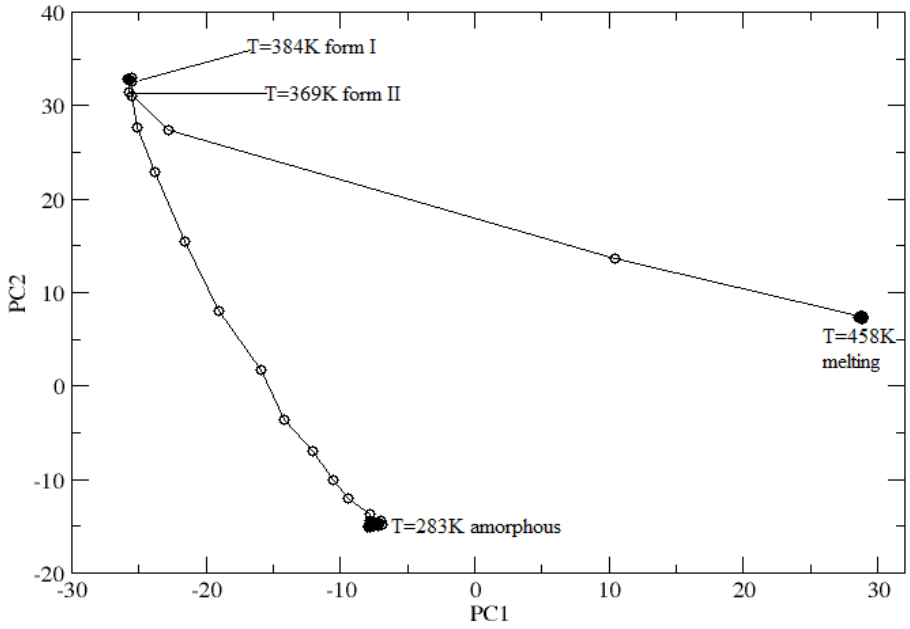

Figure 4.9c: Principal component projection of the heating of amorphous nifedipine (VTXRPD)

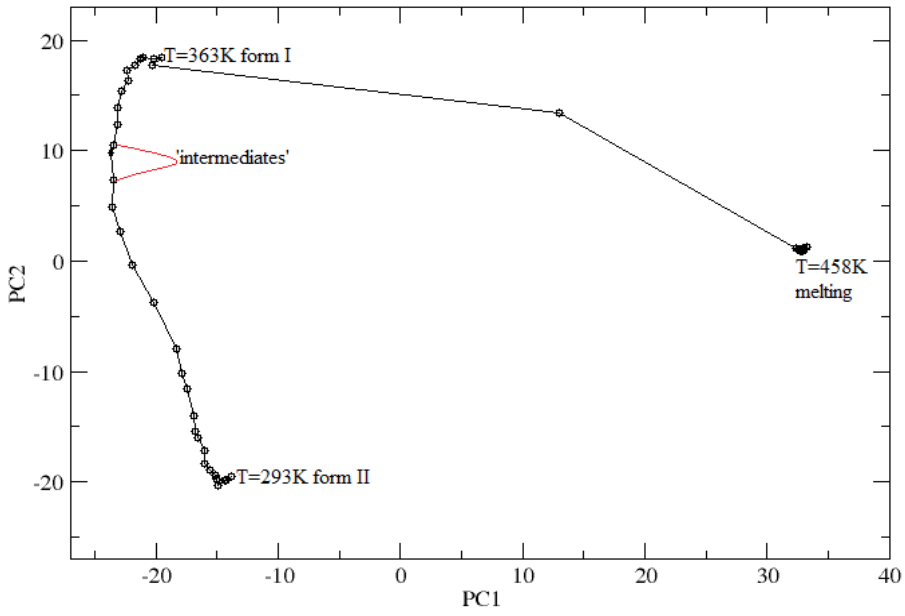

Figure 4.9d: Principal component projection from the reheating of nifedipine form II (VTXRPD)

Both projections i.e. figures 4.9c and 4.9d, are in agreement with patterns obtained from both experiments (VTXRPD).

Conclusion

We have shown that Confocal Raman spectroscopy/microscopy (coupled with hot-stage microscopy), can be used as a veritable tool in screening for polymorphism in pharmaceutical materials i.e. nifedipine; results obtained from the in situ Raman experiments are in agreement with those obtained from other techniques used in this study (DSC and XRPD) and also with those previously published in literature.

We have also reported for the first time the phonon-mode Raman spectral of nifedipine; previous studies only focused on the traditional fingerprint region. Data analysis is relatively straightforward, with visual inspection of the phonon-mode spectra reasonably sufficient to distinguish between both amorphous and crystalline forms.

The Raman analysis also afforded us the unique advantage of being able to monitor various structural/molecular changes in nifedipine such as the symmetric NO_2 stretching mode, the υ(C=O) vibration and the hydrogen bonding motifs as the heating progressed.

Sample requirements are of the order of a milligram or less. With further data treatment using principal component analysis making it easier to understand and interpret results.

5.0 Polymorphism in Tolbutamide

5.1 Monitoring polymorphic transformations in tolbutamide using constrained crystallisation

Abstract

The polymorphic transitions from amorphous tolbutamide were studied using in situ confocal Raman spectroscopy combined with Variable Temperature X-Ray Powder Diffraction (VTXRPD) and Differential Scanning Calorimetry (DSC).

Three polymorphic transformations were observed during the slow heating of the amorphous solid form of tolbutamide monitored using Raman spectroscopy; amorphous→ form IV → form II→ form I respectively.

Similar results were obtained from VTXRPD experiments, with the amorphous solid transforming first to form IV (33˚C), then to form II (48˚C) and back to the as received form I (99˚C).

While the DSC data obtained indicated an endothermic event at 83˚C, followed by two weaker endotherms at 102.3˚C and 117.9˚C respectively, before the final melting of the sample at ~128.6˚C (see details and plot in appendix).

Principal Component analysis (PCA), was used to analyse the data obtained from the Raman in situ experiment as well as the patterns obtained from the VTXRPD experiment.

5.2 Introduction

Tolbutamide an oral hypoglycemic drug used in the treatment of type II diabetes has been extensively studied,[154-168] and reported to exhibit polymorphism. Five polymorphs (I^L, I^H, and II-IV) of tolbutamide have been isolated and characterised, but while previous studies have focussed on the use of techniques such as DSC, XRPD, Infra red, solid state NMR and thermomicroscopy in monitoring the polymorphic behaviour of tolbutamide, very few studies have employed the use of Raman spectroscopy and no previous study of polymorphism in tolbutamide using in situ Raman spectroscopy has been reported.

While Simmons et al.[154] isolated two forms (A and B) of tolbutamide, Traue et al.[160] and Burger[155] suggested the presence of four different polymorphs, I-IV. Simmons's forms A and B were found to be identical to Burger's forms I and III respectively.[168]

All four forms reported by Burger have been fully characterised; I, II and III from single crystal x-ray data, while form IV was solved from conventional x-ray powder diffraction data.[168]

In 2009, Hasegawa et al.[165] confirmed the existence of conformational polymorphism in form I of tolbutamide using DSC and XRPD. Subsequently Burger's form I was renamed I^L while its conformer was named I^H. Form I^L transforms to form I^H at 38°C upon heating.[167] Also forms II, III and IV have been reported to transform into form I^H at 100°C, 106°C and 88°C respectively when heated.[167,168], while form IV also transforms into form II at 80°C.[168]

Thirunahari et al., confirmed the melting points of both forms I^H and II as 128°C and 117°C respectively.[167]

The main objective of this study therefore, is to carry out a novel study of the polymorphic transformations obtainable from amorphous tolbutamide using the constrained crystallisation approach (slow heating of the amorphous form), monitoring the observed transitions using in situ Raman spectroscopy complemented with VTXRPD and DSC.

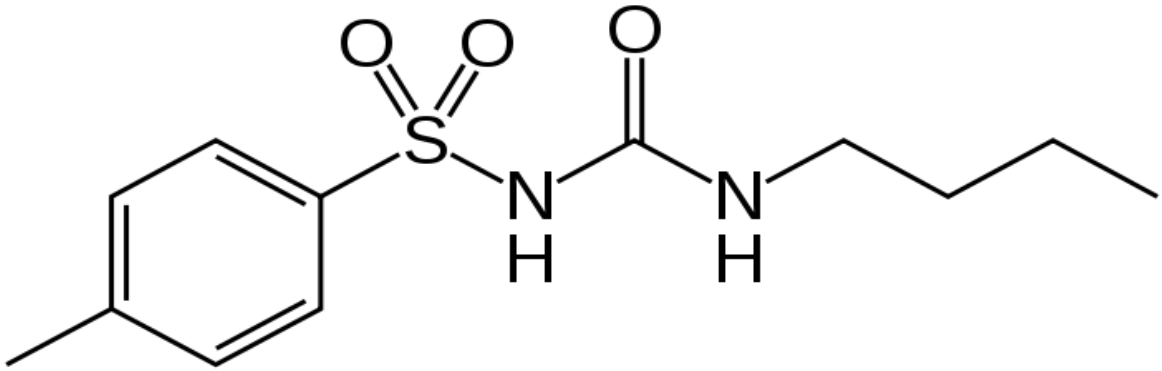

Figure 5.1: Molecular structure of tolbutamide

5.3 Experimental

5.3.1 Materials

Tolbutamide was purchased from Sigma-Aldrich Dorset UK was used in all experiment as received. The as-received sample was shown by comparison of the XRPD pattern with the reported crystal structure of Hasegawa et al.[165] to be form I^{L}.

5.3.2 DSC

A Q2000 series differential scanning calorimeter, manufactured by TA Instrument, Crawley, England, was used for the DSC analysis. Approximately 4mg of tolbutamide was first heated at 10°C/minute to 145°C, cooled down to -40°C at 10°C/minute before subsequently heating the supercooled sample slowly at a heating rate of 1°C/minute back to 145°C (modulating the temperature for 60 seconds every degree.

5.3.3 XRPD

XRPD patterns were collected on a Bruker D8 diffractometer system (Bruker AXS, Madison, WI, USA), operating in a Debye-Scherrer geometry, at a wavelength (λ) of 1.54059Å, 40kV voltage, and a current of 40mA, using a LynxEye detector. The sample was heated using a Cryostream plus controller (Oxford Cryostreams Ltd. Hanborough Oxford OX29 8LN) at 3°C/minute from -20°C to 151°C and patterns were collected at each temperature step (overall accumulation time of 8 minutes) at a scan time of 0.3 second.

5.3.4 Raman

Raman spectra were collected using a confocal Horiba-Jobin-Yvon LabRAM system (Horiba-Jobin-Yvon Ltd Middlesex U.K.), using a 600 lines/mm grating and a 785 nm excitation laser. A Synapse CCD detector was employed. Temperature control was achieved using a Linkam hot-stage (Linkam Scientific Instrument Ltd, Surrey U.K).

The tolbutamide sample was first heated to 145°C, held at this temperature for 2 minutes and quenched on a surface that had been pre-cooled to -100°C with liquid nitrogen.

The super-cooled sample was then heated at stepwise 1°C/ minute intervals, and were held at temperature during data collection (typically 10–20 seconds maximum). Data sets were collected every 1°C. Sample, approximately 1 mg was placed on a microscope slide without a cover slip.

5.3.5 Data Analysis

The Raman spectra obtained were subjected to PCA analysis using 'PCA packages' within the 'R' programming suite. Raw spectra (variance-scaled and mean-centred before analysis) were used, the phonon spectra range/mode (30-400cm^{-1}) and molecular fingerprint range/mode region (500-2000cm^{-1}) were used for the analysis.
The most important principal components (PCs) were determined from percentage variance plots and were used to investigate trends in the spectra features of the Raman data. PC1, PC2 and PC3 were selected, they accounted for over 90% variance.

5.4 Results and Discussion

5.4.1 Confocal Raman spectroscopy

The in situ Raman spectra of the slow heating of the amorphous solid sample of tolbutamide is shown in figure 5.2 below (intensities are in colours, PC1 is black, PC2 red, PC3 blue.):

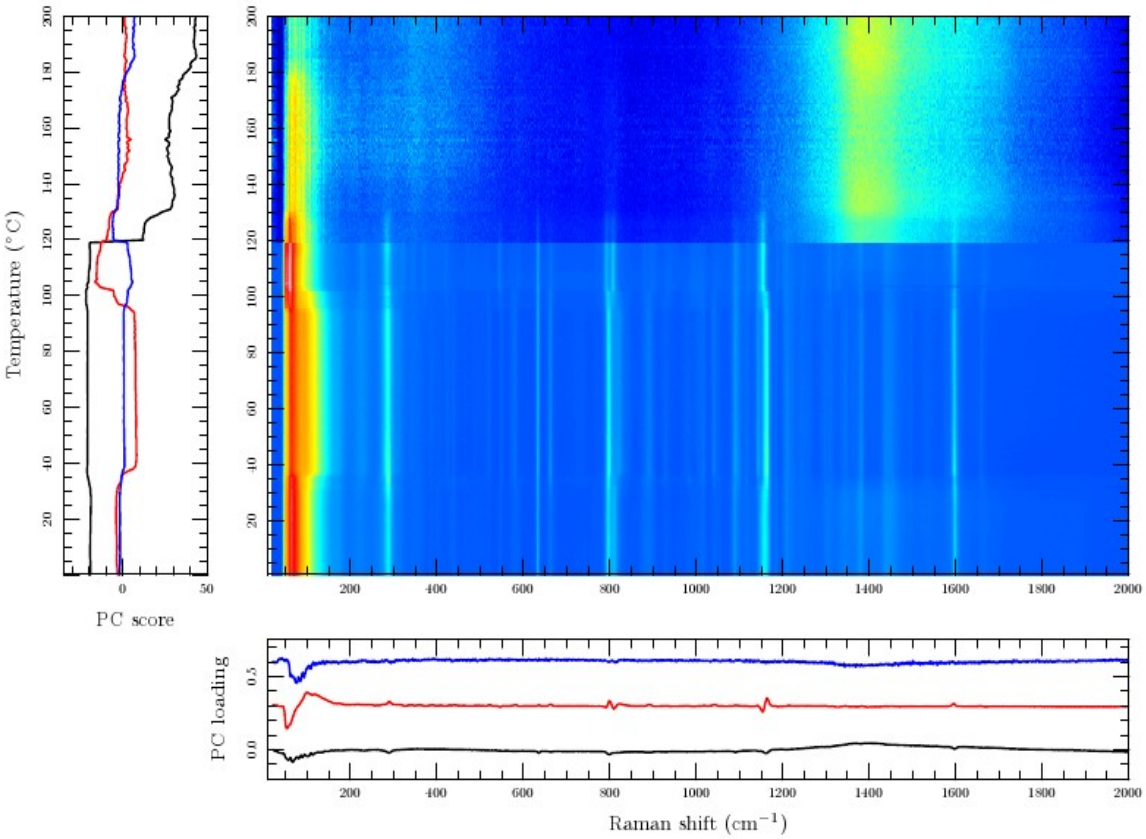

Figure 5.2: Variations in the Raman spectra (top right), PC1, PC2 (top left) with temperature and loadings (bottom), for the slow heating of amorphous tolbutamide

Visual inspection clearly shows transformations occurring has the sample is been heated from the initial amorphous phase until it starts to melt (non-abruptly) around 128°C, which is in agreement with previously published results.[167,168]

Regions within the experimental spectra window that show prominent changes in the figure above include the phonon-mode (20-350 cm^{-1}), and also in molecular-mode region i.e. 780-850cm^{-1}, 1120-1190cm^{-1} and 1580-1620cm^{-1} respectively.

To further show the transformations occurring as the in situ experiment progresses and to efficiently reduce the effect of data complexity, principal component analysis was deployed,[169] figures 5.3-5-6 below (and overleaf) show plots of the changes in the Raman spectra (Raman shift) as function of both the principal components and temperature for four different regions of the spectral window earlier mentioned (with the corresponding peaks assigned[170]).

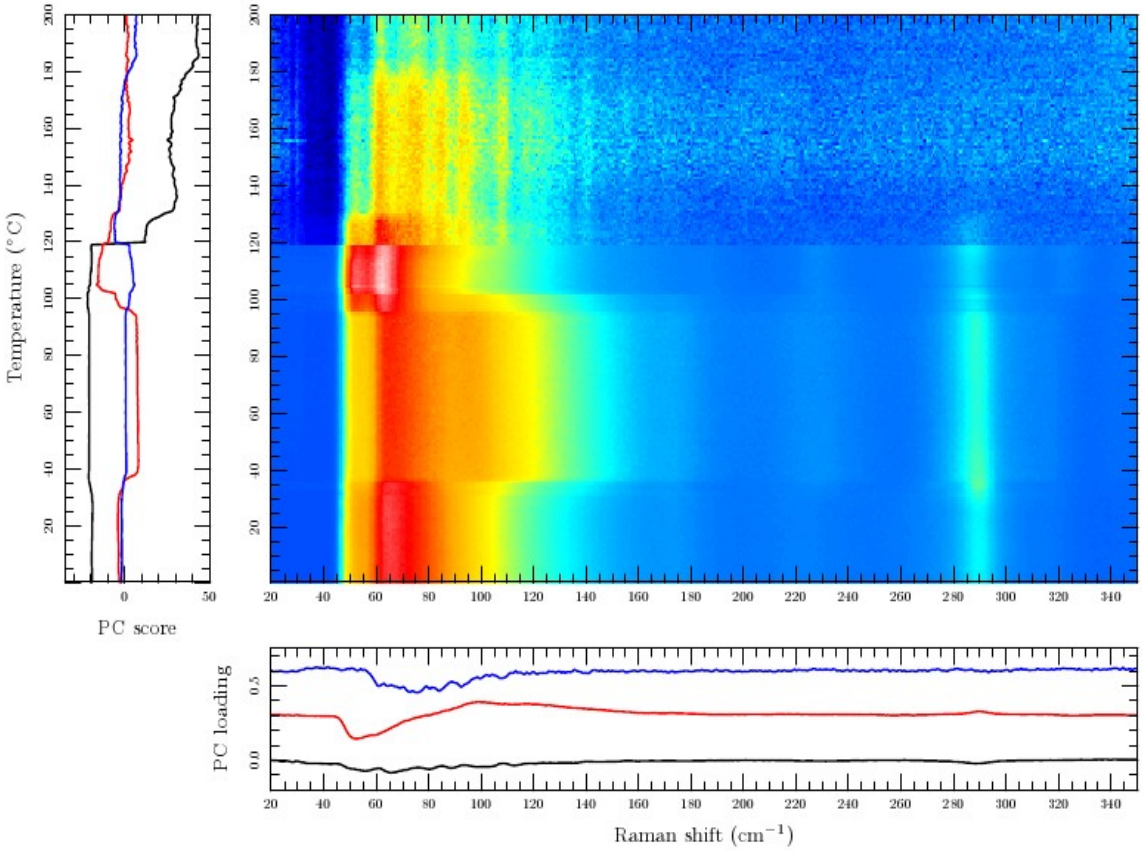

Figure 5.3: Variations in the Raman spectra (top right), PC1, PC2 (top left) with temperature and loadings (bottom), for the low wave number bands (20-340cm^{-1})

The figure above shows the changes in the low wave number or phonon-mode bands as the heating progresses, these bands due to lattice vibrational modes (this region provides useful information about lattice environment), this is the first time that these data have been presented for this system.

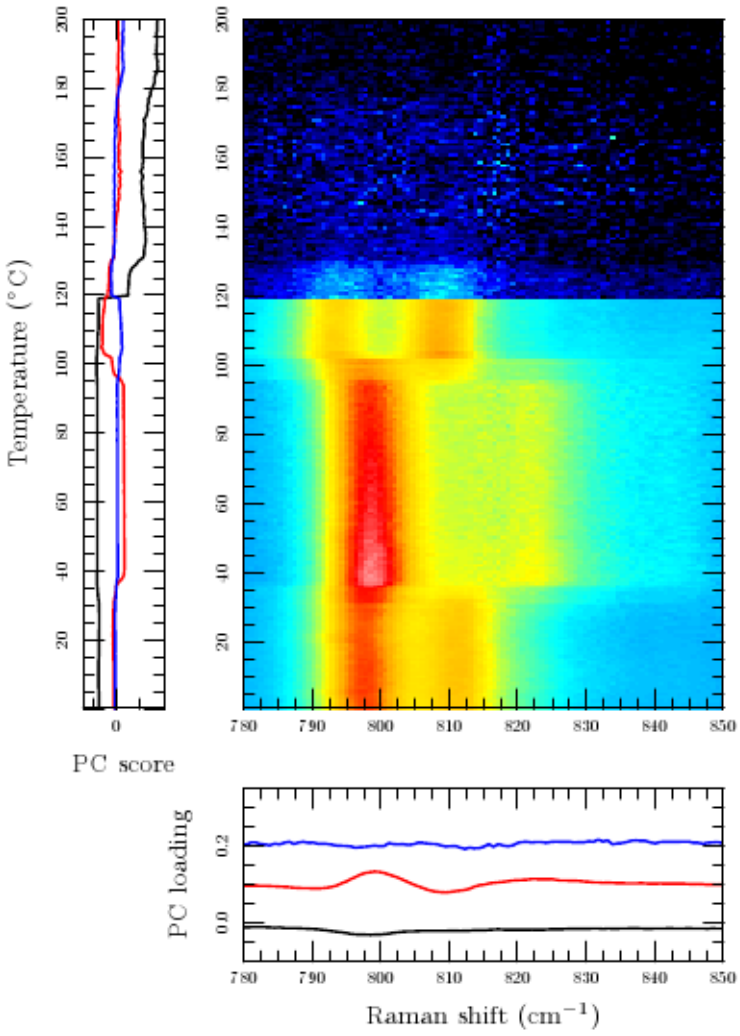

Figure 5.4: Variations in the Raman spectra (top right), PC1, PC2 (top left) with temperature and loadings (bottom), due to the O=N-C stretching vibrations (780-825cm^{-1})

Similarly, figure 5.4 shows the changes in the stretching vibrations due to the O=N-C bond in the molecule as the transition progresses.

While figure 5.5 below shows the changes in the symmetric phenyl breathing mode (1120-1190cm^{-1}) during the course of the experiment.

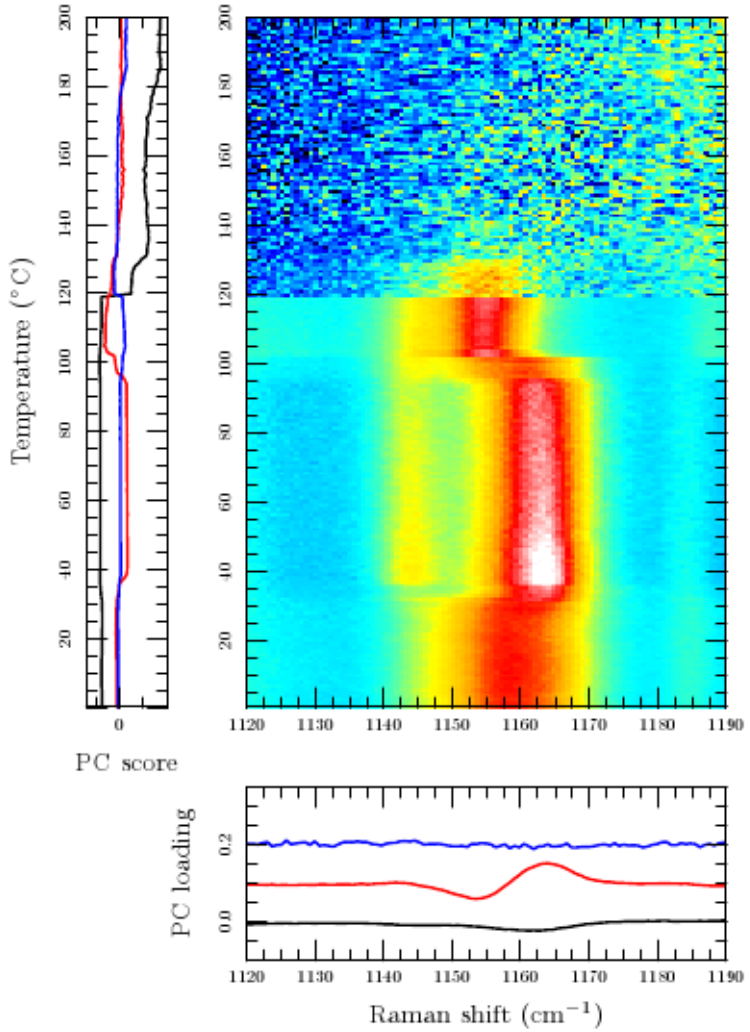

Figure 5.5: Variations in the Raman spectra (top right), PC1, PC2 (top left) with temperature and loadings (bottom),for the symmetric phenyl breathing mode (1120-1190cm^{-1})

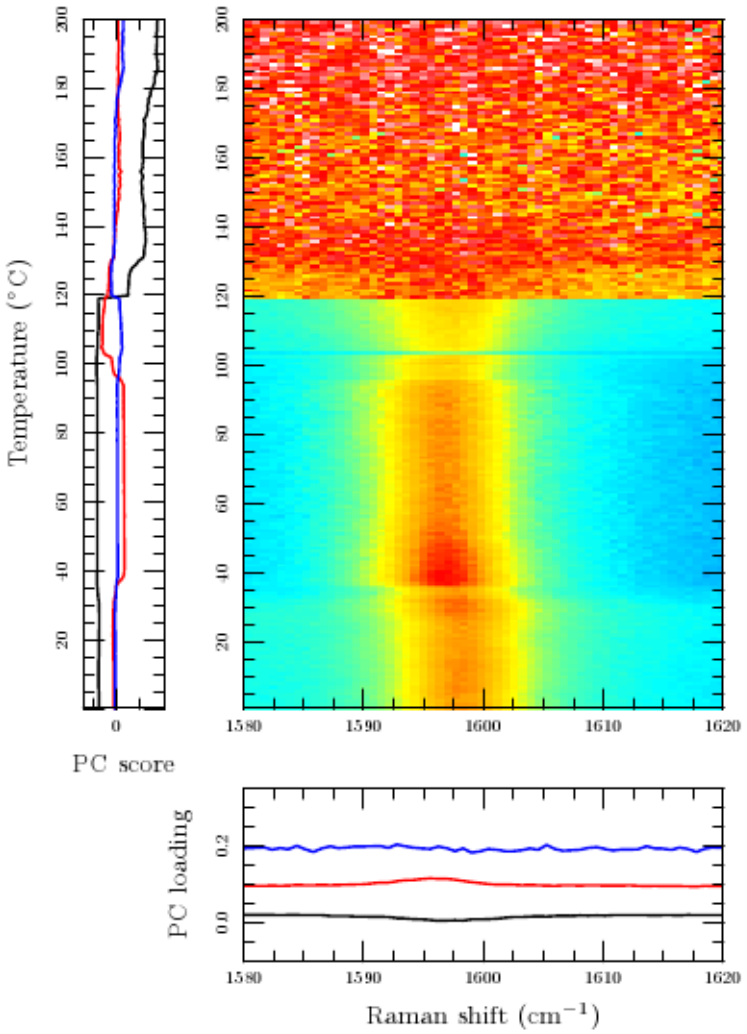

Figure 5.6: Variations in the Raman spectra (top right), PC1, PC2 (top left) with temperature and loadings (bottom), for the symmetric C=C stretching vibrations (1580-1620cm^{-1})

Figure 5.6 above also shows the variations in the C=C stretching vibrations in the molecule during the experiment.

In summary therefore, the constrained crystallisation approach monitored using in situ Raman spectroscopy has allowed a very rapid screen of this known polymorphic system, uncovering a very rich behaviour.

5.4.2 X-ray powder diffraction

The x-ray powder patterns obtained from the heating of amorphous sample of tolbutamide is shown in figure 5.7 below (using principal component analysis, PC1 is black, PC2 red, PC3 blue and PC4 is green) : indicating the following transitions, amorphous→form IV→form II→form I^{L} (patterns compared with those published by Kimura et al.)[168]

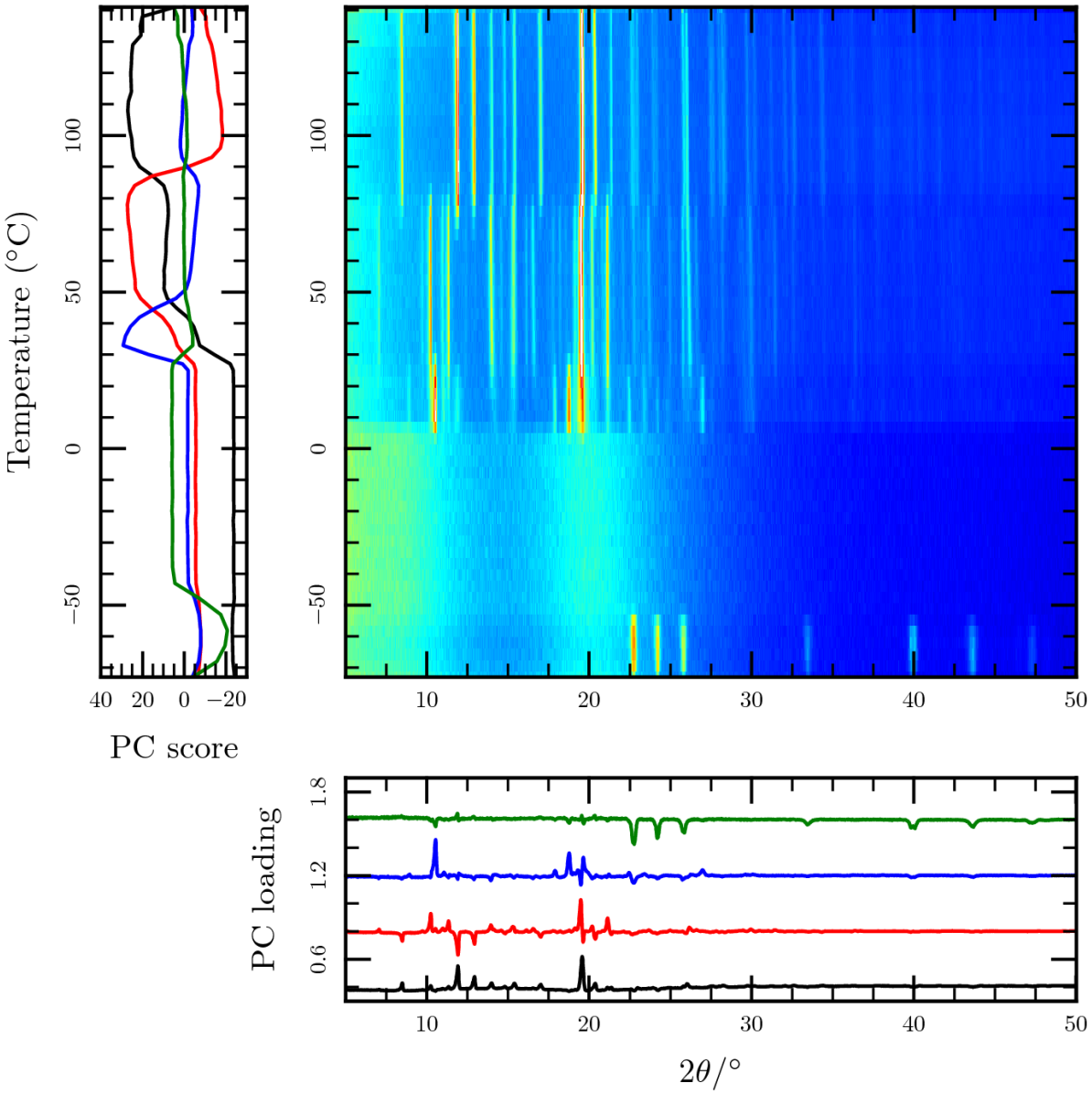

Figure 5.7: Variations in patterns (top right), PC1, PC2 (top left) with temperature and loadings (bottom), for the VTXRPD experiment

Visual inspection of figure 5.7 clearly shows the transformations as the amorphous sample is being heated, with the transitions being more apparent than in the earlier discussed Raman experiment (expected given XRPD probes crystalline order and Raman probes molecular vibrations in general). With the sample eventually melting at temperature expected from literature (128°C)[168] and also in agreement with results obtained from the Raman experiment above.

Although it is worth mentioning that the temperature of transformation between the different forms are lower in the VTXRPD experiment as compared with the in situ Raman analysis, this is likely due to larger sample volume (used in the VTXRPD) and therefore greater opportunities for new phases to nucleate.

Also the experimental set up used for XRPD analysis encouraged the formation of ice on the capillary tube used, hence the appearance of ice peaks in figure 5.7 at low temperature. Longer experiment can be used to remedy this resulting in lower temperature resolution.

Conclusion

We report for the first time the monitoring of polymorphic transformations in tolbutamide using in situ confocal Raman spectroscopy (using the constrained crystallisation approach), the results deduced from the Raman spectroscopic analysis of the experiments comparing favourably well with those obtained from traditional methods (DSC and XRPD) used to characterise polymorphic systems.
As with the previous chapter, we were able to monitor the temperature dependence of the transitions using Raman spectroscopy.
The in situ study described above is easy, fast and automated. Very small amounts of sample is required and the results obtained provides molecular and solid-state information which is very useful in structural elucidation.

6.0 Polymorphism in Imipramine Hydrochloride

6.1 Polymorphic fingerprinting using phonon-mode Raman spectroscopy

Abstract

We report for the first time the existence of polymorphism in the antidepressant drug imipramine hydrochloride. Using constrained crystallisation from the amorphous solid state to kinetically trap polymorphs via Oswald's rule of stages (this approach has proved highly effective in our previous chapters), two new polymorphs of imipramine hydrochloride were uncovered in our first attempt at screening, using in-situ Raman spectroscopy/microscopy.

The as-received form is therefore labelled form I, with form II being that which crystallises directly from the melt and form III crystallising from form II. Our results was supported by additional analysis using Variable Temperature X-ray Powder Diffraction (VTXRPD) and thermal studies using Differential Scanning Calorimetry (DSC).

Patterns from the VTXRPD experiment showed two transformations at 69°C and 75°C (the as received) via an intermediate at 30°C (mixture of amorphous and crystalline). While the DSC data obtained suggests the presence of at least two polymorphs: a low melting form (melting point at ~161.65°C) and a high melting form, with a melting point around 173.3°C respectively.

Principal Component analysis (PCA), was used to further explain the trends observed in data obtained from the Raman in situ experiment. This analysis affords a quick overview and identification followed by a more detailed appraisal.

6.2 Introduction

In this study, Imipramine hydrochloride was selected as a test case: no polymorphism has been reported to date for this system, and a single crystal structure of the known (commercially available) form has been previously determined.[171]

Imipramine is a tricyclic antidepressant, formulated as the hydrochloride (figure 6.1 overleaf) salt to enhance solubility. By slowly heating the amorphous solid form (monitored using Raman spectroscopy) of imipramine hydrochloride we were able to kinetically trap its polymorphs via the Oswald's rule of stages.[21,172]

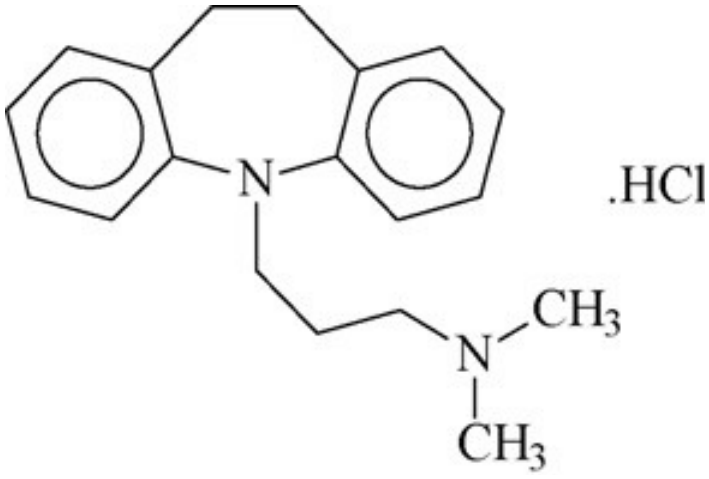

Figure 6.1: Molecular structure of imipramine hydrochloride

A previous publication[173] involving mechanical energy calculations and molecular dynamics simulations showed that the side chain folds above one of the phenyl rings, two different side chain conformations were obtained during the simulations in vacuo. Their results also concluded that tricyclic antidepressant such as imipramine hydrochloride have flexible molecules which readily may cross energy barriers between different conformations. The above findings was a major reason for choosing imipramine hydrochloride for this study.

6.3 Experimental

6.3.1 Materials

Imipramine hydrochloride was purchased from Sigma-Aldrich Dorset UK was used in all experiment as received.

6.3.2 DSC

A Q2000 series differential scanning calorimeter, manufactured by TA Instrument, Crawley, England, was used for the DSC analysis. Approximately 4mg of imipramine hydrochloride was first heated at 10°C/minute to 185°C, cooled down to -40°C at 10°C/minute before subsequently heating the supercooled sample quickly at different heating rates of 1, 2, 5,10, 20, 25, 50, and 100°C/minute back to 200°C. This was done to investigate the effect of heating the amorphous material, the 'quenching' approach allowed the amorphous form to be isolated.

6.3.3 XRPD

XRPD patterns were collected on a Bruker D8 diffractometer system (Bruker AXS, Madison, WI, USA), operating in a Debye-Scherrer geometry, at a wavelength (λ) of 1.54059Å, 40kV voltage, and a current of 40mA, using a LynxEye detector. The sample was heated using a Cryostream plus controller (Oxford Cryostreams Ltd. Hanborough Oxford OX29 8LN) at 3°C/minute from -10°C to 151°C and patterns were collected at each temperature step (overall accumulation time of 8 minutes) at a scan time of 0.3 second.

6.3.4 Raman

Raman spectra were collected using a confocal Horiba-Jobin-Yvon LabRAM system (Horiba-Jobin-Yvon Ltd Middlesex U.K.), using a 600 lines/mm grating and a 785 nm excitation laser. A Synapse CCD detector was employed. Temperature control was achieved using a Linkam hot-stage (Linkam Scientific Instrument Ltd, Surrey U.K).

The imipramine hydrochloride sample was first heated to 185°C, held at this temperature for 2 minutes and quenched on a surface that had been pre-cooled to -100°C with liquid nitrogen.

The super-cooled sample was then heated at stepwise 1°C/ minute intervals, and were held at temperature during data collection (typically 10–20 seconds maximum). Data sets were collected every 1°C. Sample, approximately 1 mg was contained between a glass microscope slide and cover slip, to allow the amorphous form to be isolated.

6.3.5 Data Analysis

The Raman spectra obtained were subjected to PCA analysis using 'PCA packages' within the 'R' programming suite. Raw spectra (variance-scaled and mean-centred before analysis) were used, the phonon spectra range/mode (30-400cm^{-1}) and molecular fingerprint range/mode region (500-2000cm^{-1}) were used for the analysis. The splitting of the data into these two ranges was to allow for a better comparison of the phonon-mode region with the conventional fingerprint region, thus showing the usefulness of the former, which is being emphasised in this study.
The most important principal components (PCs) were determined from percentage variance plots and were used to investigate trends in the spectra features of the Raman data. PC1, PC2 and PC3 were selected as they accounted for over 99% variance.

6.4 Results and Discussion

6.4.1 DSC analysis

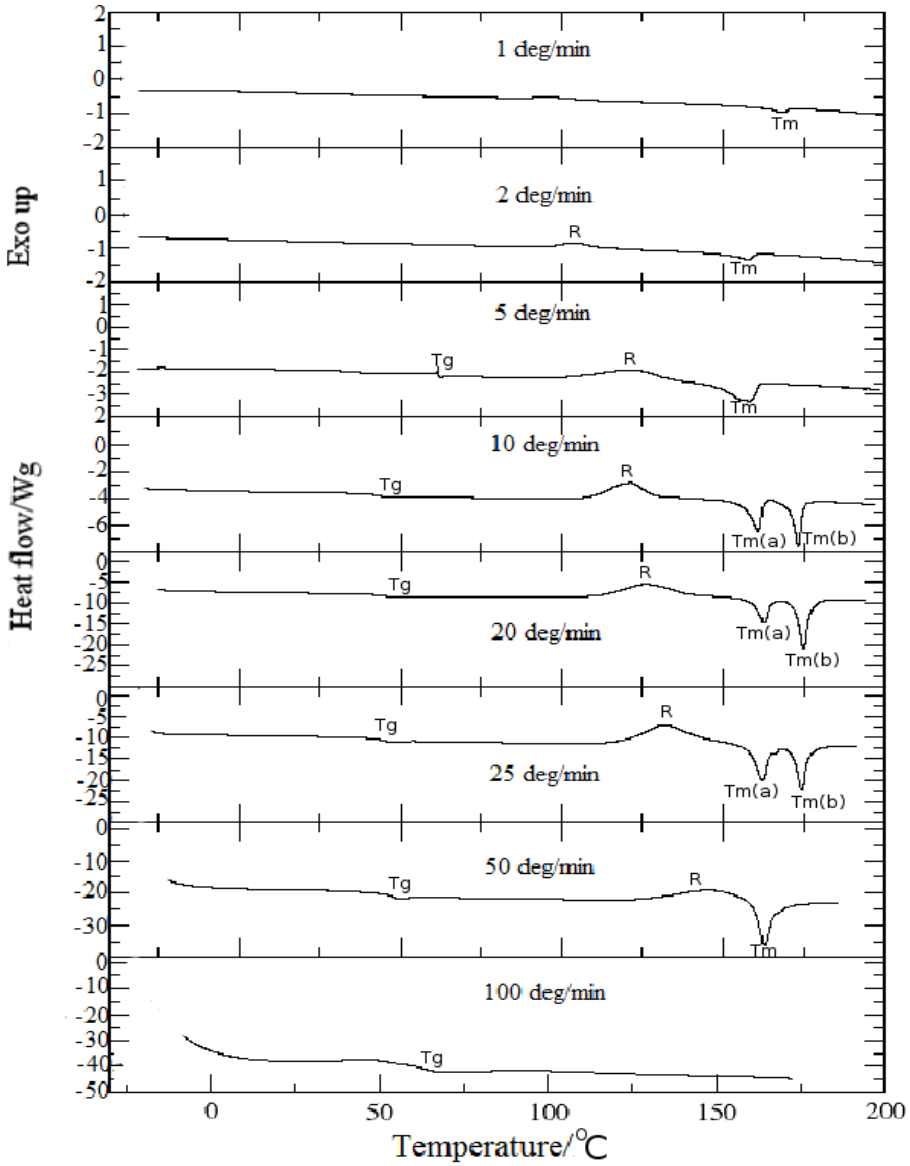

Figure 6.2: DSC plot obtained from the heating of the supercooled melt of imipramine HCl at different temperature; 1, 2, 5, 10, 20, 25, 50 100˚C/minutes (Key: Tg → glass transition temperature, R → recrystallisation peak, Tm → melting temperature: while a is the first melting and b is the second melting)

Figure 6.2 overleaf shows the DSC trace obtained from heating the super-cooled melt of imipramine hydrochloride at different temperature; 1, 2, 5, 10, 20, 25, 50 100°C/minutes, clearly suggesting that two polymorphs can be obtained from the melt using different heating rates (as shown in fig. 6.2, with two melting temperature/points (at intermediate heating rates of 10, 20 and 25°C respectively), thus indicating the existence of polymorphism in the compound, which was previously unreported. The isolation of the glass transition temperature in the experiment (not very clear at 1 and 2°C heating rates) indicated that the amorphous form of imipramine hydrochloride was obtained prior to heating. It is also interesting to note that the recrystallisation peak shifts as the heating rate changes, appearing at higher temperature as the heating rate increases.

6.4.2 Confocal Raman spectroscopy

The in situ Raman spectra of the slow heating of the amorphous solid sample of imipramine hydrochloride is shown in figure 6.3 below i.e. the phonon-mode region only (intensities is in colours, PC1 is black, PC2 red):

Simple visual inspection of figure 6.3 suggests three separate events during the experiment, but more detailed analysis (with PCA) revealed the following transitions: amorphous→ form I (60˚C) →form II (74˚C) →form III (98˚C) after which the sample melts around 173˚C.

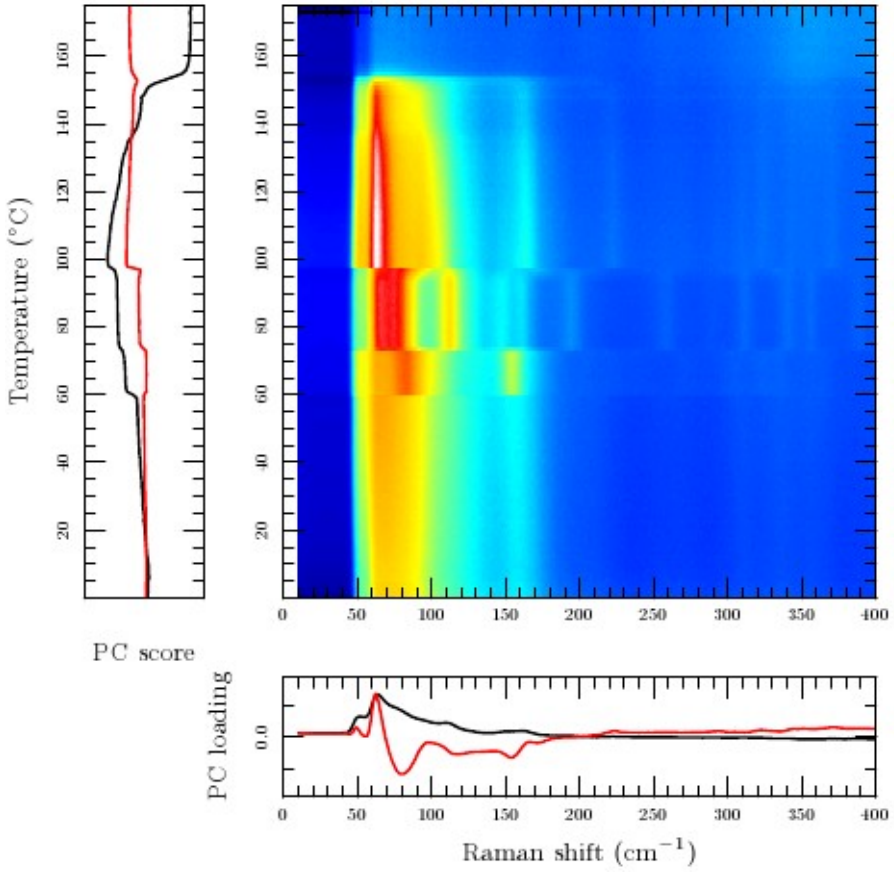

Figure 6.3: In situ Raman spectra of imipramine hydrochloride (phonon-mode region only)

The principal component projections of the Raman data obtained from the in situ experiment further elaborates the changes that occur as the solid amorphous form of imipramine hydrochloride is being slowly heated: Figure 6.4 below below shows a plot of the changes in the Raman spectra (Raman shift) as function of both the principal components and temperature.

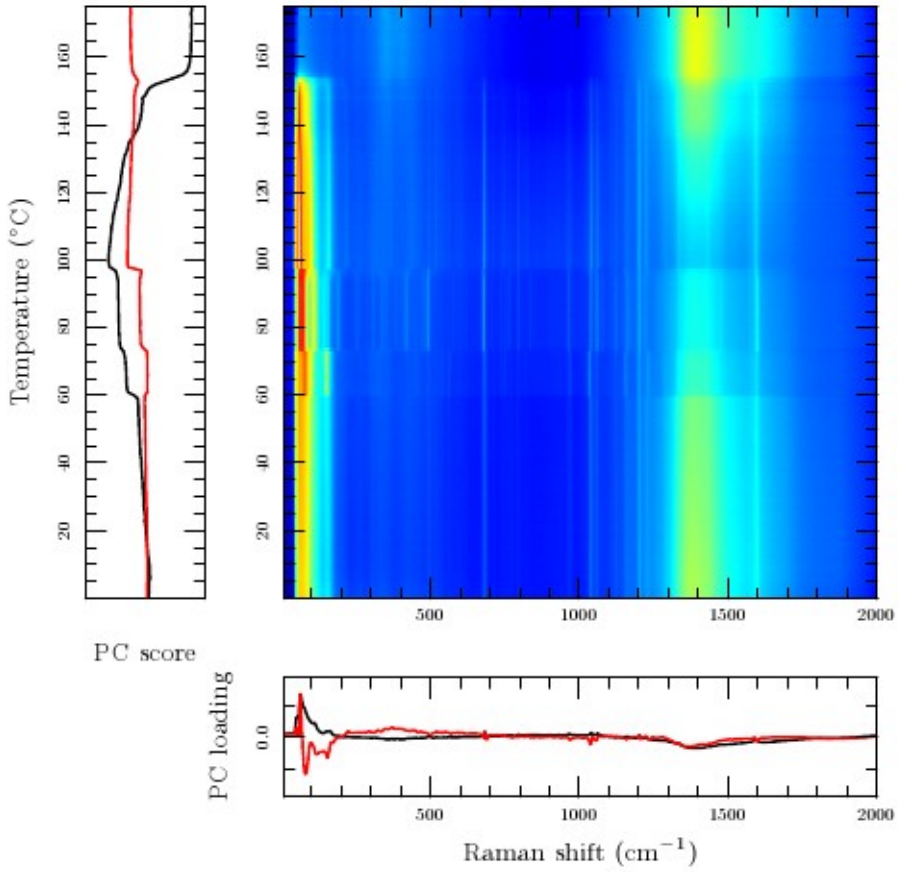

Figure 6.4: Variations in the Raman spectra (top right), PC1, PC2 (top left) with temperature and loadings (bottom), for the slow heating of amorphous imipramine hydrochloride

Two principal components (PC1, black and PC2, red) were chosen for the analysis because they accounted for over 99% of the variance. The temperature of transitions (see left hand side of picture) is in agreement with those obtained in figure 7.3, i.e. 60, 74 and 98°C respectively. With the transitions taking place in single steps at the aforementioned temperature.

With the major spectral changes occurring between 100 and 200cm^{-1} (see lower panel), which further shows the usefulness of the phonon-mode region in distinguishing polymorphic changes.

Figures 6.5a below and 6.5b overleaf shows the changes in the C-N stretching vibration and the phenyl breathing mode (due to multiple substitution) as the imipramine hydrochloride is being heated.

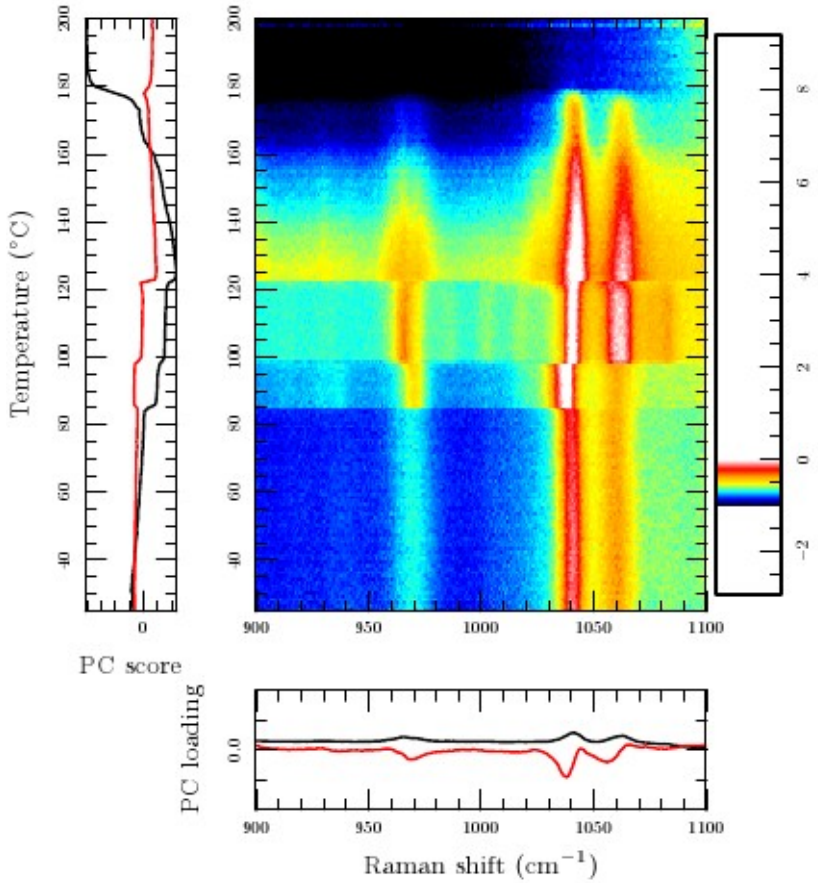

Figure 6.5a: Raman spectra showing changes in the C-N stretching vibration

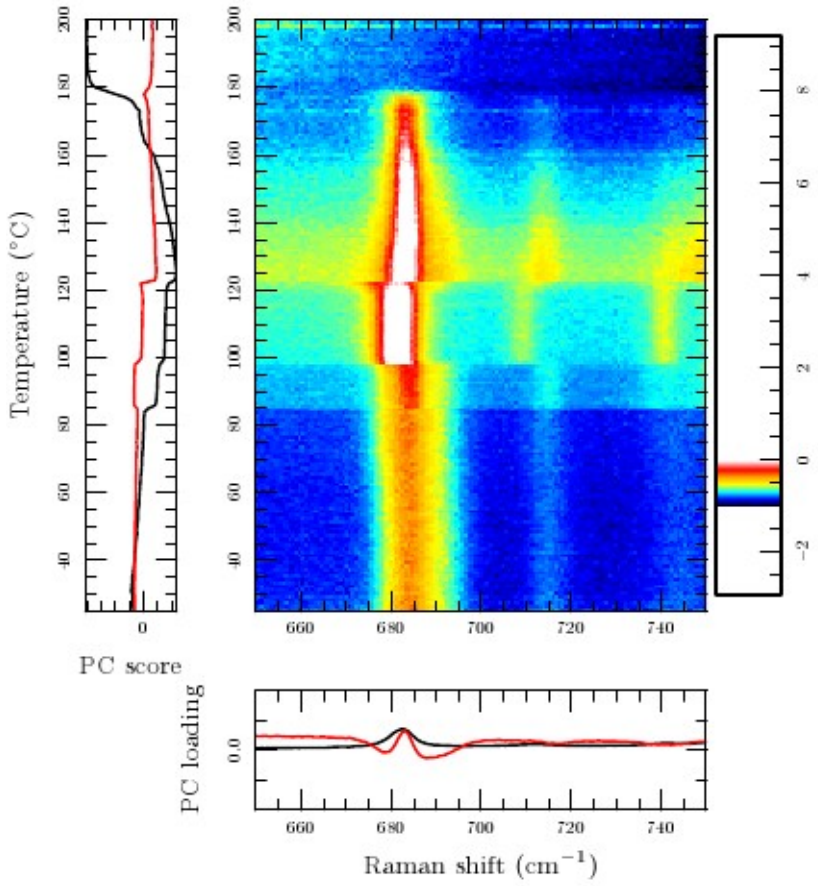

Figure 6.5b: Raman spectra showing changes in the phenyl breathing mode

Figures 6.5c and 6.5d shows the representative phonon-mode and molecular-mode Raman spectra obtained from the slow heating experiment using imipramine hydrochloride respectively:

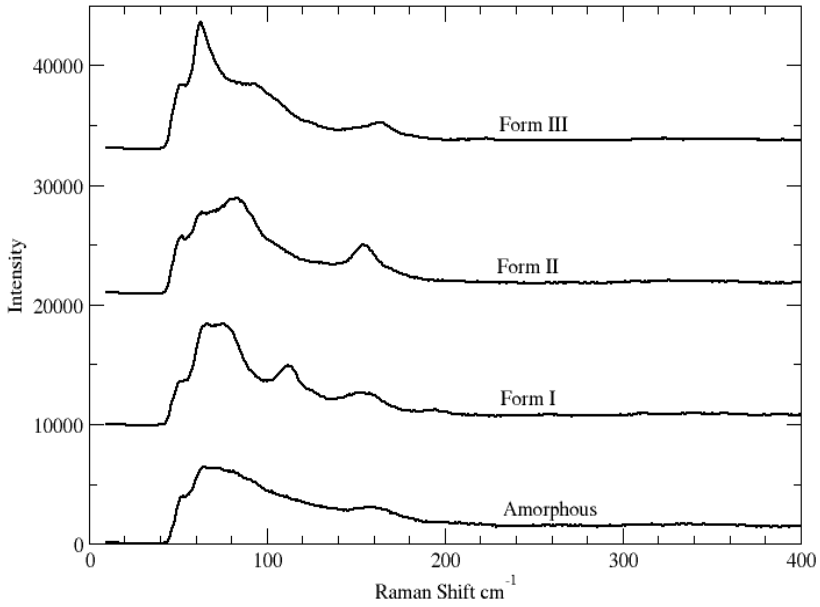

Figure 6.5c: Phonon-mode Raman spectra of imipramine hydrochloride

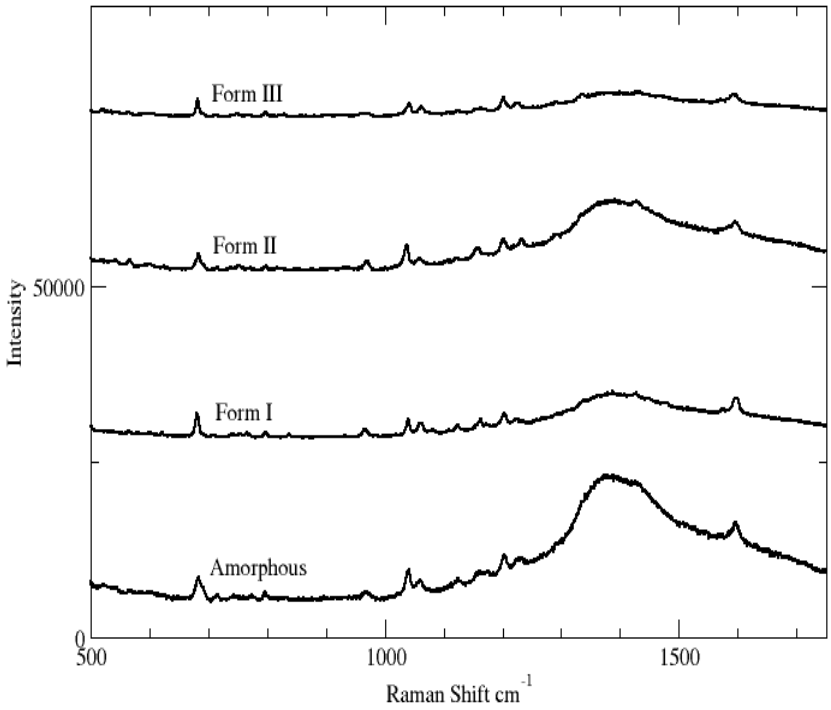

Figure 6.5d: Molecular-mode Raman spectra of imipramine hydrochloride

While the phonon peaks are different and easily distinguishable (figure 6.5c), the molecular modes appear similar as depicted in figure 6.5d, thus making it easier to differentiate among the various forms of imipramine hydrochloride using the phonon-mode spectra by visual inspection.

The change in peak position and peak width (using a Gaussian fit) of the phenyl ring deformation stretching vibration at approximately 684cm^{-1} (this peak was chosen because of its high intensity) on heating across the transition is reported in figures 6.6a and 6.6b respectively (below): Thus showing the temperature dependence of the data obtained from the in situ Raman experiment.

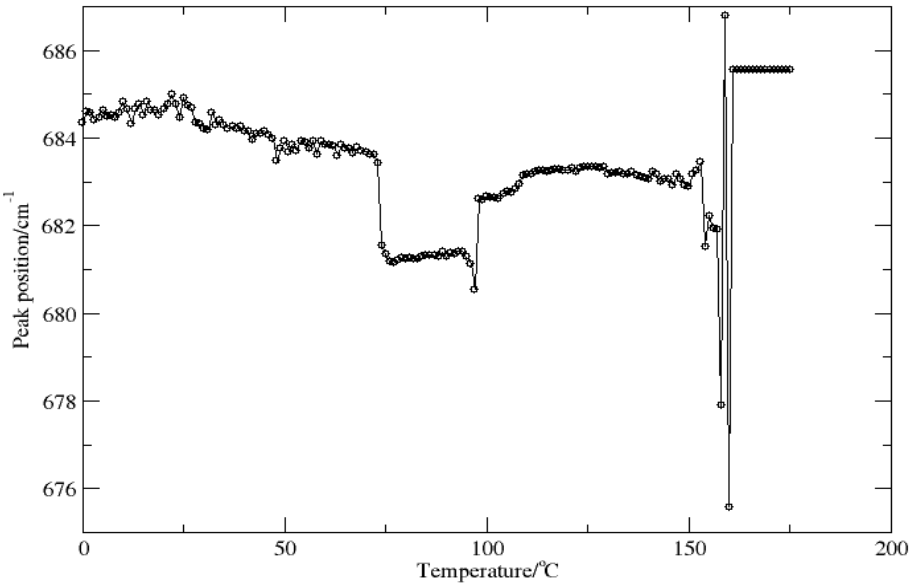

Figure 6.6a: Plot of peak position as a function of temperature

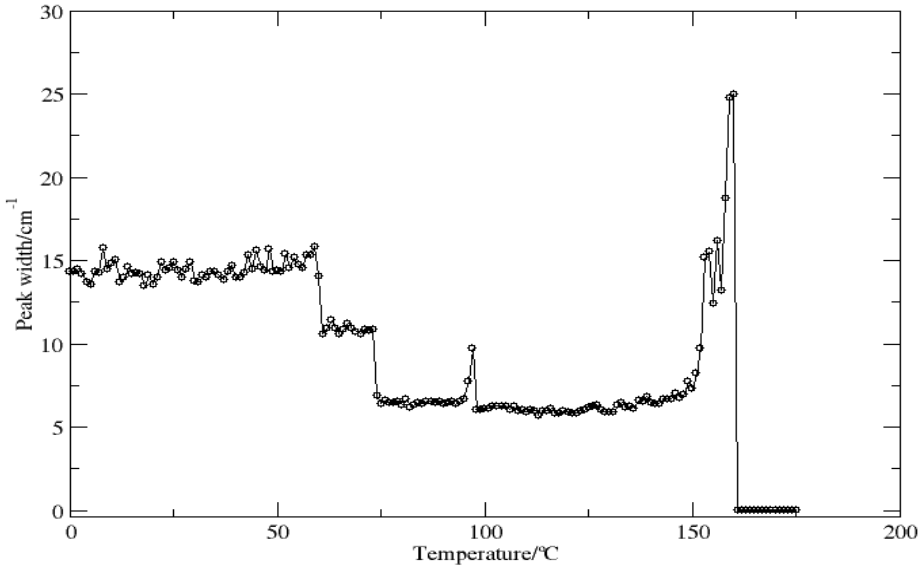

Figure 6.6b: Plot of peak width as a function of temperature

The peak widths in the amorphous state are wider than in the crystalline state due to the (static) disorder of the molecule.

6.4.3 X-ray powder diffraction

Principal component projection was also deployed to validate the transformation observed in the variable temperature XRPD experiment as shown in figure 6.7 below:

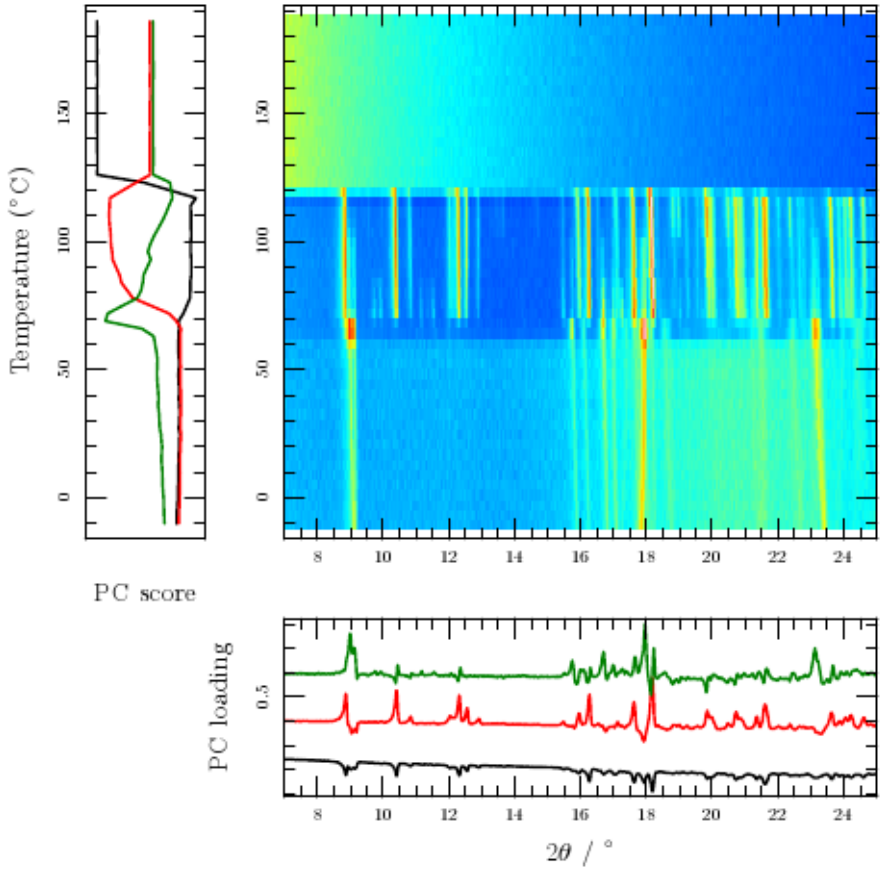

Figure 6.7: Variations in the X-ray patterns (top right), PC1, PC2 (top left) with temperature and loadings (bottom), for the slow heating of amorphous imipramine hydrochloride

Three principal components (PC1, black, PC2, red and PC3, green) were chosen for the analysis because they accounted for over 99% of the variance. Two major changes occurred during the heating experiment i.e. at 70°C and 118°C respectively, and while the first transition was in a step and sudden, the second transformation was multifarious and complex. The VTXRPD experiment was slower than the Raman analysis but has the potential of providing crystallographic information including crystal structures. The changes in x-ray patterns as the heating progressed clearly supports our findings using Raman spectroscopy. While the multi-facet nature of the second transition in fig. 6.7 is a pointer to the fact that more than one possible transformation can be obtained from heating the amorphous form of imipramine hydrochloride.

Although the temperature of transition observed with the XRPD is higher than that obtained from the Raman analysis, comparing the latter with the former allows us to be sure that the changes we see in the Raman are indeed due to polymorphic transformations.

Conclusion

In conclusion, we demonstrate that screening of pharmaceutical compounds for polymorphism can be rapidly achieved for milligram quantities of material using in situ phonon-mode Raman spectroscopy, and demonstrate that phonon-mode confocal Raman spectroscopy/microscopy (coupled with hot-stage microscopy) has the potential to offer a simple, reliable and rapid method of screening for polymorphism in pharmaceutical materials. With the results obtained from the Raman analysis comparing favourably well with both DSC and XRPD techniques in confirming that imipramine hydrochloride exhibits polymorphism (not previously reported prior to this study).

Data analysis is relatively straightforward, with visual inspection of the phonon-mode spectra sufficient to distinguish between the different polymorphs of imipramine hydrochloride. The deployment of principal component analysis in this study also makes it easier and quicker to identify transitions and the spectral changes (and therefore molecular) changes which under pin them.

7.0 Raman spectroscopy: Backscattering versus transmission geometries

7.1 Transmission Raman spectroscopy as a tool for quantifying polymorphic content of pharmaceutical formulations

Abstract

We present the first quantitative study of polymorphic content in a model pharmaceutical formulation using transmission Raman spectroscopy (TRS), and compare the results obtained with those from traditional backscattering geometry. The transmission method is shown to provide a true bulk measurement of the composition, being unaffected by systematic or stochastic sub-sampling issues that can plague traditional backscattering geometries. The accuracy of the quantification of the polymorphs using TRS was shown to surpass considerably that achieved using conventional backscattering mode.

For a model-free fit, the TRS method yielded R^2 of 0.996 compared to the backscattering value of 0.802; for a partial least squares fit with a single component the TRS method accounted for 98.09% of the variance in the data and yielded an R^2 of 0.985, compared to 89.65% of the variance and R^2 of 0.804 for the backscattering method.

7.2 Introduction

A number of analytical applications within the pharmaceutical production environment require a rapid, non-invasive and, most importantly, a non-destructive method for the assay of the bulk content of pharmaceutical formulations. In recent work, previously unexploited properties of transmission Raman spectroscopy were reported.[35,174] These include the provision of volumetric information on the sample content through the removal of sub-sampling and suppression of interfering surface layer Raman and fluorescence signals that are particularly beneficial for rapid probing of pharmaceutical capsules and coated tablets. This development stimulated new research in this area, paving the way for the establishment of a new analytical technique well suited to a number of problems faced by the pharmaceutical industry.

Although conventional backscattering Raman spectroscopy has been used in pharmaceutical applications extensively,[175-183] it suffers from sub-sampling (limited lateral interaction area and limited penetration depth) when applied to assessing the bulk content of typically highly heterogeneous formulations. This severely restricts technique's predictive power. These conventional studies also exploited the capability of conventional Raman to ascertain the polymorphic content of pharmaceutical formulations.[184]

The issue of limited lateral size of the interaction zone was addressed by expanding the laser deposition and Raman collection areas to several millimetres in the backscattering geometry.[185]

Although this approach eliminated the sub-sampling problem in lateral dimensions, the restricted penetration depth still remained an issue associated with over-sensitivity of the technique to signals originating from the surface layers of sample; e.g. fluorescence or Raman signals originating from the coating or capsule shell.

The limited penetration depth issue was effectively addressed by the recent advent of transmission Raman methodology into pharmaceutical arena. In the transmission Raman geometry, the laser beam is incident upon one side of the probed capsule and the Raman light is collected from the opposite side.

This mode of operation stems from the development of non-invasive methods such as Spatially Offset Raman Spectroscopy (SORS[186,187]) or deep probing of diffusely scattering samples.[188-191] The transmission Raman spectroscopy (TRS) concept can be considered to be a special case of SORS with the illumination and collection points displaced to the extreme and as such it shares some common characteristics with SORS.

Although the transmission Raman technique was demonstrated in the early days of Raman spectroscopy,[192] its benefits for the non-invasive probing of the bulk content of pharmaceutical samples had not been previously recognised or exploited. In addition to the elimination of the sub-sampling problem the technique also effectively suppresses both fluorescence and Raman components emanating from coating or capsule layers.[35] Although some sensitivity to the depth of probed layer within sample remains in transmission geometry it is drastically weaker than that associated with the conventional backscattering geometries.[174]

In recent research, Johansson et al.[178] established the ability of the transmission Raman technique to provide quantitative information on the binary mixture content of capsules and tablets. In this study, 20 test tablets and an unspecified number of capsules specifically formulated were used. The study achieved a relative root mean square error of prediction for Active Pharmaceutical Ingredient (API) concentration of 2.2% and 3.6%, respectively, with a 5s acquisition time. The investigation also demonstrated the robustness of the calibration model, which provided satisfactory prediction accuracy for a relatively low number of calibration points (only three).

A similar study was performed by Eliasson et al.,[193] using transmission Raman spectroscopy on production relevant formulations prepared in a laboratory environment. White development capsules were used and these presented interference that hampered the use of other process analytical technology compatible optical spectroscopic methods, such as NIR absorption and conventional Raman spectroscopy. These signals were effectively suppressed (by a factor of 30) by the transmission Raman approach.

The study was performed on 150 capsules and the measured relative root mean square error of API prediction (1.2% for a 5s acquisition time). Here we present the first quantitative measurement of polymorphs (identical chemicals of different crystalline forms) in pharmaceutical formulations using TRS and compare its performance with conventional backscattering Raman spectroscopy.

Flufenamic acid, a non-steroidal anti-inflammatory drug, was chosen as a model polymorphic system. It has been reported to adopt up to 10 polymorphs.[80] Forms I and III were chosen for this work, as they are readily obtained, are both kinetically stable under standard laboratory conditions, and are well characterised with known crystal structures.[87,91]

The molecules adopt slightly different conformations in the two polymorphs, which differ primarily in the relative orientation of the phenyl groups about the secondary amine, with dihedral angles of 42.9 between planes defined by the two phenyl rings in form III (CSD reference FPAMCA), and 53.2 in form I (CSD reference FPAMCA11). In both forms, the molecules are coupled into dimers which are linked by the hydrogen-bonded carboxylic acid groups.

An intra-molecular N–H-----O=C hydrogen bond is formed in both forms.

The molecular Raman bands are therefore expected to be rather similar. The packing of the different molecules is significantly different in the two forms, and therefore any Raman bands which are sensitive to intermolecular interactions are expected to be strongly different between the two forms.[2] This conformational polymorphism is common in pharmaceutical solids.[194]

Flufenamic acid is therefore a typical, industrially relevant (partially) conformational polymorphic compound which forms an excellent model system for this study.

7.3 Experimental

7.3.1 Materials

Flufenamic acid was purchased from Sigma-Aldrich Dorset UK. Both forms were characterised using transmission X-ray powder diffraction (XRPD) and differential scanning calorimetry (DSC) in addition to transmission and backscattering Raman spectroscopy. The as-received sample was shown by comparison of the XRPD pattern with the reported crystal structure of Krishna Murthy et. al.[87] to be form I.

This material was therefore used as the stock sample of form I. Pure form III was prepared by simple evaporative crystallisation from propanol and identified by comparison of the XRPD pattern with the reported crystal structure of McConnell.[91] From the XRPD, DSC and Raman spectroscopy, both forms I and III are estimated to have polymorphic and chemical purity in excess of 99%. Mixed samples of total individual mass of 1g were prepared by weighing suitable amounts of sample to an accuracy of 0.0001g and co-milling forms I and III in a ball mill (Retsch MM400) for 60 seconds.

A total of 27 samples of compositions 0.01, 0.02.0.09, 0.1, 0.2.0.8, 0.9, 0.91.0.98, and 0.99 (mole fraction) were prepared. XRPD and differential scanning calorimetry (DSC) were used on a sub-set of samples to confirm that no detectable (1%) transformation I / III or III / I occurs under these conditions. Visual inspection of the Raman data from both transmission and reflection is also in accord with no detectable polymorphic transformation under these conditions.

7.3.2 Instrumental

The transmission Raman spectra were measured using a Cobalt Light System Ltd TRS100 transmission Raman optical engine. The probe beam was generated using a frequency stabilised diode laser operating at 830 nm. The laser power at the sample was ~800 mW and the laser spot diameter ~3 to 4 mm at the sample. The sample was placed at one side of the holder and the laser directed through the sample and collected at 180° from the direction of the laser light.

The spectra are not corrected for the variation of the detection sensitivity across the spectral range. The spectral resolution was estimated to be 5–6 cm^{-1}. Measurement parameters were 10s (10 acquisitions of 1s duration each averaged), unless otherwise stated.

The reflection Raman spectra were collected using a HORIBA Jobin Yvon Ltd LabRAM HR system, interfaced with an Olympus BX51 optical microscope. A laser wavelength of 785nm was employed and an objective lens of x50 magnification. The laser power was 300 mW and the laser spot diameter was approximately 1 micron. In order to reduce as far as possible any issues with sub-sampling, the laser spot was scanned over a 50 x 50 $micron^2$ area during data collection using the ‘‘Duoscan’’ module supplied with the instrument.

The Raman spectra were collected under confocal conditions. The sample was placed onto a glass microscope slide, and the laser directed onto the sample and collected in backscattering geometry. The spectrometer was calibrated using the Rayleigh scattering, the peak position of silicon (520.7 cm^{-1}), and the spline files provided by the manufacturer. All spectra were collected in the same day under the same conditions in order to minimise where possible any calibration issues due to instrumental thermal drift, etc.[189]

The Raman light was collimated and dispersed by a 600 lines per mm grating, along a total beam path of 800 mm, with Raman spectra recorded using a Synapse CCD which was thermoelectrically cooled. Spectral resolution (i.e. typical peak width) is estimated to be mainly determined by the sample and of the order of 4 cm^{-1}.

The spectrum (30–2000 cm^{-1}) was collected in several windows and merged into a single spectrum using the LabSpec software supplied with the instrument. Measurement parameters were 2 seconds per window unless otherwise stated.

7.3.3 Data processing

For the chemometric analyses both datasets were handled in exactly the same manner using a partial least squares routine as implemented by the ‘‘PLS’’ package[195] within the ‘‘R’’ programming suite. Raw spectra were used, and the entire data range was used for both transmission and backscattering datasets. Kernel PLS was employed and included a multiplicative scatter correction.[196] A ‘‘leave one out’’ validation procedure was applied (cross validation yielded essentially identical results). A single PLS component was found to be appropriate for both transmission and backscattering datasets.

7.4 Results and discussion

7.4.1 Backscattering geometry

Data collected in backscattering geometry for the mixed samples are presented in figure 7.1. The spectra are of high quality with good signal : noise ratio. Visual inspection indicates some clear and obvious differences between the two polymorphic forms of flufenamic acid.

The molecular bands (ca. 400–4000 cm^{-1}) are approximately similar in intensity and position (as would be expected for two polymorphic samples which by definition contain the same molecules), but detailed differences emerge on closer inspection. The most obvious is the difference in position of the symmetric phenyl stretching mode, which occurs at 1003.8 cm^{-1} in form I and 995.1 cm^{-1} in form III.
Note that this particular peak is well-separated from other bands. In contrast to the molecular bands, the phonon-mode bands (ca. 30–400 cm^{-1}) differ strongly between the two polymorphic forms. This is expected, as the phonon-mode bands are very sensitive to inter intermolecular interactions—which are expected to be very different between the two forms—whereas the molecular bands are most sensitive to the intra-molecular interactions which are expected to be very similar.[4]

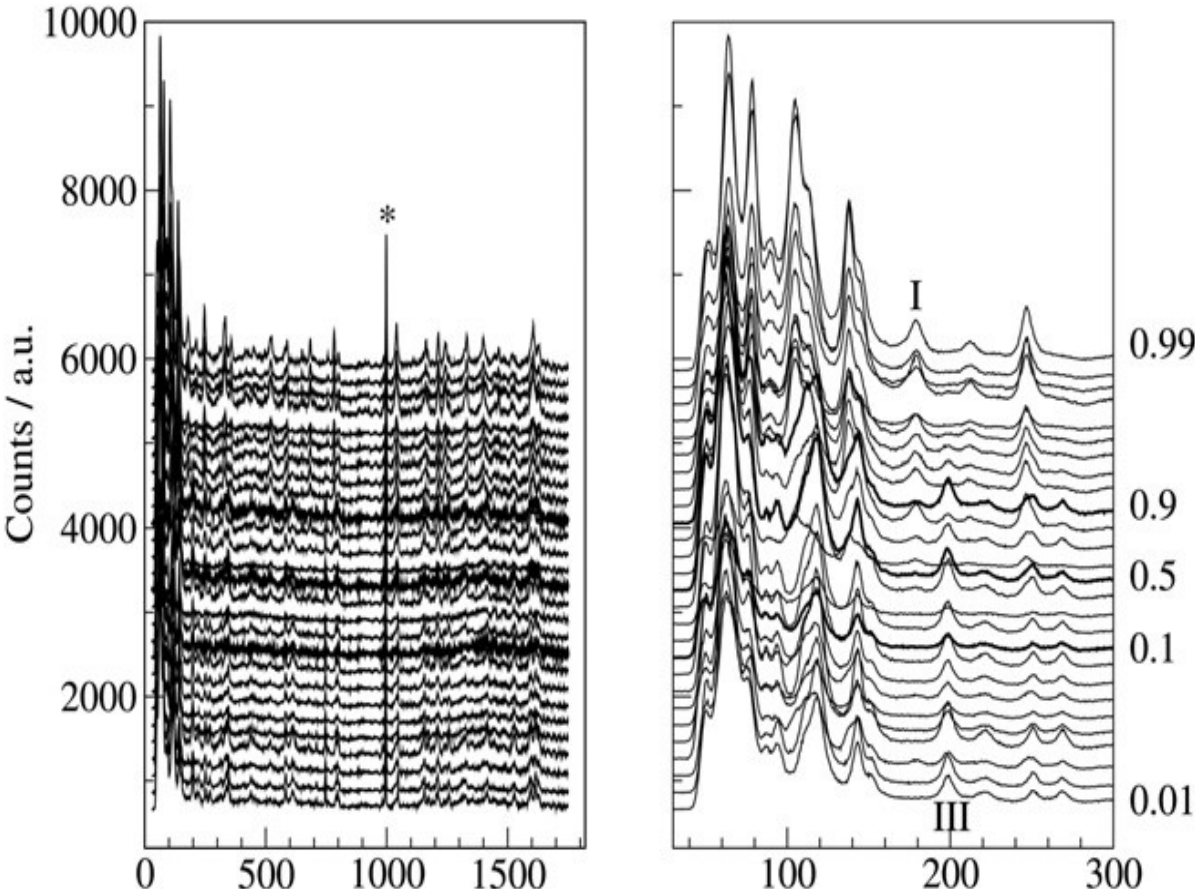

Figure 7.1: Raman spectra of polymorphic mixtures of FFA, collected in backscattering geometry, for entire spectral range (LHS). Composition (mole fraction of form I) is given at the right, spectra for 0.1, 0.5, and 0.9 are in bold. Signature peaks for forms I and III are labelled

Considering the spectra for all compositions collected under backscattering geometry, it is clear (again from visual inspection of the data) that although, globally, the spectra change across the series from form I to form III, this trend is not reproducible from one composition to another. There is no locally smooth change in the spectra as a function of composition. Note in particular the two ‘‘fingerprint’’ peaks for forms I and III which are labelled in the figure. For example, the spectrum for 0.91 mole fraction of form I more closely resembles that for 0.8 rather than 0.9. Also, the backscattering spectra do not exhibit the expected symmetry around 0.5 mole fraction: far more spectra resemble form III than form I.

There are therefore two issues with the backscattering data which render them unsuitable for any reliable and quantitative studies in this situation: firstly, there is some inherent variability in the data; and secondly, there is a strong over-representation of form III in the data for the mixed samples.

This latter issue is systematic, whereas the former is stochastic. We emphasise at this point, and will clearly demonstrate later, that these issues with the backscattered Raman spectra do not reflect any variability in the bulk composition of the samples but are inherent in the use of backscattering data to characterise this model pharmaceutical system.

7.4.2 Transmission geometry

Data collected in transmission geometry are presented in figure 7.2 (overleaf). The spectra for the pure forms are comparable with those collected in backscattering geometry which were fully discussed earlier, albeit at slightly lower spectral resolution (full width at half maximum of the phenyl peak 7cm^{-1} for transmission mode versus 4cm^{-1} for backscattering, data not shown). The primary difference between the backscattering and transmission data is for the mixed samples. A clear and obvious smooth variation in the spectra as a function of composition is readily apparent even from visual inspection of the data.

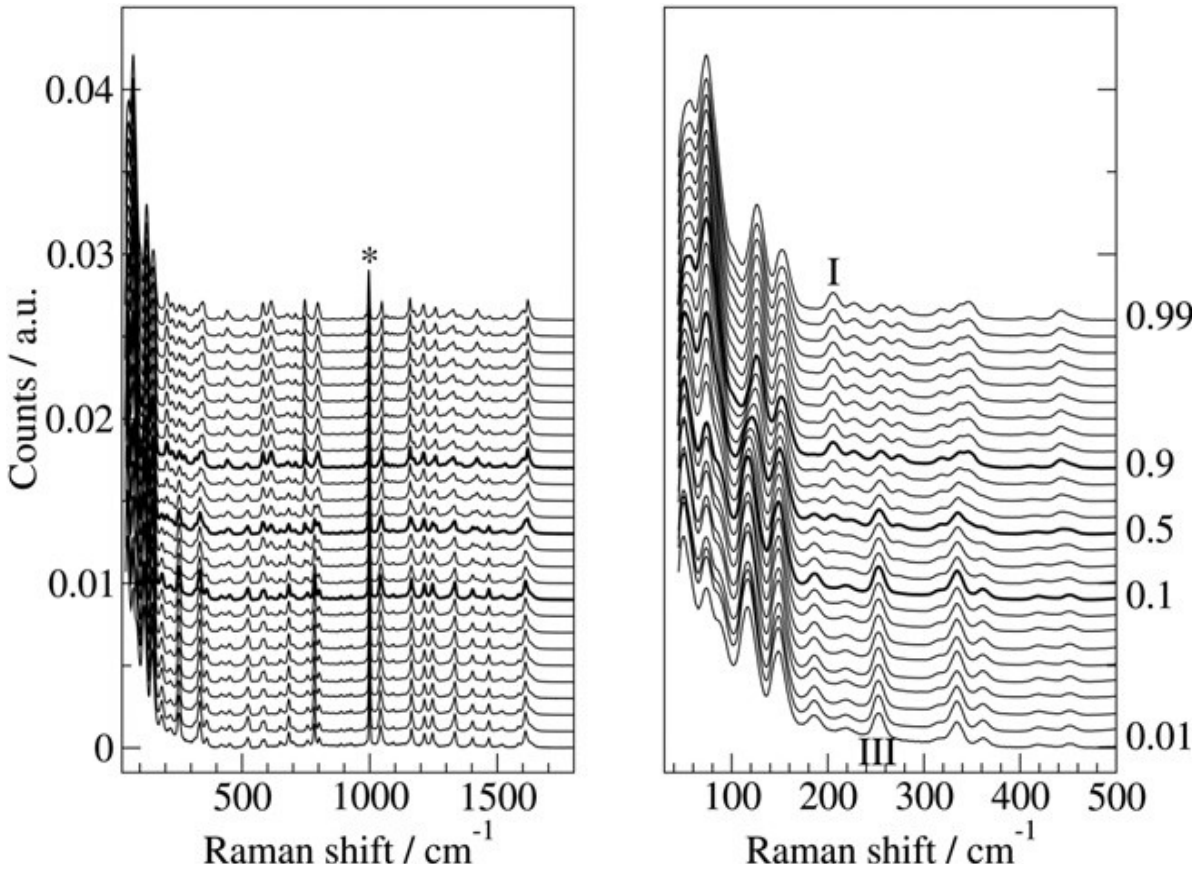

Figure 7.2: Raman spectra of polymorphic mixtures of FFA, collected in transmission geometry, for entire spectral range (LHS) and phononmode bands (RHS). Composition (mole fraction of form I) is given at the right, spectra for 0.1, 0.5, and 0.9 samples are in bold. Signature peaks for forms I and III are labelled and the symmetric phenyl breathing mode is indicated with *.

7.4.3 Chemometric analyses

The results of the chemometric analysis (partial least squares, PLS) for all 27 mixed samples are presented in figure 7.3. Analysis of the backscattering data clearly does not yield a wholly reliable model, in that the observed and predicted values are spread significantly from the expected straight line with gradient of one.

The single component PLS model in this case only explains 89.7% of the variance in the data. There also appears to be a systematic trend overlaid on the scattered data points, with form I being under-represented in the PLS model (many data points lie below the ideal straight line, indicating an under-estimation of the amount of form I). This is thought to arise from the previously noted over-representation of form III in the raw spectra, and will be addressed below.

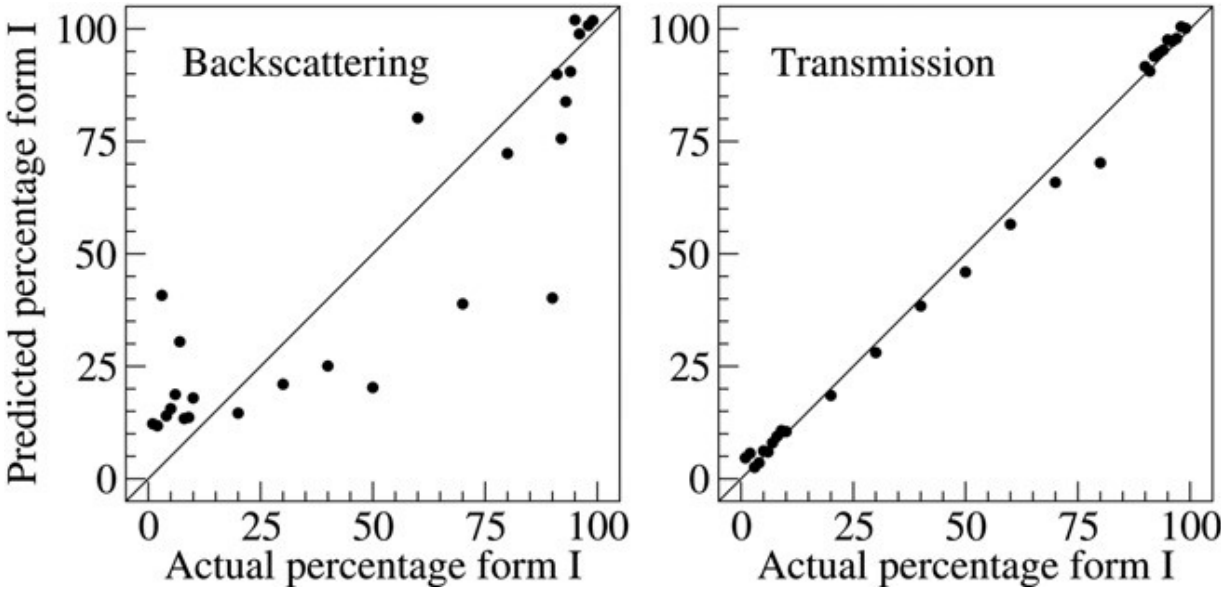

Figure 7.3: Results of PLS analysis (validation plot, all data) for transmission and backscattering data

In contrast to the scatter observed in the backscattering data, analysis of the transmission data (also figure 4.4) yields a highly satisfactory model, with the points correlating well with the expected straight line. In this case the single component model explains 98.09% of the variance in the data, and yields a linear regression R^2 of 0.985.

A PLS analysis was also performed employing data in the spectral windows below 500 cm^{-1}, in order to investigate whether the increased variance of the spectra in the region below 500 cm^{-1} (compared to above 500 cm^{-1}) would produce a more robust model than the one described above, which employed the entire spectral range. The amount of variance modelled increased from 98.09% (entire range) to 99.4% (below 500 cm^{-1} only), i.e. the use of only the data below 500 cm^{-1} further improves the robustness of our model.

For the transmission data, but not the backscattering, the agreement between observed and calculated is very satisfactory, and demonstrates for the first time that TRS data are suitable for quantitative chemometric analysis of polymorphic mixtures.

The fit of the chemometric model to the TRS data is pleasing, however, the model constructed required input of all 27 experimental datasets, i.e. the model was constructed from the experimental data. In order to fully validate the use of TRS data for quantitative analysis of polymorphic mixtures, a model-free approach analysis (with less potential for possible or potential bias) has also been performed to further investigate the validity of using TRS data for polymorphic quantification.

7.4.4 Model-free analysis

For a model-free comparison of the relative merits of transmission and backscattering Raman spectra for quantitative analysis of polymorphic mixtures, we have employed the average position of the phenyl breathing mode peak which arises from the two overlapping peaks from the two polymorphic forms at ca. 1000 cm^{-1} as an approximation of the composition.

It is expected to vary in a linear manner with composition. The averaged position of these two peaks was determined by fitting a single Gaussian function (plus single-parameter background); this peak was selected as it is very intense and the position is significantly different for the two polymorphs, as well as the lack of overlap with neighbouring peaks.

The peak position was chosen as this should be unaffected by sample preparation, Raman scattering cross-sections for the two polymorphs, etc., unlike perhaps the peak intensity. Results for this simple modelfree analysis are presented in figure 7.4.

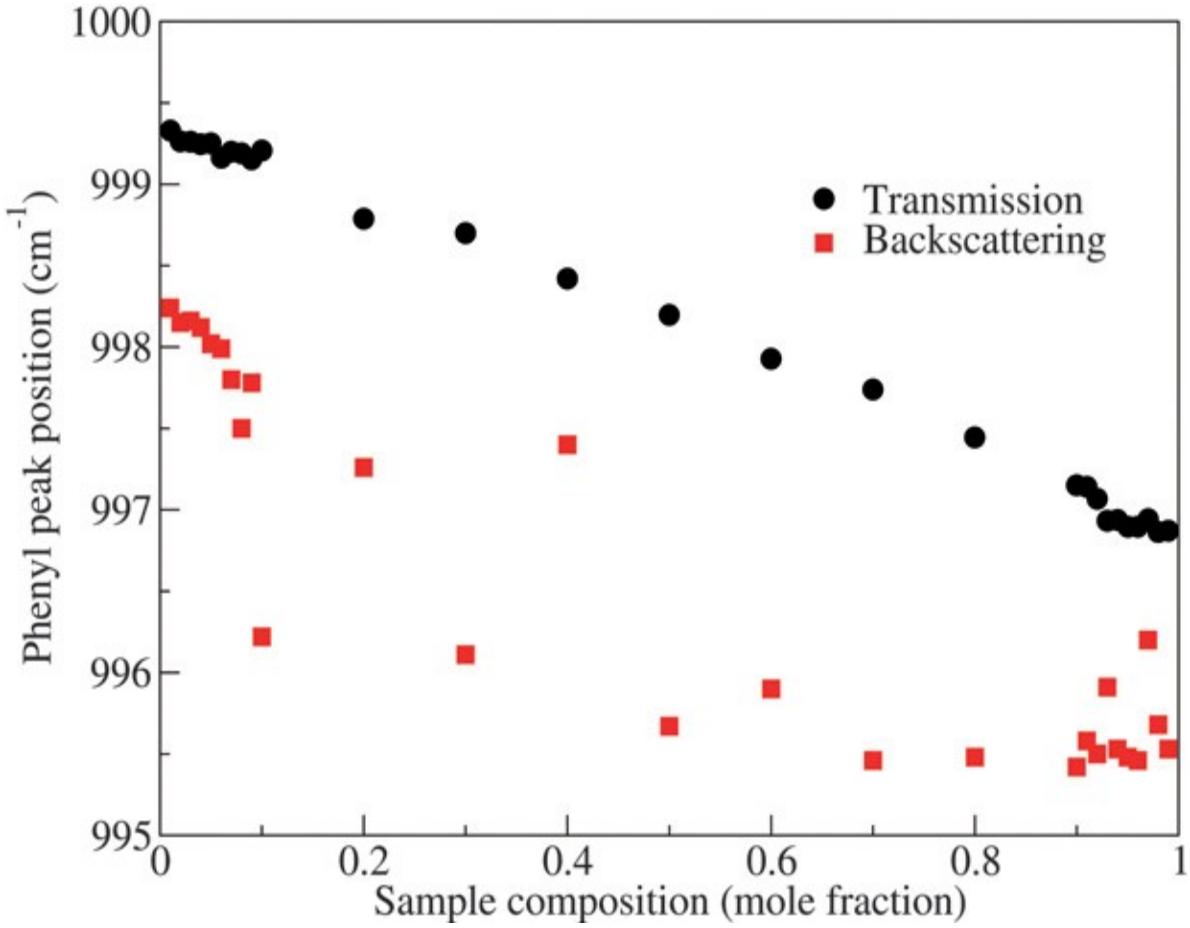

Figure 7.4: Results of fitting the two symmetric breathing bands of the phenyl rings in forms I and III with a single Gaussian

Absolute peak positions vary systematically between backscattering and transmission experiments by approximately a wave number due to instrumental effects, vagaries of calibration, etc.; this is well within the expected range.[189]

It can be seen that for the transmission data, the averaged position of the two phenyl peaks varies very smoothly in a linear manner as a function of sample composition ($R^2 = 0.996$). In contrast, for the backscattering data the peak positions are extremely scattered ($R^2 = 0.802$), and there is a clear over-representation of form III (under-representation of form I).

The scatter of the data points and the over-representation of form III are exactly the same issues that became apparent upon initial, visual inspection of the backscattering data and on performing the PLS analysis of the same. Overall, this model-free comparative study has strongly validated the PLS analysis of the TRS data, and has again highlighted some problems with the use of backscattering Raman data for quantitative analysis, at least in the current case.

7.4.5 Data pre-treatment approach

To further test the robustness of the PLS model for the transmission data, the raw data from both the transmission and backscattering experiments were subjected to different sorts of data pre-treatment before generating the plots of the predicted versus the actual weights of form I in all the 27 samples prepared for the study, i.e. switching mean-centring off and leaving esd normalisation on (figure 7.5a and 7.5b), switching mean-centring on and leaving esd normalisation off (figure 7.6a and 7.6b) and leaving both mean-centring and esd normalisation off (figure 7.7a and 7.7b).

In all cases (below and overleaf), the plots for the transmission data showed a better correlation between the predicted and the actual weights of form I in all the samples used.

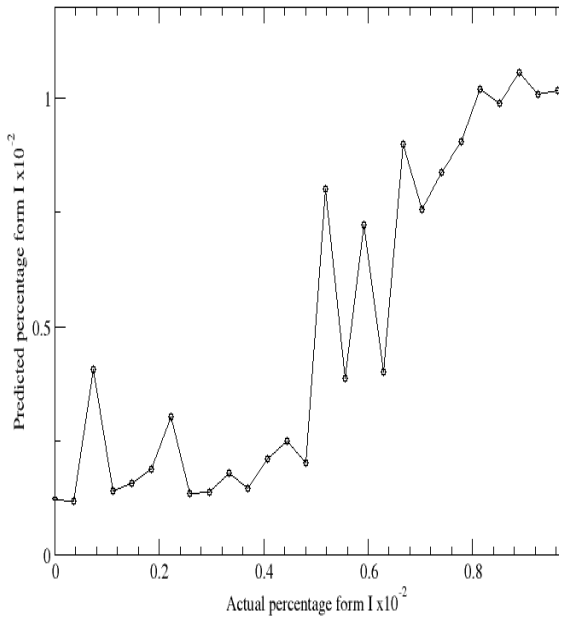

Figure 7.5a: Results of PLS analysis (validation plot, all data) for backscattering data (mean-centring off and esd normalisation on)

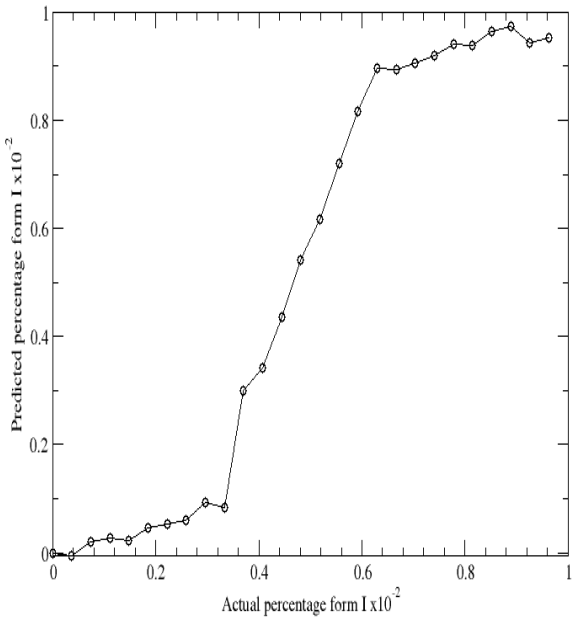

Figure 7.5b: Results of PLS analysis (validation plot, all data) for transmission data (mean-centring off and esd normalisation on)

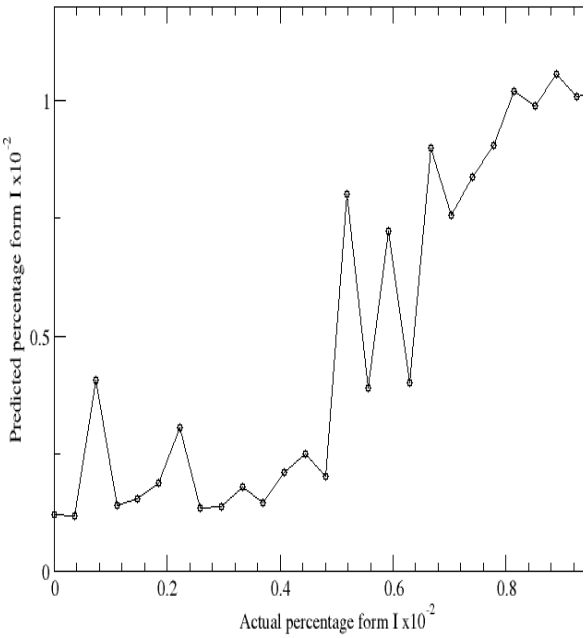

Figure 7.6a: Results of PLS analysis (validation plot, all data) for backscattering data (mean-centring on and esd normalisation off)

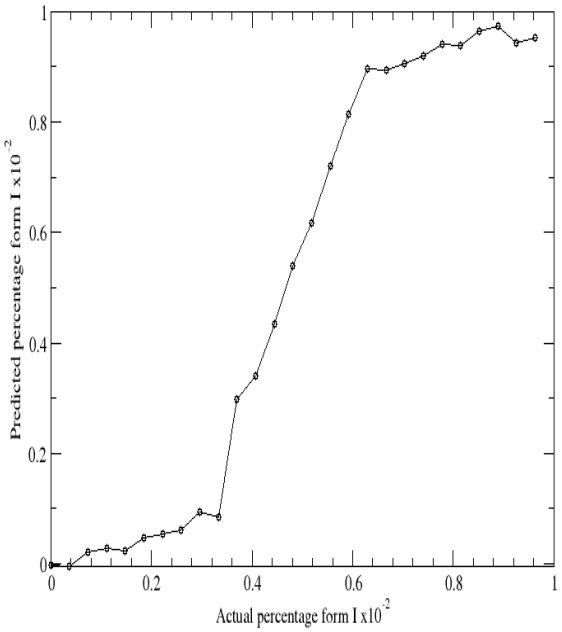

Figure 7.6b: Results of PLS analysis (validation plot, all data) for transmission data (mean-centring on and esd normalisation off)

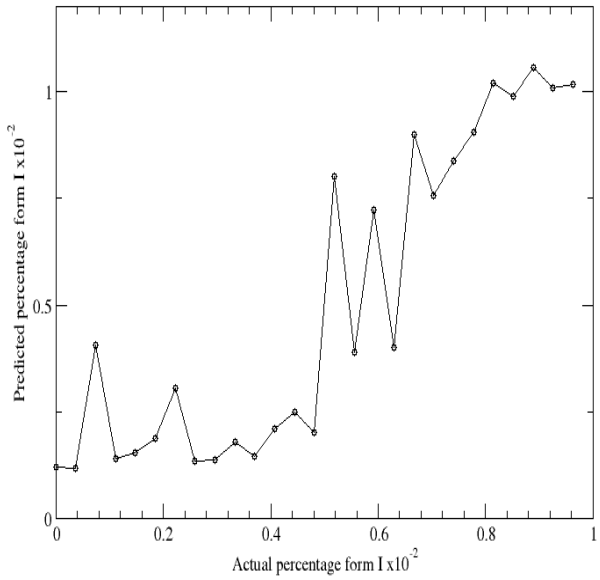

Figure 7.7a: Results of PLS analysis (validation plot, all data) for backscattering data (mean-centring off and esd normalisation off)

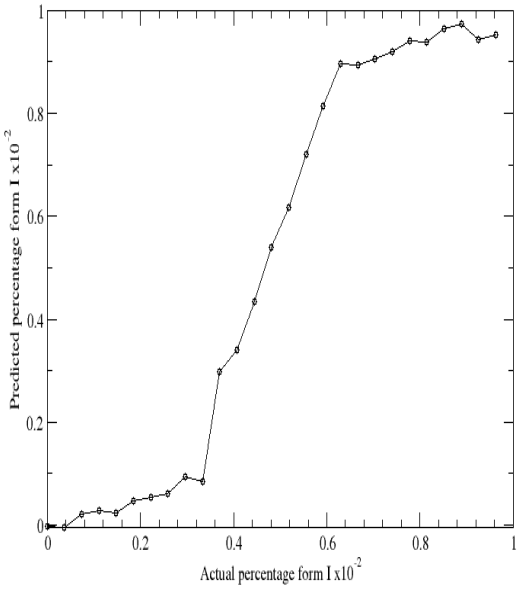

Figure 7.7b: Results of PLS analysis (validation plot, all data) for transmission data (mean-centring off and esd normalisation off)

7.4.6 Issues with the use of backscattering data

We therefore now turn to consider the two issues which render the backscattering data unsuitable for quantitative analysis of the composition of the mixture, namely the large scatter in the raw data, and the systematic over-representation of form III (and under-representation of form I) which was clearly observed in both the chemometric and model-free analyses.

The likely cause of the variability of the backscattering spectra is a lack of true averaging of the sample, i.e. a sub-sampling issue. As outlined earlier this is a well-known issue in the use of traditional backscattering Raman spectroscopy. To investigate the possibility of this sub-sampling problem, a series of 20 spectra were recorded on different areas of form I, form III and the 50 : 50 mixture.

The peak position of the symmetric phenyl breathing mode around 1000 cm^{-1}, which is significantly different for form I and form III, was measured for each spectrum, and a standard deviation (i.e. reproducibility) for the position of this peak in the different samples was calculated. For mixtures with sub-sampling problems the reproducibility is expected to be lower and the standard deviation higher than for samples without this issue.

Results were as follows: form I, 1.169; 50 : 50, 2.274; and form III, 0.253 cm^{-1}. The higher standard deviation for the 50 : 50 mix compared to the pure forms clearly indicates the presence of some sub-sampling problems. We can therefore conclude that the use of a Raman microscope in backscattering geometry, and the associated small sample volume, is not appropriate for accurately measuring the composition of bulk samples, even when great care is taken to reduce lateral sub-sampling problems as far as possible by co-milling samples prior to measurement to encourage thorough sample mixing, and also by rastering the laser over a 50 x 50 $micron^2$ area during the measurement.

The sub-sampling problem explains the variability in the spectra, but not the systematic trend in which more spectra resemble form III than form I. In backscattering geometry, Raman spectroscopy is to some extent a surface technique. This systematic over-sampling of form III is suggestive of some type of surface segregation of the mixed samples, driven for example by different size reduction behaviours of the two polymorphs during milling, different surface energies of the polymorphs, etc., coupled with a limited penetration depth in the backscattering geometry.

In order to probe the possibility of surface segregation during the sample preparation a series of scanning electron microscope (SEM) images were collected. Figure 7.8 shows the images for forms I, III (unmilled) and the 50 : 50 sample (after a minute of milling), taken after identical sample preparation to that employed in the Raman measurements.

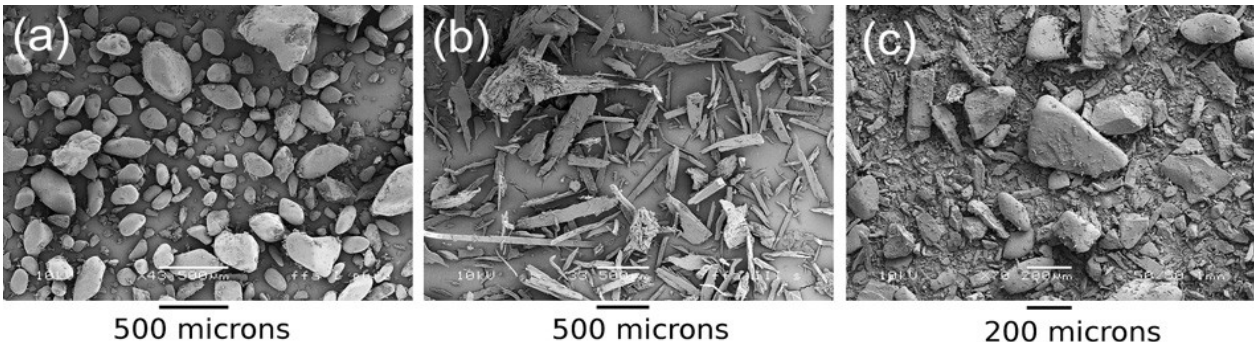

Figure 7.8: Scanning electron micrographs of: (a) FFA I; (b) FFA III; and (c) 50 : 50 mixture milled for 60 seconds. Scale bars are 500, 500 and 200 microns respectively

The particles of forms I and III exhibit very different external morphologies: form I is present as lozenge-shaped particles, whereas form III has a less isotropic, more sawdust-like appearance. In the image of the 50 : 50 mixed sample, the larger particles more closely resemble those of form I than form III, with the smaller particles resembling form III rather than form I. It is clear that co-milling leads to a greater size reduction of form III than form I.
There are a number of ways in which this could affect the spectra of the mixed samples. A surface layer of form III on form I could lead to the systematic over-representation of form III. Likewise, a more efficient powder packing of III and resultant higher bulk density would also lead to this phenomenon. Regardless of the underlying cause of the over-representation of form III, in the backscattering Raman microscopy experiments strong evidence of sub-sampling problems is apparent, despite the careful sample preparation (co-milling) and data collection (laser spot rastering) designed to minimise these issues.
Sub-sampling occurs both laterally and vertically, and ultimately means that the backscattering data are unsuitable for quantification of the model polymorphic mixtures studied here, with both systematic and stochastic problems apparent.

In contrast, the TRS data appear to be completely unaffected by sub-sampling and offer a reliable method of quantitatively characterising polymorphic mixtures. It is likely that the results presented will be widely applicable, beyond the simple model system selected for study here.

Conclusion

For the first time we have investigated the use of transmission Raman spectroscopy for the quantitative analysis of polymorphic mixtures. It is a rapid technique which provides a true bulk measurement and is unaffected by systematic or stochastic sub-sampling issues that can plague traditional backscattering geometries, as demonstrated clearly in the current study.

Transmission Raman data are suitable for reliable, quantitative studies of polymorphic mixtures using either chemometric methods, or simple model-free peak position averages, and offer significant advantages over backscattering methods for bulk characterisation of polymorphs.

General Conclusion

The use of Raman spectroscopy in monitoring pharmaceutical crystallisation (by adopting the constrained crystallisation approach) has been shown in this study to be extremely useful. It is fast, sample requirement are of the order of 1mg or less (with no sample preparation needed) and the whole process can be easily automated. Data obtained from the study has compared favourably well with other techniques such as DSC and XRPD and also with those previously published in literature. The phonon-mode spectral was particularly useful as it helps to easily distinguish between both amorphous and crystalline forms and also provided information about the lattice environment. Structural/molecular changes could also be easily monitored during the course of the experiments using Raman spectroscopy, this is not the case with other techniques used in this study e.g. DSC and XRPD. Although it must be mentioned that a typical Raman spectrometer is expensive.

The deployment of principal component analysis in the study for data elucidation helped greatly in simplifying and interpreting the large data sets generated throughout the study.

The novel technique of transmission Raman spectroscopy was also used to carry out quantitative studies of a model pharmaceutical formulation and was found to provide a true bulk measurement of the compositions used.

Future Work

Improve on the experimental set up used in the study so that individual isolation of different polymorphic forms can be achieved.

Isolate the new forms of imipramine hydrochloride discovered during the study, characterise them using XRPD, DSC and eventually solve their crystals structures. Carry out solubility/dissolution studies on them as well.

Also solve the crystal structure FFA form two from the XRPD pattern obtained in the study.

References

1. Jarkko Pirttimäki, E. Laine, J. Ketolainen, and P. Paronen, Efffects of grinding and compression on crystal structure of anhydrous caffeine, *Int. J. Pharm*.(1993), **95**, 93-99
2. Sarah Al-Dulami, Adeyinka Aina and Jonathan Burley, Rapid polymorph screening on milligram quantities of pharmaceutical material using phonon-mode Raman spectroscopy, *CrystEngComm*, (2010), **12**, 1038–1040
3. Jain, P., Banga, A.K., Inhibition of crystallization in drug-in-adhesive-type transdermal patches. *Int. J. Pharm*.(2010), doi:10.1016/j.ijpharm.2010.04.042
4. Preface, Pharmaceutical solid polymorphism in drug development and regulation; *Advanced Drug delivery Reviews,* (2004), **56,** 235-236
5. Eun Hee Lee, Stephan X.M. Boerrigter, Alfred C.F. Rumondor, Sai P. Chamathy and Stephen Byrn, Formation and solid-state characterization of a salt-induced metastable polymorph of Flufenamic Acid, *Crystal Growth and Design,* (2008), Vol **8,** No 1, 91-97
6. Polymorphism in the Pharmaceutical Industry, Edited by R. Hilfiker 2006 WILEY-VCH verlag GmbH & Co KgaA, Weinheim, ISBN 3-527-31146-7
7. Threlfall, T.L., Analysis of organic polymorphs. A review. *Analyst*, (1995), **120** , 2435-2460
8. Grant, D.W.J., Theory and origin of polymorphism in polymorphism in pharmaceutical Solids, H.G. Brittain, Editor. 1999, Marcel Dekker, Inc., New York. 1-33
9. Di Martino, P., Guyot-Hermann, A.M., Conflant, P., Drache, M., and Guyot, J.C., A new pure paracetamol for direct compression: The orthorhombic form. *International Journal of Pharmaceutics*, (1996), **128**, 1-8
10. Norbert Rasenack, B. W. Müller, Crystal habit and tableting behaviour, *Int. J. Pharm*.(2002), **224**, 45-57
11. Sun, C. and Grant, D.J.W., Influence of crystal structure on the tableting properties of sulfamerazine polymorphs, *Pharmaceutical Research*, (2001), **18**, 274-280
12. Suihko, E., Lehto, V.-P., Ketolainen, J., Laine and Paronen, P., Dynamic Solid-State and tableting properties of four theophylline forms, *International Journal of Pharmaceutics*, (2001), **158**, 225-236
13. Kahela, P., Aaltonen, R., Lewing, E., Anttila, M., and Kristofferson, E., Pharmacokinetics and dissolution of two crystalline forms of carbamazepine, *International Journal of Pharmaceutics*, (1983), **14**, 103-112
14. Meyer, M.C., Straughn, A.B., Jarvi, E.J., Wood, G.C., Pelsor, F.R. and Shah, V.P., The bioinequivalence of carbamazepine tablets with a history of clinical failures, *Pharmaceutical Research*, (1992), **9**, 1612-1616
15. Chemburkar, S.R., Bauer, J., Deming, K., Spiwek, H., Patel, K., Morris, J., Henry, R., Spanton, S., Dziki, W., Porter, W., Quick, J., Bauer, P., Donaubauer, J., Narayanan, B.A., Soldani, M., Riley, D., and McFarland, K, Dealing with the impact of ritonavir polymorphs on the late stages of bulk drug process development, *Organic Process Reasearch & Development*, (2000), **4**, 413-417

16. Cushla M. McGoverin, L. C. H. Ho, J. A. Zeitler, C. J. Strachan, K. C. Gordon and Thomas Rades, Quantification of binary polymorphic mixtures of ranitidine hydrochloride using NIR spectroscopy, *Vibrational Spectroscopy*, (2006), **41**, 225-231

17. Norman Chieng, S. Rehder, D. Saville, T., T. Rades and J. Aaltonen, Quantitative solid-state analysis of three forms of ranitidine hydrochloride in ternary mixtures using Raman spectrscopy and X-ray powder diffraction, *Journal of Pharmaceutical and Biomedical Research*, (2009), **49**, 18-25

18. Singhal D., W. Curatolo, Drug polymorphism and dosage form design: a practical perspective, *Adv. Drug Del. Rev.*, (2004), **56,** 335-347

19. Dr. Jan-OlavHenck, Diversity amidst Similarity: A multidisciplinary approach to polymorhs, solvates & phase relations, Bayer HealthCare, Erice, June 2004

20. Artur Burger and R. Ramberger, On the polymorphism of pharmaceuticals and other molecular crystals. I. Theory of thermodynamic rules, *Mikrochim. Acta* **11** (1979), 259–271

21. Ostwald, W. Z. Studien ueber die Bildung und Umwandlung fester Koerper, *Phys. Chem*. (1897), **22**, 289

22. Terry Threlfall, Structural and thermodynamic explanation of Oswald's Rule, *Organic Process Research & Development*, (2003), **7**, 1017-1027

23. 6th *International conference on pharmacy and applied physical chemistry*, Ascona, Switzerland, May 26-30, 2002

24. Beckmann W., Otto W., Budde U. Crystallisation of the stable polymorph of hydroxytriendione: Seeding process and effects of purity. *Organic Process Reasearch & Development,* (2001), **5,** 387-392

25. Shachtshneider T. P., Boldryrev V. V., Phase transformations in sulfathiazole during mechanical activation, *Drug Dev. Ind. Pharm*., (1993), **19**, 2055-2067

26. Otsuka M., Otsuka K., Nobuyoshi K., Relation between polymorphic transformation pathway during grinding and the physicochemical properties of bulk powders for pharmaceutical preparations, *Drug Dev. Ind. Pharm*., (1994), **20**, 1649-1660

27. Aaltonen J.,Koradia V., Gordon K.C., Solid form screening-a review, *Eur. J. Biopharm.* (2009) Jan;71(1):23-37. Epub 2008 Jul 31

28. Bhadeshia H. K. D. H., Lecture notes, University of Cambridge, Material Science and Metallurgy 2002

29. Christopher Hammond, The basics of crystallography and diffraction (second edition), Oxford University Press, Oxford UK, 2001

30. Barbara L. Dutrow, Christine M. Clark, Geochemical instrumentation and analysis, X-ray Powder Diffraction, Geochemsheets Carleton University U.S.A 2008

31. David E. Bugay, Solid-state nuclear magnetic resonance spectroscopy: Theory and pharmaceutical application, *Pharmaceutical Research*, (1993), **10**, 317-327

32. Andrew E. R., The narrowing of NMR spectra of solids by high-speed specimen rotation and the resolution of chemical shift and spin-multiplet structures for solids, *Prog. NMR Spectroscopy* (1971), **8**, 1-39

33. Andrew E. R., A. Bradbury and R. G. Eades, Removal of dipolar broadening of nuclear magnetic resonance spectra of solids by specimen rotation, *Nature,* (1959), **183**, 1802-1803

34. Mark R. Witkowski, The uses of Raman spectroscopy in the detection of counterfeit and adulterated pharmaceutical products, *American Pharmaceutical Review*, (2005), 1-5

35. Pavel Matousek and A. W. Parker, Non-invasive probing of pharmaceutical capsules using transmission Raman spectroscopy, *J. Raman Spectrosc.,* (2007), **38,** 563–567

36. Direct Communications with Professor Pavel Matousek

37. Eliasson C., N. A. Macleod and P. Matousek, Non-invasive detection of powders concealed within diffusely scattering plastic containers, *Vibrational Spectroscopy*, (2008),Vol. **48**, Issue 1, 8-11

38. Adeyinka Aina, Michael D. Hargreaves, Pavel Matousek and Jonathan C. Burley, Transmission Raman spectroscopy as a tool for quantifying polymorphic content of pharmaceutical formulations, *Analyst,* (2010), **135**, 2328 - 2333, **DOI:** 10.1039/c0an00352b

39. Nicholas Stone, P. Matousek, Advanced Transmission Raman Spectroscopy: A Promising Tool for Breast Disease Diagnosis *Cancer Res*, (2008), **68**, 4424-4430

40. McCrone W. C., Fusion methods in chemical microscopy, Interscience Publishers, Inc., New York, 1957

41. Maria, Kuhnert-Brandstätter, Thermomicroscopy in the analysis of pharmaceuticals, Pergamon Press, Oxford, 1971

42. David J. Berry, Colin C. Seaton, William Clegg, Ross W. Harrington, Simon J. Coles, Peter N. Norton, Michael B. Hursthouse, Richard Storey, William Jones, Tomislav Friščič, and Nicholas Blagden, Applying hot-stage microscopy to co-crystal screening: A study of nicotinamide with seven active pharmaceutical ingredients, *Crystal Growth and Design*, (2008), Vol. **8**, No 5, 1697-1712

43. Imre M. Vitez1, Ann W. Newman, Martha Davidovich, Chris Kiesnowski, The evolution of hot-stage microscopy to aid solid-state characterizations of pharmaceutical solids, *Thermochimica Acta,* (1998), **324**, 187-196

44. Mura P., M.T. Faucci, A. Manderioli, G. Bramanti, L. Ceccarelli, Compatibility study between ibuproxam and pharmaceutical excipients using differential scanning calorimetry, hot-stage microscopy and scanning electron microscopy, *Journal of Pharmaceutical and Biomedical Analysis,* (1998), **18**, 151–163

45. Bartolomei M., P. Bertocchi, M. Cotta Ramusino, E. Ciranni Signoretti, Thermal studies on the polymorphic modifications of (R,S) propranolol hydrochloride, *Thermochimica Acta,* (1998), **321**, 43-52

46. Haitao Li 1, Y.-H. Kiang, Janan Jona, Multiple approaches to pharmaceutical polymorphism investigation-A case study, *European Journal of Pharmaceutical Sciences,* (2009), **38,** 426–432

47. Lian Yu, Susan M. Reutzel and Gregory A. Stephenson, Physical characterization of polymorphic drugs: an integrated characterization strategy, Reviews, *Research Focus*, PSTT Vol. 1, No. 3 June 1998, 118-127

48. W. J. Krzanowski, Principles of multivariate analysis, a user's perspective, revised edition, Oxford University press, (2000)

49. Louis Ferre, Selection of components in principal component analysis: a comparison method *Computational statistics & Data Analysis*, (1995), **19**, 669-682

50. Derya Kara, Evaluation of trace metal concentrations in some herbs and herbal teas using principal component analysis, *Food Chemistry*, (2009), **114**, 347-354

51. Patricia Henson and Steve Lowry, Analysing Polymorphs with Raman spectroscopy, Drug Discovery & Development, Webcast series, January 2006

52. Wolfgang Beckmann, Seeding the desired polymorph: Background, possibilities, limitations and case studies, *Organic Process Research & Development*, **4**, (2000), 372-383

53. Li T., Kenneth R. Morris, Kinam Park, Influence of Tailor-made additives on etching patterns of acetaminophen single crystals, *Pharm. Res*., **18**, (2001), 398-402

54. Weissbuch I., L. Leiserowitz, M. Lahav, Crystal morphology control with tailor-made additives; A stereochemical control: In *Advances in Crystal Growth Research* (Sato K., ed.), 381-400, Elvesier

55. Rubin-Preminger, J.M. and Bernstein, J., 3-Aminobenzenesulfonic acid: a disappearing polymorph. *Cryst. Growth Des*., **5,** (2005), 1343–1349

56. Kwon O.P., M. Jazbinzek, A. Choubey, P. A. Losio, V. Gramlich and P. Günter, Morphology and polymorphism control of organic polyene crystals by tailor-made auxiliaries, *Cryst. Growth Des*., **6**, (2006), 2327–2332

57. Kellogg, R.M., Kaptein B., Vries T.R., Dutch resolution of racemates and the roles of solid solution formation and nucleation inhibition, *Top. Curr. Chem*. **269**, (2007), 159–197 (Novel Optical Resolution Technologies)

58. Mitchell C.A., Yu L., Ward M. D., Selective nucleation and discovery of organic polymorphs through epitaxy with single crystal substrates. *J. Am. Chem. Soc*., **123**, (2001), 10830-10839

59. Blagden, N., Crystal engineering of polymorph appearance: the case of sulphathiazole, *Powder Technol*. **121**, (2001), 46–52

60. Rafilovich, M. and Bernstein, J., Serendipity and four polymorphic structures of benzidine $C_{12}H_{12}N_2$, *J. Am. Chem. Soc*. **128**, (2006), 12185–12191

61. Day, G.M., J.A. Zeitler, W. Jones, T.Rades , Investigating the latent polymorphism of maleic acid, (2006), *Chem. Commun.* 54–56

62. Fages, J., Hubert Lochard, Jean-Jacques Letourneau, Martial Sauceau and Elisabeth Rodier, Particle generation for pharmaceutical applications using supercritical fluid technology. *Powder Technol*., **141**, (2004), 219–226

63. Krukonis,V. (1984) Supercritical fluid nucleation of difficult-to-comminute solids. In Proceedings of the Annual Meeting AIChE, paper 140 f, T-214

64. Kordikowski, A., T. Shekunov, P. York, Polymorph control of sulfathiazole in supercritical CO_2, *Pharm. Res*., **18**, (2001), 682–688

65. Hooton, J.C., Caroline S. German, Martyn C. Davies, Clive J. Roberts A comparison of morphology and surface energy characteristics of sulfathiazole polymorphs based upon single particle studies, *Eur. J. Pharm. Sci*., **28**, (2006), 315–324

66. Garetz, B.A., Aber J. E., Goddard N. L., Young R. G., Myerson A. S., Non-photochemical, polarization-dependent, laser induced nucleation in supersaturated aqueous urea solutions. Phys. Rev. Lett. **77**, (1996), 3475–3476

67. Sun, X., Bruce A. Garetz, Allan S. Myerson, Supersaturation and polarization dependence of polymorph control in the non-photochemical laser-induced nucleation (NPLIN) of aqueous glycine solutions, *Cryst. Growth Des*. **6**, (2006), 684–689

68. Blundell, T. L., Jhoti H., Abell C., High-throughput crystallisation for lead discovery in drug design, *Nat. Rev. Drug Discov.* **1**, (2002), 45-54

69. Peterson, M.L., Morissette S.L., McNulty C., Coldsweig A., Shaw P., LeQuesne M., Monagle J., Encina N., Marchionna J., Johnson A., Gonzalez-Zugasti J., Lemmo A.V., Ellis S.J., Cima M.J., Almarsson O., Iterative high-throughput polymorphism studies on acetaminophen and an experimentally derived structure for form III, *J. Am. Chem. Soc.,* **124**, (2002), 10958-10959

70. Stewart, L. Clark R. and Behnke C., High-throughput crystallisation and structure determination in drug discovery, *Drug Discov. Today* **7**, (2002), 187-196

71. Storey, R. A., R. Docherty and P. D. Higginson, Integration of high throughput screening methodologies and manual processes for solid form selection, *Am. Pharm. Rev.*, **6**, (2003), 100-105

72. Sherry L. Morissette, Orn Almarsson, Matthew L. Peterson, Julius F. Remenar, Michael J. Read, Anthony V. Lemmo, Steve Ellis, Michael J. Cima, Colin R. Gardner, High-throughput crystallisation: polymorphs, salts, co-crystals and solvates of pharmaceutical solids, *Adv. Drug. Deliv. Rev.*, **56**, (2004), 275-300

73. Rupp, B., Automated high throughput drug target crystallography, *Am. Pharm. Rev.*, (2005), 127-131

74. Chayen, N. E., Optimisation techniques for automation and high throughput, *Methods in Molecular Biology*, Vol. **363**, (2007), 175-190

75. Sudha R. Vippagunta, Harry G. Brittain, D. J. W. Grant, Crystalline solids, *Adv. Drug Delivery Rev.*, **48**(1), 3, (2001), 3-26

76. Chan F. C., J. Anwar, R. Cernik and R. M. Wilson, *Ab initio* structure determination of sulfathiazole polymorph V from synchrotron X-ray powder diffraction data, *J. Appl. Cryst.,* **32**, (1999), 436-441

77. Caroline McGregor and Emma Bines, The use of high-speed differential scanning calorimetry (Hyper-DSC™) in the study of pharmaceutical polymorphs, *International Journal of Pharmaceutics*, Vol. **350**, Issues 1-2, (2008), 48-52

78. Graeme M. Day, J. A. Zeitler,W. Jones, T. Rades, and P. F. Taday,Understanding the Influence of Polymorphism on Phonon Spectra: Lattice Dynamics Calculations and Terahertz Spectroscopy of Carbamazepine, *J. Phys. Chem. B*, **110**(1), (2006), 447-456

79. Nicholas Stone, P. Matousek, Advanced Transmission Raman Spectroscopy: A Promising Tool for Breast Disease Diagnosis *Cancer Res*, (2008), **68**, 4424-4430

80. Krc J., Jr., Crystallographic properties of flufenamic acid, *Microscope*, (1977), 25 31-45

81. Xiaoming Chen, Joseph G. Stowell, Kenneth R. Morris and Stephen R. Byrn, Quantitative study of solid-state acid–base reactions between polymorphs of flufenamic acid and magnesium oxide using X-ray powder diffraction, *Journal of Pharmaceutical and Biomedical Analysis,*(2010), **51,** 866–874

82. Maria Kuhnert-Brandstatter, L. Borka and G. Friedrich-Sander, Zur Polymorphie Von Arzneimittelm: flufenaminsaure und BL 191, *Arch. Pharm. Ber. Dtsch. Pharm*., (1974), Ges. 307, 845-853

83. Zdzislaw Galdecki, Marek Leszek Glowka and Zbigniew Gorkiewicz, Examination of the polymorphism of 2-[(3-Trifluoromethyl)Phenyl]Aminobenzoic acid, *Acta. Polon. Pharm. XXXV*, No.1, (1978), 77-79

84. Gilpin R. K.,and W. Zhou, Infrared Studies of the Polymorphic states of the fenamates, *Journal of Pharmaceutical and Biomedical Analysis*, (2005), **37**, 509-515

85. Artur Burger and Rudolf Ramberger, Thermodynamishe Beziehungen Zwischen Polymorphen Modifikationen: Flufenaminsaure and Mefenaminsaure, *Mikrochimita Acta. Wien*, **I**, (1980), 17-28

86. German L. Perlovich, Artem O. Surov and Annette Bauer-Brandl, Thermodynamic properties of Flufenamic and Niflumic acids- Specific and non-specific interactions in solution and in cystal lattices, mechanism of solvation, partitioning and distribution, *Journal of Pharmaceutical and Biomedical Analysis*, (2007), **45**, 679-687

87. Krishna Murthy H. M., T. N. Bhat and M. Vijayan, Structure of a new crystal form of 2- {[3-(Trifluoromethyl)phenyl]amino}benzoic acid, *Acta Cryst.* B38, (1982), 315-317

88. Juan Jose Lozano, Ramon Pouplana, Manuel Lopez and Juan Ruiz, Conformational analysis of the antiinflammatory fenmates: A molecular mechanics and semiempirical molecular orbital study, *Journal of Molecular Structure (Theochem)*, (1995), **335**, 215-227

89. Facchin G., M. H. Torre, E. Kremer, O. E. Piro and E. J. Baran, Crystal structure and spectrocopic behaviour of a binuclear Copper(II) complex of Flufenamic Acid and Dimethlformamide, *Z. Anorg. Allg. Chem*., (1998), **264**, 2025-2028

90. Yuerong Hu, Hakan Wikstrom, Stephen R. Byrn, Lynne S. Taylor, Estimation of the transition temperature for an enantiotropic polymorphic sytem from the transformation kinetics monitored using Raman spectroscopy, *Journal of Pharmaceutical and Biomedical Analysis*, (2007), **45**, 546-551

91. McConnell J. F., 3-Trifluoromethyldiphenylamine-2-carboxylic acid, $C_{14}H_{10}F_3NO_2$ flufenamic acid, *Cryst. Struct. Commun*., (1973), **3,** 459– 461

92. Romero S., P. Bustamante, B. Escalera, M. Cirri, P. Mura, Characterization of the solid phases of paracetamol and fenamates at equilibrium in saturated solutions, *J. Therm. Anal. Calorim*., (2004), **77,** 541–554

93. Jenkins R., R.W. Gould, D. Gedcke, Quantitative X-ray Spectrometry, second ed., Marcel Dekker, New York, 1995

94. Alexander L., H.P. Klug, Basic aspects of X-ray absorption in quantitative diffraction analysis of powder mixtures, *Anal. Chem*., (1948), **20,** 886–889

95. Hassan Refat H. Ali, Howell G.M. Edwards, Michael D. Hargreaves, Tasnim Munshi, Ian J. Scowen, Richard J. Telford, Vibrational spectroscopic characterization of salmeterol xinofoate polymorphs and a preliminary investigation of their transformation using simultaneous in situ portable Raman spectroscopy and differential scanning calorimetry, *Analytica Chimica Acta*, (2008), **620**, 103-112

96. Szafran M., J. Koput, Z. Dega-Szafran, Theoretical and experimental vibrational spectra of two polymorphic 4-hydroxy-1-methylpiperidine betaine hydrochlorides, *Journal of Molecular Structur*e, (2008), **887,** 100-116

97. Aldo Brillante, Ivano Bilotti, Fabio Biscarini, Raffaele Guido Della Valle, Elisabetta Venuti, Polymorphs of α-sexithiophene probed by lattice phonon Raman microscopy, *Chemical Physics*, (2006), **238**, 125-131

98. Gamberini M. C., C. Baraldi, A. Tinti, F. Palazzoli, V. Ferioli, Vibrational study of tamoxifen citrate polymorphism, *Journal of Molecular Structure*, (2007), **840,** 29-37

99. Tomasz Zych, Tomasz Misiaszek, M. Magdalena Szostak, Polymorphism of 2-nitroaniline studied by calorimetric (DSC), structural (X-ray diffraction) and spectroscopic (FT-IR, Raman, UV-Vis) methods, *Chemical Physics*, (2007), **340**, 260-272

100. Yu. A. Chesalov, V.P. Baltakhinov, T.N. Drebushchak, E. V. Boldyreva, N.V. Chukanov, V.A. Drebushchak, FT-IR and FT-Raman spectra of five polymorphs of chlorpropamide. Experimental study and *ab initio* calculations, J*ournal of Molecular Structure,* (2008), **891** 75-86

101. Martin E. Auer, Ulrich J. Griesser and Juergen Sawatzki, Oualitative and quantitative study of polymorphic forms in drug formulations by near infrared FT-Raman spectroscopy, *Journal of Molecular Structure,* (2003), 661-662, 301-317

102. Goryainov S. V., E.V. Boldyreva, E.N. Kolesnik, Raman observation of a new (ζ) polymorph of glycine?, *Chemical Physics Letters*, (2006), **419**, 496-500

103. Gamberini M. C., C. Baraldi, A. Tinti, C. Rustichelli, V. Ferioli, G. Gamberini, Solid state characterization of chloramphenicol palmitate. Raman spectroscopy applied to pharmaceutical polymorphs, *Journal of Molecular Structure*, (2006), **785**, 216-224

104. Babkov L., J. Baran, N.A. Davydova, V.I. Mel'nik, K.E. Uspenskiy, Raman spectra of metastable phase of benzophenone, Journal of Molecular Structure, (2006), 792-793, 73-77

105. Baraldi C., M.C. Gamberini, A. Tinti, F. Palazzoli, V. Ferioli, Vibrational study of acetazolamide polymorphism, *Journal of Molecular Structure*, (2009), **918**, 88-96

106. Zoltan Nemet, Adam Demeter, Gyorgy Pokol, Quantifying low levels of polymorphic impurity in clopidogrel bisulphate by vibrational spectroscopy and chemometrics, Journal of Pharmaceutical and Biomedical Analysis, (2009), **49**, 32-41

107. Silvia L. Cuffini, Javier F. Ellena, Yvonne P. Mascarenhas, Alejandro P. Ayala, Heinz W. Sielser, Josue Mendes Filho, Gustavo A. Monti, Virginia Aiassa, Norma R. Sperandeo, Physicochemical characterization of deflazacourt: *Thermal analysis, crystallographic and spectroscopic study, Steroids*, (2007), **72**, 261-269

108. Eric Da Silva, Serge Bresson, Derick Rousseau, Characterization of the three major polymorphic forms and liquid state of tristearin by Raman spectroscopy, *Chemistry and Physics of Lipids*, (2009), **157**, 113-119

109. Zoltan Nemet, Gyozo Csonka Kis, Gyorgy Pokol, Adam Demeter, Quantitative determination of famotidine polymorphs: X-ray powder diffractometric and Raman spectrometric study, *Jouurnal of Pharmaceutical and Biomedical Analysis*, (2009), **49**, 338-346

110. Carina Schoenherr, Thomas Haefele, Kurt Paulus, Giancarlo Francese, Confocal Raman microscopy to probe content uniformity of a lipid based powder for inhalation: A quality by design approach, *Eur. J. Pharm. Sci.*, (2009), doi: 10.1016/j.ejps.2009.05.011

111. Teiteira A. M. R., P.T.C. Freire, A.J.D. Moreno, J.M. Sasaki, A.P. Ayala, J. Mendes Filho, F.E.A. Melo, High-pressure Raman study of L-alanine crystal, *Solid State Communications*, (2000), **116**, 405-409

112. Alejandro P. Ayala, H.W. Siesler, R. Boese, G.G. Hoffmann, G.I. Polla, D.R. Vega, Solid state characterization of olanzapine polymorphs using vibrational spectroscopy, *International Journal of Pharmaceutics*, (2006), **326**, 69-79

113. Alejandro P. Ayala, H.W. Siesler, S.M.S.V. Wardell, N. Boechat, V. Dabbene, S.L. Cuffini, Vibrational spectra and quantum mechanical calculations of antiretroviral drugs: Nevirapine, *Journal of Molecular Structure*, (2007), **828**, 201-210

114. Alejandro P. Ayala, H.W. Siesler and S.L. Cuffini, Polymorphism incidence in commercial tablets of mebendazole: a vibrational spectroscopy investigation, *Journal of Raman Spectroscopy*, (2008), **39**, 1150-1157

115. Tandon P., G. Forster, R. Neubert, and S. Wartewig, Phase transitions in oleic acid as studied by X-ray diffraction and FT-Raman spectroscopy, *Journal of Molecular Structure*, (2000), 524, 201-215

116. Vankeirsbilck T., A. Vercauteren, G. Van der Weken, F. Verpoort, G. Vergote, J.P. Remon, Applications of Raman spectroscopy in pharmaceutical analysis, *Trends in Analytical Chemistry*, **21**, (2002) ,No. 12, 869-877

117. Gandhi R. B., J.B. Bogardus, D.E. Bugay, R.K. Perrone, M.A. Kaplan, Pharmaceutical relationships of three solid state forms of stavudine, *International Journal of Pharmaceutics*, (2000), **201**, 221-237

118. Alejandro Pedro Ayala, Polymorphism in drugs investigated by low wave number Raman Scattering, *Vibrational Spectroscopy*, (2007), **45**, 112-116

119. Paul W. Findlay, David E. Bugay, Utilization of Fourier transform-Raman spectroscopy for the study of pharmaceutical crystal forms I, *Journal of Pharmaceutical and Biomedical Analysis*, (1998), **16**, 921-930

120. David E. Bugay, Characterization of the solid-state: spectroscopic techniques, *Advanced Drug Delivery Reviews*, (2001), **48**, 43-65

121. McCrone W. C., Fusion methods in chemical microscopy, Interscience Publishers, Inc., New York, 1957

122. Mura P., M.T. Faucci, A. Manderioli, G. Bramanti, L. Ceccarelli, Compatibility study between ibuproxam and pharmaceutical excipients using differential scanning calorimetry, hot-stage microscopy and scanning electron microscopy, *Journal of Pharmaceutical and Biomedical Analysis,* (1998), **18**, 151–163

123. Scott M. Reed, T. J. R. Weakley, J. E. Hutchison, Polymorphism in a conformationally flexible substituted anthraquinone; a crystallographic, thermodynamic and molecular modelling studies, *Crystal Engineering*, (2000), **3**(2), 85-99

124. Sendhil K. Poornachary, P. S. Chow R. B. H. Tan, Impurity effects on the growth of molecular crystals: experiments and modelling, *Advanced Powder Technology*, (2008), **19**(5), 459-473

125. Martin C. J., and D. A. O'Connor, An experimental test of Lindemann's melting law, *J. Phys. C: Solid State Phys*., **10**, (1977), 3521-3526

126. Frank D. Stacey, Spiro S. Spiliopoulos and Mark A. Barton, A critical re-examination of the thermodynamic basis of the Lindemann's melting law, *Physics of the Earth and Planetary Interiors*, **55**, (1989), 201-207

127. Lindemann F. A., Über die Berechnung molecularen Eigen Frequenzen, *Phys. Z*., **11**, (1910), 609-612

128. Wolf G. H., R. Jeanloz, Lindemann melting law: anharmornic correction and test of its validity for minerals, *J. Geophys. Res*., **89**, (1984), 7821-7835

129. Gilvary J. J., The Lindemann and Grüneisen laws, *Phys. Rev.*, **102**, (1956), 308-316

130. Kuhlmann-Wilsdorf D., Theory of melting, *Phys. Rev.*, 140A, (1965), 1599-1610

131. Ross M., Generalised Lindemann melting law, *Phys. Rev.*, **184**, (1969), 233-242

132. Shapiro J. N., Lindemann law and lattice dynamics, *Phys. Rev.*, B1, (1970), 3982-3989

133. Stacey F. D. and Irvine R. D., Theory of melting: thermodynamic basis of Lindemann's law, *Aust. J. Phys*., **30**, (1977a), 631-640

134. Stacey F. D. and Irvine R. D., A simple dislocation theory of melting, *Aust. J. Phys*., **30**, (1977b), 641-646

135. Direct Communications with Dr. Jonathan C. Burley

136. Zhou D., E.A. Schmitt, G.G. Zhang, D. Law, S. Vyazovkin, C.A. Wight, D.J.W. Grant, (2003). Crystallisation kinetics of Amorphous Nifedipine Studied by Model-fitting and Model-free approaches, *J. Pharm. Sci.*, **92**, 1779-1792

137. Eckert T. and J. Muller (1976). On Polymorphic Forms of Nifedipine from Supercooled Melts, *Archiv der Pharmazie,* Vol. 310 Issue **2**, 116-116

138. Artur Burger, K.T. Koller (2006). Polymorphism and Pseudopolymorphism on Nifedipine, *Sci. Pharm.* **64**, 293-301

139. Fumitoshi Hirayama, Zheng Wang and Kaneto Uekama (1994). Effect of 2-Hydroxyl-beta-cyclodextrin on Crystallisation and Polymorphic Transition of Nifedipine in Solid State, *Pharmaceutical Research*, Vol. **11**, No. 12, 1766-1770

140. Aso, Y., Yoshioka, S., Otsuka, T., Kojima, S. (1995). The Physical Stability of Amorphous Nifedipine Determined by Isothermal Microcalorimetry, *Chemical and Pharmaceutical Bulletin,* Vol. **43**, Issue 2, 300-303

141. Tamaki Miyazaki, Sumie Yoshioka, Yukio Aso, Toru Kawanishi, (2007). Crystallisation rate of amorphous nifedipine analouges unrelated to the glass transition temperature *International Journal of Pharmaceutics,* 336, 191-195

142. Yukio Aso, Sumie Yoshioka, Shigeo Kojima, (2001). Feasibilty of using Isothermal Microcalorimetry to evaluate the Physical Stability of Amorphous Nifedipine and Phenobarbital, *Thermochimica Acta*, 380, 199-204

143. Bram Keymolen, James L. Ford, Mark W. Powell, Ali R. Rajabi-Siahboomi, (2003). Investigation of the Polymorphic Transformations from Glassy Nifedipine, *Thermochimica Acta*, 397, 103-117

144. Grooff D., M.M. De Villiers, W. Liebenberg, (2007). Thermal Methods for Evaluating Polymorphic transitions in Nifedipine, *Thermochimica Acta*, 454, 33-42

145. Chan K. L. A., O.S. Fleming, S.G. Kazarian, D. Vassou, G.D. Chryssikos and V. Gionis, (2004). Polymorphism and Devitrification of Nifedipine under Controlled Humidity: a combined FT-Raman, IR and Raman microscopic investigation, *Journal of Raman Spectroscopy*, **35**, 353-359

146. Chan K. L. A., S.G. Kazarian, D. Vassou, G.D. Chryssikos and V. Gionis, (2007). In situ High-throughput Study of Drug Polymorphism under Controlled Temperature and Humidity using FT-IR Spectroscopic Imaging, *Vibrational Spectroscopy*, **43**, 221-226

147. Mino R. Caira, Yolande Robbertse, Jacobus J. Bergh, Mingna Song, Melgardt M. De Villiers, (2003). Structural Characterisation, Physicochemical Properties, and Thermal Stability of Three Crystal Forms of Nifedipine, *Journal of Pharmaceutical Science,* Vol. **92**, No. 12, 2519-2533

148. Triggle A. M., E. Shefter and D.J. Triggle, (1980). Crystal Structures of Calcium Channel Antagonists: 2,6-Dimethyl-3,5-dicarbomethoxy-4-[2-nitro-, 3-cyano, 4-(dimethylamino)-, and 2,3,4,5,6-pentafluorophenyl]-1,4-dihydropyridine, *J. Med. Chem*., **23**, 1442-1445

149. Jervis H., S.G. Kazarian, K.L.A. Chan, D. Bruce, N. King (2004). Water vapour-induced mesoporous structure collapse observed by VGI and FT-IR spectroscopy, *Vibrational Spectroscopy*, Vol. **35**, Issues 1-2, 225-231

150. Xia Yang, Xiujuan Wang and Chi Bun Ching (2009). In situ monitoring of solid-state transition of p-aminobenzoic acid polymorphs using Raman spectroscopy, *J. Raman Spectrosc*., **40**, 870-875

151. Frausto-Reyes C., C. Medina-Gutierrez, R. Sato-Berru, L. R. Sahagun (2004). Qualitative study of ethanol content in Tequilas by Raman spectroscopy and principal component analysis, *Spectrochemica Acta* Part A 61 2657-2662

152. Sato-Berru R. Y., E. V. Mejia-Uriarte, C. Frausto-Reyes, M. Villagran-Muniz, H. Murrieta S, J. M. Saniger (2006). Application of principal component analysis and Raman spectroscopy in the analysis of polycrystalline $BaTiO_3$ at high pressure, *Spectrochemica Acta* Part A 66, 557-560

153. Norman Chieng, Sonke Rehder, Dorothy Saville, Thomas Rade, Jaakko Aaltonen (2009). Quantitative solid-state analysis of three forms of ranitidine hydrochloride in ternary mixtures using Raman spectroscopy and X-ray powder diffraction, *Journal of Pharmaceutical and Biomedical Analysis*, **49**, 18-25

154. Simmons D. L., Ranz R. J., Gyanchandani N. D., Picotte P., Polymorphism in pharmaceuticals II (tolbutamide). *Can. J. Pharm. Sci., (*1972), **7**, 121-123

155. Burger, A. Zur polymorphie oraler antidiabetika. *Sci. Pharm.* (1975), **43,** 161-168

156. Burger A., Ramberger R., On the polymorphism of pharmaceuticals and other molecular crystals. II. Applicability of thermodynamic rules, *Mikrochim. Acta* (1979), 273-316

157. Al-Saieq S. S., Riley G. S., Polymorphism in sulphonylurea hypoglycaemic agents: I. Tolbutamide, *Pharm. Acta Helv.,* (1981), **56**, 125-129

158. Leary J. R., Ross S. D., Thomas M. J. K., On characterization of the polymorphs of tolbutamide, *Pharm. Weekblad. Sci. Ed.,* (1981), **3**, 62-66

159. Umeda T., Ohnishi N., Yokoyama T., Kuroda T., Kita Y., Kuroda K., Tatsumi E., Matsuda Y., A kinetic study on the isothermal transition of polymorphic forms of tolbutamide and mefenamic acid in the solid state at high temperatures, *Chem. Pharm. Bull,* (1985), **33**, 2073-2078

160. Traue J., Kala, H. Kohler, M. Wenzel, U. Wiegeleben, A. Forster, B.;Pollandt, P. Pintye-Ho ´di, K. Szabo´-Revesz, P. Selmeczi, B., Untersuchungen zur polymorphie von arzneistoffen in pulvern und tabletten, *Pharmazie,* (1987), **42**, 240-241

161. Georgarakis M., Untersuchungen zur polymorphie von tolbutamid, *Pharmazie,* (1989), **44**, 209-210

162. Olives A. I., Martin M. A., del Castillo, B., Barba, C., Influence of the presence of trace amounts of metals on the polymorphism of tolbutamide, *Int. J. Pharm.,* (1996), **14**, 1069-1076

163. Stephenson G. A., Pfeiffer R. R., Byrn, S. R., Solid-state investigation of the tautomerism of acetohexamide. *Int. J. Pharm.,* (1997), **146**, 93-99

164. Hasegawa G., T. Komasaka, R. Bando, Y. Yoshihashi, E. Yonemochi, K. Fujii, H. Uekusa, K. Terada, Reevaluation of solubility of tolbutamide and polymorphic transformation from form I to unknown crystal form, *Int. J. Pharm*. (2009), **369**, 12-18

165. Subra-Paternault P., C. Roy, D. Vrel, A. Vega-Gonzalez, C. Domingo, Solvent effect on tolbutamide crystallisation induced by compressed CO_2 as antisolvent, *Journal of Crystal Growth*, (2007), **309**, 76-85

166. Chakravarty P., K. S. Alexander, A. T. Riga, K. Chartterjee, Crystal forms of tolbutamide from acetonitrile and 1-octanol: effect of solvent, humidity and compression pressure, *Int. J. Pharm*., (2005), **288**, 335-348

167. Thirunahari S., S. Aitipamula, P. C. Chow, R. G. H. Tan, Conformational polymorphism of tolbutamide: A structural, spectroscopic, and thermodynamic characterisation of Burger's forms I-IV, *Journal of Pharmaceutical Sciences*, (2009), 1-16, DOI 10.1002/jps.22061

168. Kimura K., F. Hiramaya and K. Uekama, Characterisation of tolbutamide polymorphs (Burger's forms II and IV) and polymorphic transition behavior, *Journal of Pharmaceutical Sciences*, (1999), **88**, 385-391

169. Jonathan C. Burley, Dermot O'Hare and Gareth R. Williams, The application of statistical methodology to the analysis of time-resolved X-ray diffraction data, *Analytical Methods,* (2011), DOI: 10.1039/C0AY00772B

170. Infra red and Raman characteristic group frequencies, tables and charts by George Socrates, third edition, Wiley and sons, 2004

171. Jonathan C. Burley, M. J. Duer, R. S. Stein and R. M. Vrcelj, Enforcing ostwald's rule of stages: Isolation of paracetamol forms III and II, *European Journal of Pharmaceutical Sciences,* **31**, (2007), 271-276

172. Post M. L., O. Kennard and A. S. Horn, The tricyclic antidepressants: imipramine hydrochloride. The crystal and molecular structure of 5-(3-dimethylaminopropyl)-10,11-dihydro-5*H*-dibenz[*b*,*f*]azepine hydrochloride, *Acta Cryst.,* B**31**, (1975), 1008-1013

173. Heimstad E., Ø. Edvardsen and S. G. Dahl, Molecular structure and dynamics of trycyclic antidepressant drugs, *European Neurpsychopharmacology,* **1**, (1991), 127-137

174. Matousek, P., Parker, A.W., Bulk Raman Analysis of Pharmaceutical Tablets, *Applied Spectroscopy*, (2006), **60,** Issue 12, 1353-1357

175. Adrian C. Williams, V. Brett Cooper, Lisa Thomas, Letecia J. Griffith , Catherine R. Petts and Steven W. Booth, Evaluation of drug physical form during granulation, tabletting and storage, *International Journal of Pharmaceutics*, (2004), **275**, 29-39

176. Chao Wang, Thomas J. Vickers and Charles K. Mann, Direct assay and shelf-life monitoring of aspirin tablets using Raman spectroscopy, *Journal of Pharmaceutical and Biomedical Analysis,* (1997), **16**, 87-94

177. Dyrby, M., Engelsen, S.B., Nørgaard, L.Bruhn, M.Lundsberg-Nielsen, L., Chemometric Quantification of the Active Substance (Containing C≡N) in a Pharmaceutical Tablet Using Near-Infrared (NIR), Transmittance and NIR FT-Raman Spectra, *Applied Spectroscopy,* (2002), **56**, 579-585

178. Jonas Johansson, Staffan Pettersson and Staffan Folestad, Characterization of different laser irradiation methods for quantitative Raman tablet assessment, *Journal of Pharmaceutical and Biomedical Analysis,* (2005), **39,** 510-516

179. Steven E. J. Bell, D. Thorburn Burns, Andrew C. Dennis, Lindsay J. Matchett and James S. Speers, Composition profiling of seized ecstasy tablets by Raman spectroscopy, *Analyst*, (2000), **125**, 1811-1815

180. Debra S. Hausman, R. Thomas Cambron and Adel Sakr, Application of on-line Raman spectroscopy for characterizing relationships between drug hydration state and tablet physical stability, *International Journal of Pharmaceutics,* (2005), **299**, 19-33

181. Roman Szostak and Sylwester Mazurek, Quantitative determination of acetylsalicylic acid and acetaminophen in tablets by FT-Raman spectroscopy, *Analyst,* (2002), 127, 144-148

182. Breintenbach J., Wolfgang Schrof and J. Neumann, Confocal Raman-Spectroscopy: Analytical Approach to Solid Dispersions and Mapping of Drugs, *Pharmaceutical Research*, (1999), **16**, 1109-1113

183. Cushla M. McGoverin, Thomas Rades and Keith C. Gordon, Recent pharmaceutical applications of raman and terahertz spectroscopies, *Journal of Pharmaceutical Sciences,* (2008), **97**, 4598-4621

184. Johansson Jonas, Sparén Anders, Svensson Olof, Folestad Staffan and Claybourn Mike, Quantitative Transmission Raman Spectroscopy of Pharmaceutical Tablets and Capsules, *Applied Spectroscopy*, (2007), **61**, 1211-1218

185. Wikström Håkan, Lewis Ian R., Taylor Lynne S., Comparison of Sampling Techniques for In-Line Monitoring Using Raman Spectroscopy, *Applied Spectroscopy*, (2005), **59**, 934-941

186. Matousek P., Clark I.P., Draper E.R.C., Morris M.D., Goodship A.E., Everall N., Towrie M., Finney W.F., and Parker, A.W., Subsurface Probing in Diffusely Scattering Media Using Spatially Offset Raman Spectroscopy, *Applied Spectroscopy*, (2005), **59**, 393-400

187. Pavel Matousek, M. Morris, N. Everall, I. Clark, M. Towrie, E. Draper, A. Goodship and A. Parker, Numerical Simulations of Subsurface Probing in Diffusely Scattering Media Using Spatially Offset Raman Spectroscopy, *Applied Spectroscopy*, (2005), **59**, 1485-1492

188. Pavel Matousek, Deep non-invasive Raman spectroscopy of living tissue and powders, *Chem. Soc. Rev.*, (2007), **36**, 1292–1304

189. Neil Macleod and P. Matousek, Emerging Non-invasive Raman Methods in Process Control and Forensic Applications, *Pharmaceutical Research*, (2008), **25**, 2205–2215

190. Neil Macleod and P. Matousek, Deep noninvasive Raman spectroscopy of turbid media, (2008), *Applied Spectroscopy,* **62**, 291A–304A

191. Pavel Matousek and M. D. Morris, Emerging Raman Applications and Techniques in Biomedical and Pharmaceutical Fields, Springer, 1st edn, 2010

192. Schrader B., and G. Bergmann, Die Intensität des Ramanspektrums polykristalliner Substanzen, *Fresenius' Z. Anal. Chem.*, (1967), **225**, 230–247

193. Eliasson C., N. Macleod, L. Jayes, F. Clarke, S. Hammond, M. Smith and P. Matousek, Non-invasive quantitative assessment of the content of pharmaceutical capsules using transmission Raman spectroscopy, *Journal of Pharmaceutical and Biomedical Analysis,* (2008), **47,** 221-229

194. Joel Bernstein, *Polymorphism in Molecular Crystals*, Oxford University Press, 2002

195. Mevik B. and R. Wehrens, The pls package: Principal component and partial least squares regression in R, *J. Stat. Software*, 2007, **18**(2), 1–24 142

196. Geladi P., D. MacDougall and H. Martens, Linearization and scatter-correction for near-Infrared reflectance spectra of meat, *Appl. Spectrosc.*, **39**, (1985), 491–500

APPENDICES

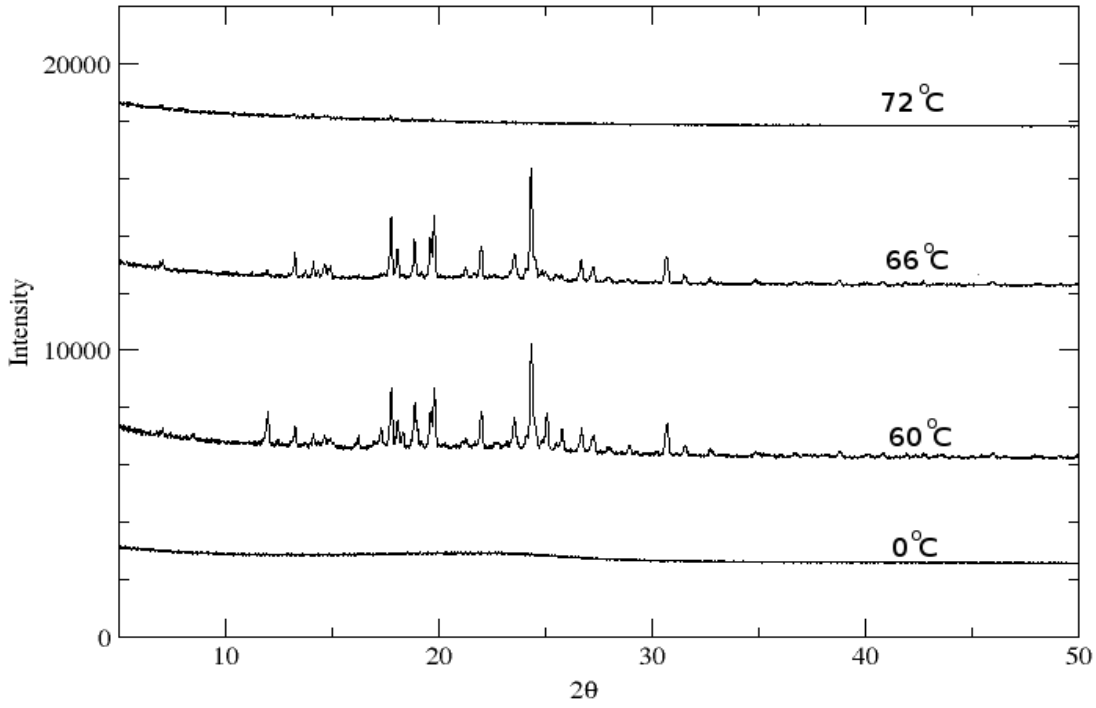

Figure A: In situ XRPD pattern from the heating of amorphous FFA III

Amorphous FFA III transforms back to form I at 66°C via an intermediate (mixture of forms I and III, at 60°C), before melting at a much lower temperature of 72°C as shown above (figure A). These differences in behaviour can be adduced to experimental set up, likely causes include several separate areas of amorphous material, caused by entrapment of bubbles in the capillary tube when the FFA sample was melted. Slightly different thermal conditions in each part of the capillary, coupled with stochastic nature of nucleation makes things difficult.

Figure B: In situ XRPD pattern from the reheating of nifedipine form II (below), form II transforms via a mixture of both forms I and II (at 63°C and 66°C) to form I (69°C).

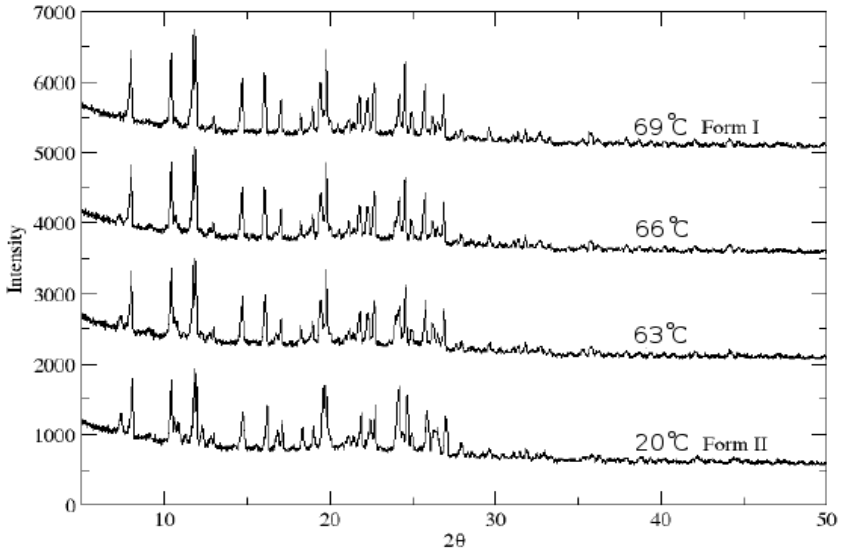

Figure C: DSC trace of the slow heating of amorphous tolbutamide: inset are the two weak endothermic events at at 102.3°C and 117.9°C (below)

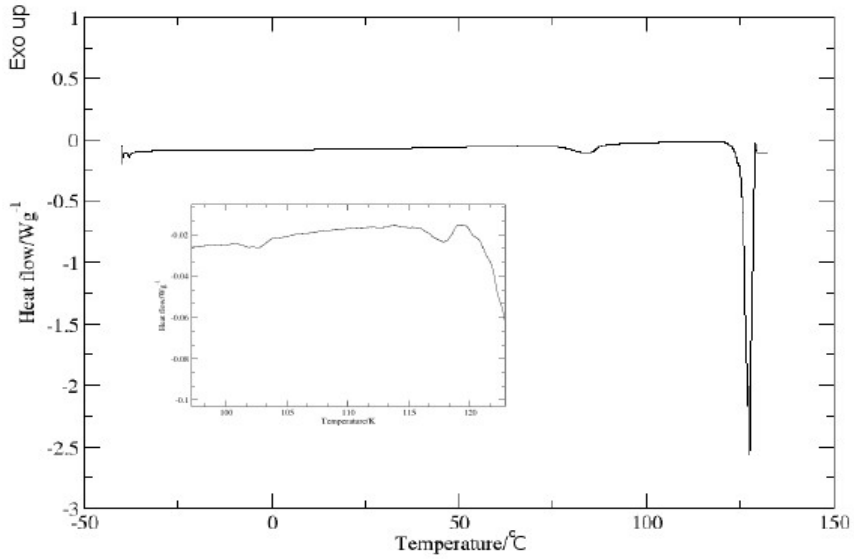

List of Conferences Attended

The British Crystallographic Association (BCA),Pharmaceutical Special Interest Group Autumn Meeting held at AstraZeneca, Charnwood site, Loughborough, on the 5th November 2008.

Control and Prediction of the Organic Solid State (CPOSS) conference tagged: 'State of the Art and Challenges', held at the old refectory, University College London, on the 31st March 2009.

The British Crystallographic Association (BCA), Annual Spring Meeting with the theme 'Dynamic Crystallography', held at the University of Loughborough, from the 21st -23rd April 2009.

The Real McCoy Royal Society of Chemistry (RSC) Meeting tagged: 'The Analysis of Counterfeit Products', held at AstraZeneca, Charnwood site, Loughborough, on the 29th of April 2009.

First World Conference on Physico-Chemical Methods in Drug Discovery and Development held at Rovinj, Croatia, from the 27th September to October 1st 2009.

Symposium on Mechanochemistry and Solvent-free Synthesis held at the Queen's University Belfast from the 6th - 7th November 2009.

Infra-red and Raman Discussion Group 191st Christmas meeting, held at the University College London, on the 17th December 2009.

The Academy of Pharmaceutical Sciences 'Industrial Insights' held at AstraZeneca Loughborough, from the 8th-9th April 2010.

Control and Prediction of the Organic Solid State (CPOSS) conference tagged: 'Characterisation and Computational Modelling of Complex Behaviour', held at the old refectory, University College London, on the 19th April 2010.

Biomaterials for Ageing Populations: 1st UK-CHINA Summer School, held at Sichuan University, China from the 19th - 25th July 2010.

UK Pharmaceutical Characterisation Seminar, held at the School of Pharmacy, University of London, on the 14th September 2010.

Infra-red and Raman Discussion Group 194st General meeting, held at the University College London, on the 6th December 2010.

Control and Prediction of the Organic Solid State (CPOSS) conference tagged: 'Towards Understanding the Pharmaceutical Solid State', held at the old refectory, University College London, on the 30th March 2011.

Presentations

1. Poster titled, 'Polymorphism in Flufenamic Acid', presented at the Control and Prediction of the Organic Solid State (CPOSS) conference tagged: 'State of the Art and Challenges', held at the old refectory, University College London, on the 31st March 2009.

2. Poster titled, 'Polymorphic fingerprinting using phonon-mode Raman spectroscopy', presented at the 1st RCUK China Summer School, Tagged Biomaterials for ageing population, held at Sichuan University, Chengdu, China, 19th-26th July, 2010.

Prize

1. Best research proposal/ idea (as part of a team), at the 1st RCUK China Summer School, Tagged Biomaterials for ageing population, held at Sichuan University, Chengdu, China, 19th-26th July, 2010.
2. RCUK Travel Award - £800

Journal Publications

1. Sarah Al-Dulami, Adeyinka Aina and Jonathan Burley, Rapid polymorph screening on milligram quantities of pharmaceutical material using phonon-mode Raman spectroscopy, CrystEngComm, 2010, 12, 1038–1040.
2. Adeyinka Aina, Michael D. Hargreaves, Pavel Matousek and Jonathan C. Burley, Transmission Raman spectroscopy as a tool for quantifying polymorphic content of pharmaceutical formulations, Analyst, (2010),DOI: 10.1039/c0an00352b.